

UNIVERSITY OF OKLAHOMA  
GRADUATE COLLEGE

EFFECT OF NANOPARTICLES AND SOLVENT BASED EMULSION ON HEAVY  
OIL VISCOSITY

A THESIS  
SUBMITTED TO THE GRADUATE FACULTY  
in partial fulfillment of the requirements for the  
Degree of  
MASTER OF SCIENCE

By  
HARSHKUMAR PATEL  
Norman, Oklahoma  
2016

EFFECT OF NANOPARTICLES AND SOLVENT BASED EMULSION ON HEAVY  
OIL VISCOSITY

A THESIS APPROVED FOR THE  
MEWBOURNE SCHOOL OF PETROLEUM AND GEOLOGICAL ENGINEERING

BY

---

Dr. Subhash N. Shah, Chair

---

Dr. Ramadan Ahmed

---

Dr. Maysam Pournik

© Copyright by HARSHKUMAR PATEL 2016  
All Rights Reserved.

*To my Parents, Teachers, and Friends*

## **Acknowledgements**

Foremost, I would like to express my sincere gratitude to Dr. Subhash Shah for his continuous academic guidance and financial support. His immense knowledge and vast industry experience, coupled with supportive nature, have played a significant role in shaping my professional career. It has been a great honor working under him as a graduate research assistant.

I would also like to thank Dr. Ramadan Ahmed for his insightful suggestions to improve quality of this work. I am also grateful to Dr. Maysam Pournik for taking interest in my research and providing valuable recommendations as a thesis committee member.

Special thanks to Dr. Ucan Sezai for providing me with heavy oil samples. Without his generous support, this study could not have been conducted. I am also thankful to Aditya Srinivasan for conducting a study that served as a foundation for this research work.

I am grateful to entire research team of Well Construction Technology Center (WCTC) for being the family away from home. Special thanks to Jeff McCaskill, for his technical support with equipment and help with preparation of fluid samples. I am extremely grateful to Sarvesh, Abhishek, Soham and Vineet for teaching me know-hows of various experimental works and making my stay at WCTC a memorable one. All my friends, especially Varun, Deep, Parth, Viral and Vimlesh, deserve my heartfelt thanks, for always believing in me and supporting me through thick and thin.

Last but not the least, I am profoundly grateful to my parents for their love and support. Thank you dad, for being the greatest inspiration in my life, and providing me with all necessary resources. Thanks mom, for raising me to become a better person that I am today. I have no words to acknowledge the sacrifices that you have made. I will always be indebted to both of you.

# Table of Contents

<b>Acknowledgements</b> .....	<b>iv</b>
<b>Abstract</b> .....	<b>xviii</b>
<b>1. Introduction</b> .....	<b>1</b>
1.1 Heavy Oil.....	1
1.2 Heavy Oil Recovery Techniques .....	2
1.2.1 Non-Thermal Recovery Methods .....	2
1.2.2 Thermal Recovery Methods .....	4
1.3 Basic Principles of Chemical EOR.....	6
1.3.1 Mobility Ratio .....	6
1.3.2 Capillary Number .....	7
1.3.3 Interfacial Tension.....	9
1.4 Surfactants .....	9
1.5 Macro- vs Micro- Emulsions .....	12
1.6 Nanoparticles .....	13
1.6.1 Nanotechnology in Oil and Gas Industry.....	14
1.7 Research Opportunities.....	16
1.8 Scope of Research and Objectives.....	17
1.9 Overview of Thesis.....	19
<b>2. Heavy Oil Viscosity</b> .....	<b>21</b>
2.1 Rheological Behavior .....	21
2.1.1 Effect of Shear Rate.....	21
2.1.2 Effect of Composition .....	21
2.1.3 Effect of Temperature.....	22
2.2 Importance of Viscosity Data .....	23
2.3 Reliability of Viscosity Data.....	24
2.3.1 Sampling.....	25
2.3.2 Handling and Transportation.....	26
2.3.3 Sample Preparation.....	26

2.3.4	Viscosity Measurement .....	26
2.4	Ideal vs Practical Heavy Oil Viscosity .....	27
<b>3.</b>	<b>Heavy Oil Viscosity Alteration by Nanoparticles .....</b>	<b>29</b>
3.1	Low Temperature Viscosity Alteration .....	31
3.1.1	Decrease in Viscosity .....	31
3.1.2	Increase in Viscosity.....	35
3.2	High Temperature Viscosity Alteration.....	38
3.2.1	Aquathermolysis.....	38
3.2.2	Improved Thermal Conductivity .....	39
3.3	Optimum Concentration of Nanoparticles.....	41
3.3.1	Effect of Temperature.....	41
3.3.2	Effect of Metal Type and Particle Size.....	42
3.3.3	Effect of Oil Composition .....	43
3.4	Field Application .....	43
<b>4.</b>	<b>Characteristics of Solvent Based Emulsion.....</b>	<b>45</b>
4.1	Benefits of S/W Emulsion .....	46
4.1.1	Mobility Control.....	46
4.1.2	Viscosity Reduction.....	47
4.1.3	In-Situ Emulsification .....	47
4.2	Phase Behavior of a S/W Emulsion System .....	48
4.3	Rheology of S/W Emulsion .....	49
4.4	Optimum Composition of S/W Emulsion.....	50
<b>5.</b>	<b>Properties of Solvent Based Emulsion Containing Nanoparticles .....</b>	<b>51</b>
5.1	Rheological Behavior .....	52
5.2	Interfacial Tension Alteration.....	54
5.3	Emulsion Stability.....	56
<b>6.</b>	<b>Experimental Setup and Methodology .....</b>	<b>57</b>
6.1	Equipment Used.....	57
6.1.1	Viscometer.....	57
6.1.2	Heater Cup.....	64



6.1.3	Blender .....	65
6.2	Materials Used .....	65
6.2.1	Triton™ X-100 Surfactant .....	65
6.2.2	Xylene.....	66
6.2.3	NaCl Brine.....	67
6.2.4	Copper (II) Oxide Nanoparticles .....	67
6.2.5	Iron (III) Oxide Nanoparticles.....	68
6.2.6	Nickel (II) Oxide Nanoparticles .....	68
6.3	Fluid Preparation.....	69
6.3.1	Heavy Oil Containing Nanoparticles.....	69
6.3.2	Solvent-in-Water (S/W) Micro-Emulsion .....	71
6.3.3	Heavy Oil Emulsion .....	71
6.3.4	Heavy Oil Nano-Emulsion .....	72
6.4	Challenges in Viscosity Measurement.....	72
6.4.1	Temperature Control .....	72
6.4.2	Viscosity Measurement Approach .....	73
6.4.3	Artificial Shear-Thinning Behavior.....	77
6.5	Procedure of Viscosity Measurement .....	78
6.6	Models Employed for Rheological Characterization of Fluids .....	79
<b>7.</b>	<b>Results and Discussion .....</b>	<b>82</b>
7.1	Rheology of Heavy Oil Samples .....	82
7.1.1	Reproducibility .....	87
7.2	Effect of Nanoparticles .....	91
7.2.1	Copper Oxide (CuO) .....	91
7.2.2	Iron Oxide (Fe <sub>2</sub> O <sub>3</sub> ) .....	96
7.2.3	Nickel Oxide (NiO) .....	100
7.2.4	Optimum Concentration .....	103
7.3	Effect of S/W Emulsion.....	107
7.3.1	Rheological Behavior .....	108
7.3.2	Viscosity Reduction.....	111

7.4	Effect of S/W Emulsion Containing Nanoparticles .....	114
7.4.1	Heavy Oil Nano-Emulsion Containing Copper Oxide Nanoparticles....	114
7.4.2	Heavy Oil Nano-Emulsion Containing Iron Oxide Nanoparticles.....	118
7.4.3	Heavy Oil Nano-Emulsion Containing Nickel Oxide Nanoparticles.....	121
7.5	Economic Analysis .....	124
<b>8.</b>	<b>Conclusions and Recommendations .....</b>	<b>129</b>
8.1	Conclusions.....	129
8.2	Future Work and Recommendations .....	131
	<b>Nomenclature.....</b>	<b>133</b>
	<b>References .....</b>	<b>134</b>
	<b>Appendix A: Rheology of Heavy Oil Containing Nanoparticles.....</b>	<b>141</b>
	<b>Appendix B: Rheology of Heavy Oil Emulsion Containing S/W Emulsion .....</b>	<b>153</b>
	<b>Appendix C: Rheology of Heavy Oil Nano-Emulsion Containing S/W Emulsion and Nanoparticles .....</b>	<b>157</b>

## List of Tables

Table 1.1: Classification of surfactants (Akstinat, 1981) .....	11
Table 4.1: Interfacial tension of an Alaskan crude oil with brine, air and optimized micro-emulsion (Qiu, 2010).....	50
Table 6.1: Shear stress measurement limit of various spring and bob configuration as provided by the manufacturer.....	59
Table 6.2: Shear rate range for different bobs as provided by the manufacturer .....	60
Table 6.3: Specifications of the spring and bob configuration used in the viscometer ..	62
Table 6.4: Specifications of the surfactant used .....	66
Table 6.5: Specifications of xylene .....	67
Table 6.6: Properties of copper (II) oxide nanopowder .....	68
Table 6.7: Properties of iron (III) oxide nanopowder.....	68
Table 6.8: Properties of nickel (II) oxide nanopowder.....	69
Table 6.9: Test matrix for each heavy oil sample .....	70
Table 7.1: Power law parameters of heavy oil samples at various temperatures .....	84
Table 7.2: Newtonian viscosity of heavy oil samples as a function of temperature .....	85
Table 7.3: Sample calculation of reproducibility error .....	88
Table 7.4: Reproducibility of viscosity measurement for heavy oil samples.....	91
Table 7.5: Summary of viscosity alteration by copper oxide nanoparticles.....	92
Table 7.6: Summary of viscosity alteration by iron oxide nanoparticles .....	96
Table 7.7: Summary of viscosity alteration by nickel oxide nanoparticles.....	100
Table 7.8: Optimum concentration (% wt.) of nanoparticles at different temperatures	104

Table 7.9: Power law parameters of heavy oil emulsions containing 5 vol% S/W emulsion .....	109
Table 7.10: Power law parameters of heavy oil emulsions containing 10 vol% S/W emulsion .....	109
Table 7.11: Power law parameters of heavy oil emulsions containing 15 vol% S/W emulsion .....	110
Table 7.12: Power law parameters of heavy oil emulsions containing 20 vol% S/W emulsion .....	110
Table 7.13: Summary of average viscosity reduction caused by S/W emulsion.....	111
Table 7.14: Power law parameters of heavy oil nano-emulsions containing 5 vol% S/W emulsion and 0.002 wt% copper oxide nanoparticles .....	116
Table 7.15: Power law parameters of heavy oil nano-emulsions containing 10 vol% S/W emulsion and 0.002 wt% copper oxide nanoparticles .....	116
Table 7.16: Power law parameters of heavy oil nano-emulsions containing 5 vol% S/W emulsion and 0.002 wt% iron oxide nanoparticles.....	119
Table 7.17: Power law parameters of heavy oil nano-emulsions containing 10 vol% S/W emulsion and 0.002 wt% iron oxide nanoparticles.....	119
Table 7.18: Power law parameters of heavy oil nano-emulsions containing 5 vol% S/W emulsion and 0.002 wt% nickel oxide nanoparticles .....	122
Table 7.19: Power law parameters of heavy oil nano-emulsions containing 10 vol% S/W emulsion and 0.002 wt% nickel oxide nanoparticles .....	122
Table 7.20: Cost of nano-sized metal oxide particles.....	124

Table 7.21: Cost of chemicals used in preparing S/W emulsion.....	125
Table 7.22: Summary of cost and viscosity performance of all test fluids prepared with heavy oil Sample A .....	126
Table 7.23: Summary of cost and viscosity performance of all test fluids prepared with heavy oil Sample B.....	127

## List of Figures

Figure 1.1: Distribution of world's total oil reserves (Schlumberger, 2006) .....	1
Figure 1.2: Displacement front for two different mobility ratios (Miscible Processes, SPE, 1965).....	7
Figure 1.3: A typical relationship of capillary number with (a) residual oil saturation (Johannesen and Graue, 2007), and (b) relative permeability (Lohne and Fjelde, 2012)	8
Figure 1.4: Interfacial tension at the interface between two immiscible liquids (Torsaeter and Abtahi, 2003) .....	9
Figure 1.5: A typical molecular structure of surfactant (Akstinat, 1981) .....	10
Figure 1.6: Graphical representation of critical micelle concentration (Lake, 1989).....	12
Figure 1.7: Change in free energy as a function of droplet size of dispersed medium of emulsions (Sharma and Shah, 1985) .....	13
Figure 1.8: Change in surface area with decreasing particle size (Yokoyama, 2008) ...	14
Figure 2.1: Effect of asphaltene concentration on viscosity of xylene base fluid (Pierre et al., 2004).....	22
Figure 2.2: Effect of temperature on asphaltene structure in a typical heavy oil (Pierre et al., 2004).....	23
Figure 3.1: Zeta potential of NiO nanoparticles as a function of pH (El-Kemary et al., 2013).....	32
Figure 3.2: Microscopic image of nickel nanoparticles dispersed in (a) heavy oil, and (b) water (Shokrlu et al., 2014) .....	33
Figure 3.3: Low temperature viscosity alteration by nanoparticles (Not to scale).....	37

Figure 3.4: Effect of nano- and micron-sized metal particles on heat transfer rates (Shokrlu et al., 2014) .....	41
Figure 3.5: Illustration of in-situ injection of nanoparticle to improve heavy oil recovery (Nassar et al., 2011).....	44
Figure 4.1: Isothermal ternary diagram for xylene-in-2% NaCl brine emulsion system (Qiu, 2010) .....	48
Figure 5.1: Double network structure formation in presence of nanoparticles by entanglement of micelles (Helgeson et al., 2010) .....	53
Figure 5.2: Effect of copper oxide nanoparticles on viscosity of xylene-in-brine micro emulsion (Qiu, 2010).....	54
Figure 5.3: Spreading of nanofluids on solids surface through ‘disjoining pressure’ (Wasan et al., 2010).....	55
Figure 6.1: (a) Model 900 OFITE viscometer (b) Couette principle (source: viscopedia.com).....	58
Figure 6.2: Shear stress limit of different spring-bob configuration plotted with the estimated rheogram of both heavy oil samples (at 75 and 140°F) .....	61
Figure 6.3: Viscometer calibration plot.....	64
Figure 6.4: Heater cup used with the viscometer .....	64
Figure 6.5: Commercial blender used to prepare heavy oil emulsion.....	65
Figure 6.6: Effect of viscous heating on apparent viscosity (at a constant shear rate and in absence of external heat energy) .....	74
Figure 6.7: Hysteresis effect (absence of external heat source).....	75

Figure 6.8: Graphical representation of shear stress variation during step down shear rate approach .....	76
Figure 6.9: Graphical representation of shear stress variation during step up shear rate approach .....	76
Figure 6.10: Graphical representation of artificial shear-thinning behavior introduced by shear degradation and viscous heating .....	77
Figure 6.11: Graphical representation of typical temperature variation during test.....	79
Figure 7.1: Rheogram for heavy oil sample A at various temperatures .....	83
Figure 7.2: Rheogram for heavy oil sample B at various temperatures .....	83
Figure 7.3: Newtonian viscosity of heavy oil samples as a function of temperature .....	86
Figure 7.4: Newtonian viscosity of used heavy oil samples as a function of temperature .....	86
Figure 7.5: Graphical representation of reproducibility tests for Sample A at (a) 100°F, (b) 120°F, (c) 140°F, and (d) 160°F .....	89
Figure 7.6: Graphical representation of reproducibility tests for Sample B at (a) 100°F, (b) 120°F, (c) 140°F, and (d) 160°F .....	90
Figure 7.7: Newtonian viscosity of heavy oil sample A in presence of copper oxide nanoparticles at various temperatures .....	93
Figure 7.8: Newtonian viscosity of heavy oil sample B in presence of copper oxide nanoparticles at various temperatures .....	93
Figure 7.9: Percentage change in apparent viscosity of heavy oil sample A caused by copper oxide nanoparticles at various temperatures.....	94



Figure 7.10: Percentage change in apparent viscosity of heavy oil sample B caused by copper oxide nanoparticles at various temperatures..... 94

Figure 7.11: Newtonian viscosity of heavy oil sample A in presence of iron oxide nanoparticles at various temperatures ..... 97

Figure 7.12: Newtonian viscosity of heavy oil sample B in presence of iron oxide nanoparticles at various temperatures ..... 97

Figure 7.13: Percentage change in apparent viscosity of heavy oil sample A caused by iron oxide nanoparticles at various temperatures ..... 98

Figure 7.14: Percentage change in apparent viscosity of heavy oil sample B caused by iron oxide nanoparticles at various temperatures ..... 98

Figure 7.15: Newtonian viscosity of heavy oil sample A in presence of nickel oxide nanoparticles at various temperatures ..... 101

Figure 7.16: Newtonian viscosity of heavy oil sample B in presence of nickel oxide nanoparticles at various temperatures ..... 101

Figure 7.17: Percentage change in apparent viscosity of heavy oil sample A caused by nickel oxide nanoparticles at various temperatures..... 102

Figure 7.18: Percentage change in apparent viscosity of heavy oil sample B caused by nickel oxide nanoparticles at various temperatures..... 102

Figure 7.19: Percentage change in viscosity of heavy oil Sample A as a function of nanoparticle concentration at (a) 100°F, (b) 120°F, (c) 140°F, and (d) 160°F..... 105

Figure 7.20: Percentage change in viscosity of heavy oil Sample B as a function of nanoparticle concentration at (a) 100°F, (b) 120°F, (c) 140°F, and (d) 160°F..... 106

Figure 7.21: Average reduction in apparent viscosity of heavy oil sample A caused by varying volume fraction of S/W emulsion as a function of temperature .....	112
Figure 7.22: Average reduction in apparent viscosity of heavy oil sample B caused by varying volume fraction of S/W emulsion as a function of temperature .....	112
Figure 7.23: Effect of S/W emulsion containing copper oxide nanoparticles on viscosity of heavy oil sample A.....	117
Figure 7.24: Effect of S/W emulsion containing copper oxide nanoparticles on viscosity of heavy oil sample B.....	117
Figure 7.25: Effect of S/W emulsion containing iron oxide nanoparticles on viscosity of heavy oil sample A .....	120
Figure 7.26: Effect of S/W emulsion containing iron oxide nanoparticles on viscosity of heavy oil sample B .....	120
Figure 7.27: Effect of S/W emulsion containing nickel oxide nanoparticles on viscosity of heavy oil sample A.....	123
Figure 7.28: Effect of S/W emulsion containing nickel oxide nanoparticles on viscosity of heavy oil sample B.....	123

## Abstract

Considering the fact that heavy oil and bitumen constitutes about 70% of world's total oil resources, it is not surprising that the quest to produce heavy oil has attained industry wide attention. Because of extremely high viscosity, heavy oil reservoirs generally yield low-energy and low-productivity wells. Technical and economic challenges associated with heavy oil production, indicate a need for extensive research and development activities.

The objective of study presented in this document is to investigate three different approaches for reducing viscosity of heavy oil. In the first set of experiments, three types of metal oxide nanoparticles (CuO, Fe<sub>2</sub>O<sub>3</sub>, and NiO) were employed and their effect on heavy oil viscosity was investigated at different concentrations. The second approach was to mix a solvent-in-water (S/W) emulsion with heavy oil sample in different proportions and inspect rheological changes in resultant emulsion. In third phase of the study, both nanoparticles and solvent based emulsion were added to heavy oil sample and viscosity of resultant nano-emulsion was examined. For all test fluids, rheological measurements are presented at four different temperatures ranging from 100°F to 160°F. This unprecedented experimental work was conducted with two extremely viscous heavy oil samples having viscosity of approximately 77,000 cP and 350,000 cP at room temperature.

Addition of nanoparticles resulted in notable reduction in viscosity of both heavy oil samples. For each type of nanoparticles, viscosity reduction of 50 to 70% was achieved.

The degree of viscosity alteration was observed to be a function of type of nanoparticles, their concentration, and fluid temperature. Moreover, optimum concentrations for maximum viscosity reduction, were identified for each metal oxide nanoparticles at different temperatures.

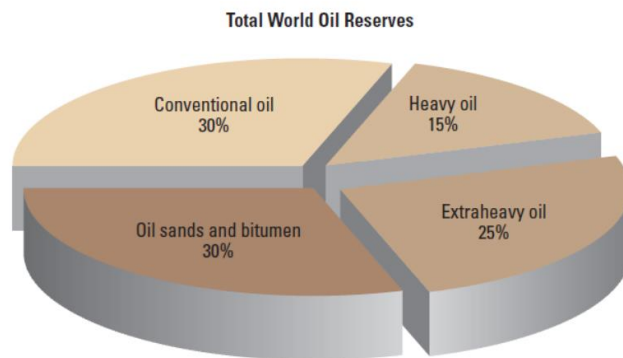
Using S/W emulsion, depending on volume fraction, viscosity reduction varying from 20 to 93% was achieved. In case of S/W emulsion containing nanoparticles, viscosity alteration strongly depended on type of nanoparticles added. Addition of copper oxide nanoparticles in S/W emulsion resulted in additional viscosity reduction of 10 to 30%. Iron oxide nanoparticles had adverse effect, if any, on the performance of S/W emulsion. Interestingly, nickel oxide nanoparticles either had improving or deteriorating effect depending on its concentration in S/W emulsion.

Cost analysis revealed that some of the test fluids cost less than \$16 per barrel of oil and provided 40 to 50% viscosity reduction. The results are promising considering the fact that the cost presented were calculated based on purchase quote for a very small quantity and they will reduce significantly for field scale applications.

Remarkable results obtained in this study, confirm efficacy of nanoparticles and solvent based emulsion in reducing viscosity of heavy oil. This work rekindles the interest in non-thermal heavy oil recovery techniques such as chemical flooding, and provides a foundation for future core flooding studies.

# 1. Introduction

Diminishing ‘easy oil’ resources and ever-increasing energy demand have made it essential to explore unconventional resources such as heavy oil, shale oil, shale gas, tar sands, gas hydrates etc. Among these resources, heavy oil, extra heavy oil and bitumen constitutes about 70% of world’s total oil reserves (see **Fig. 1.1**). Therefore, it is not surprising that quest to produce heavy oil has gained industry wide attention over the past few decades.



**Figure 1.1:** Distribution of world’s total oil reserves (Schlumberger, 2006)

## 1.1 Heavy Oil

Heavy oil is characterized by high density and high resistance to flow i.e. high viscosity, in comparison to conventional oil. Most of heavy oil reservoirs were originally formed in deep formations and contained light oil. However, over the period of time, oil migrated upward and was degraded by bacteria or chemical weathering process. This permitted lighter hydrocarbon compounds to escape, leaving behind viscous heavy oil.

Heavy oil is defined as an oil with gravity between 10 to 20°API and a viscosity value greater than 100 cP at reservoir temperature. Denser oil with gravity less than 10°API are further classified based on in-situ viscosity as extra heavy oil (<10,000 cP) and bitumen (>10,000) (Meyer et al., 2007). Typically, heavy oil is characterized by high viscosity that increases as API gravity decreases. In general, heavy oil exhibits low hydrogen/carbon ratio, low gas/oil ratio, and significant sulfur, asphaltene and heavy metal compounds.

## **1.2 Heavy Oil Recovery Techniques**

World-wide heavy oil production has been on incline in recent years and is believed to increase rapidly in future. Heavy oil exhibits low mobility at reservoir temperature which results in very low production rates. Common production phases such as primary and secondary recovery are usually bypassed because of financial restrictions. It is often decided to proceed directly to tertiary or enhanced oil recovery.

### **1.2.1 Non-Thermal Recovery Methods**

Even though thermal recovery techniques are the most widely used methods for heavy oil production, non-thermal recovery techniques are given first consideration because of their relatively low cost and technical simplicity.

#### ***1.2.1.1 Primary and Secondary Recovery / Cold Production***

Primary recovery techniques rely entirely on natural drive mechanisms for oil to flow into wellbore. The main issue with cold production is low recovery factors of less than 10-15% of original oil-in-place. Operators always try to produce as much oil as they can

using cold production technique before considering other options. Once reservoir pressure starts depleting, secondary recovery techniques such as artificial lift systems, waterflooding, or gas injection are employed.

Recently, *Cold Heavy Oil Production with Sand (CHOPS)* has emerged as a promising non-thermal recovery technique. In this method, sand is intentionally produced in order to create high permeability channels known as wormholes which can enhance drainage area by a factor of 10 or more (Chen, 2006). *Pressure Pulse technology (PPT)* is a relatively new method, which uses steady, non-seismic pulse vibrations to create low velocity wave effect and excite oil molecules and solid particles to flow (Speight, 2009). In *Solvent Methods*, diluents like naphtha or light oil are injected near the wellbore to reduce viscosity of the fluid at pump and improve outflow performance of the well.

#### ***1.2.1.2 Tertiary Recovery***

Chemical flooding makes up the majority of non-thermal tertiary enhance oil recovery techniques. *Micellar Polymer Flooding* and *Alkaline Flooding* are the most common chemical flooding methods. These methods rely on emulsification of heavy oil to improve mobility ratio. In *micellar polymer flooding*, surfactant is injected along with displacing fluid while in *alkaline flooding*, surfactants are formed by inducing reaction between alkaline chemical and certain compounds of oil.

*Carbon Dioxide* or *Nitrogen Flooding* have also emerged as attractive options. Miscibility with oil and vaporization of lighter fraction are the dominant mechanisms of

improved recovery. Sometimes, these gases and water are injected alternatively to achieve better sweep efficiency.

*Microbial Enhanced Oil Recovery (MEOR)* involves injection of a solution containing nutrients and microorganisms. These specially selected bacteria upgrade heavier components of oil into lighter fractions and reduces viscosity.

### **1.2.2 Thermal Recovery Methods**

In some reservoirs, subsurface heavy oil is too viscous to flow on its own. As a result, non-thermal methods do not yield economic production rates. In such cases, it becomes imperative to introduce heat into the reservoir to reduce viscosity of heavy oil.

During thermal recovery, crude oil undergoes significant physical and chemical changes. Physical changes involve alteration of viscosity, specific gravity, interfacial tension, etc. While chemical changes are reflected by processes like cracking and dehydrogenation.

*Hot Fluid Injection* is a process wherein fluids such as water, air, natural gas, carbon dioxide, exhaust gases, solvents, etc are heated at the surface and then injected into relatively cold subsurface formation.

*Steam Injection* is the most common method for heavy oil extraction mainly because of high heat content per pound of steam. There are several mechanisms that contribute to oil recovery during steam injection; such as viscosity reduction, steam distillation, relative permeability alteration, solution gas drive, solvent drive, and gravity segregation (Wu, 1977). *Cyclic Steam Stimulation (CSS) or Huff-'n-Puff* is another variant of steam



injection method in which steam is continuously injected into producing formation for several days or weeks. Next, the injection is shut-off to permit soaking of the reservoir and then, the well is open for production. Steam based methods have been in commercial use since 1960s and they have been widely applied in California, Canada, Indonesia, Oman, and China (Speight, 2009).

*In-Situ combustion (IC)* process involves underground ignition of reservoir oil. The fire generated is sustained by continuous injection of air. Thermal cracking and miscible drive are the dominant mechanisms responsible for additional oil recovery. This is probably the most technically challenging thermal recovery method because of complex designing and difficulty in controlling fire front. IC method is not new and in fact, it has been applied in over a hundred fields (Speight, 2009).

*Steam Assisted Gravity Drainage (SAGD)* has emerged as the most promising thermal recovery technique since the emergence of directional drilling. In this technique, two parallel horizontal wells are drilled. The top well is used to inject steam into formation. As heavy oil becomes less viscous, it starts to drain downward due to gravity and is produced from the bottom well. Major advantage of this method is high steam to oil ratio resulting in ultimate recovery of as high as 60 to 70%.

*Electromagnetic Heating* is a relatively new thermal oil recovery method in which electromagnetic waves are radially transmitted into the reservoir. Temperature is increased by dielectric heating, i.e. heat is generated by vibration of molecules. Recently some researchers (Hascakir, 2008; Greff et al., 2011; shokrlu et al., 2011) have proposed

that the use of nano-sized metal particles along with electromagnetic heating can produce catalytic effect and greatly reduces energy requirement.

### **1.3 Basic Principles of Chemical EOR**

Many of the heavy oil reservoirs are thin and have relatively low oil in place. Moreover, some reservoirs have overlying gas cap or underlying water or both. All these factors render them poor candidates for expensive and technically challenging thermal recovery methods. For such reservoirs, chemical flooding has emerged as an ideal EOR technique.

As discussed in previous section, there are various types of chemical EOR methods. These methods are based on one or more of the following principles: (i) reducing the mobility of displacing fluid, (ii) decreasing interfacial tension between injected fluid and heavy oil, (iii) reduction of heavy oil viscosity, (iv) wettability alteration, and (v) oil swelling. All of these mechanisms are directly or indirectly reflected as changes in two parameters, namely mobility ratio and capillary number.

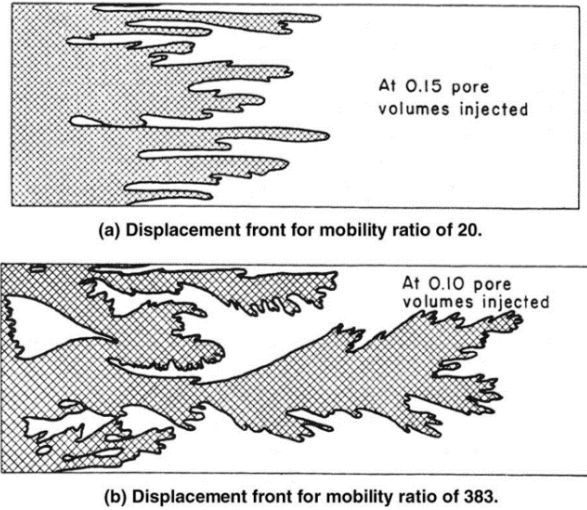
#### **1.3.1 Mobility Ratio**

Mobility ratio determines sweep efficiency of chemical flooding. It is defined as the ratio of mobility of displacing fluid to mobility of displaced fluid (oil). Mathematically, it can be expressed as,

$$M = \frac{k_{rd}}{k_{ro}} \times \frac{\mu_o}{\mu_d}$$

where,  $k_r$  is relative permeability and  $\mu$  is viscosity. Subscript 'd' stands for displacing fluid and 'o' corresponds to oil. All parameters are in consistent units.

Mobility ratio of greater than 1 means that mobility of displacing fluid is higher than mobility of oil. This is an unfavorable condition which leads to viscous fingering, resulting in poor displacement efficiency and therefore less oil recovery (see **Fig. 1.2**).



**Figure 1.2:** Displacement front for two different mobility ratios (Miscible Processes, SPE, 1965)

Considering extremely high viscosity of heavy oil, it is difficult to achieve mobility ratio of 1 or less. Therefore, to minimize it as much as possible, most of the methods focus not only on decreasing oil viscosity but also on reducing mobility and relative permeability of displacing fluid.

### 1.3.2 Capillary Number

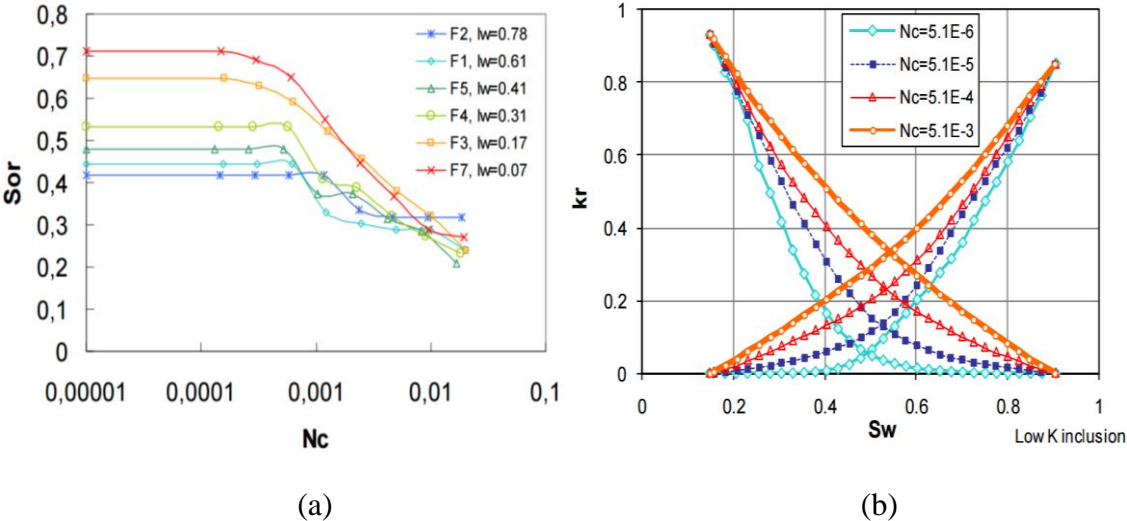
Capillary number is a dimensionless group that relates viscous force with capillary force.

It is denoted by  $N_c$  and is defined as,

$$N_c = \frac{U\mu_d}{\sigma}$$

where,  $v$  is Darcy velocity,  $\mu$  is dynamic viscosity of displacing fluid and  $\sigma$  is surface or interfacial tension. All variables are in consistent units.

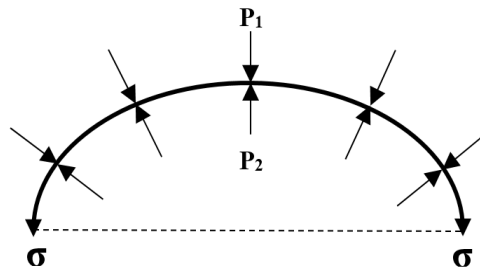
Capillary number is a governing parameter for chemical flooding technique. Various researchers have confirmed through laboratory studies that additional residual oil can be recovered by decreasing retaining capillary forces (i.e. interfacial tension) or increasing viscous forces (i.e. better displacement efficiency). Both of these effects are reflected as increase in capillary number. As capillary number increases, residual saturation of oil decreases (see **Fig. 1.3**). Once capillary number reaches a critical value, oil blobs break down into smaller droplets, resulting in additional recovery. Capillary number also reflects alteration in relative permeability. Increasing capillary number increases relative permeability of both wetting and non-wetting phase (see **Fig. 1.3**).



**Figure 1.3:** A typical relationship of capillary number with (a) residual oil saturation (Johannesen and Graue, 2007), and (b) relative permeability (Lohne and Fjelde, 2012)

### 1.3.3 Interfacial Tension

Interfacial tension (IFT) is a property of the interface between two immiscible phases. When one of the phases is air, it is referred to as surface tension. It is a measure of imbalance of molecular forces at an interface. It arises from the tendency of a liquid to expose minimum free surface in presence of another immiscible liquid. It acts perpendicular to the interface as shown in **Fig. 1.4**.



**Figure 1.4:** Interfacial tension at the interface between two immiscible liquids  
(Torsaeter and Abtahi, 2003)

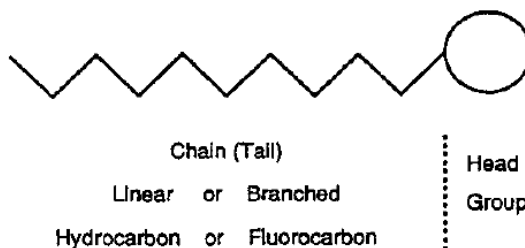
All chemical EOR methods aim to decrease interfacial tension between oil and displacement phase. Reduction in IFT encourages formation of emulsion. There are various ways to alter IFT such as use of surfactant, mechanical agitation, change in temperature, electrostatic forces etc. However, usage of surfactant is the most practical method to form an in-situ emulsion. Surfactant molecules preferentially position themselves at the oil-water interface and reduces IFT.

### 1.4 Surfactants

Surfactants are surface active agents that are widely used in many industries. Surfactants molecules have capability to adsorb on or concentrate at an interface between two

immiscible liquids. They alter interfacial properties such as free energy and reduce surface or interfacial tension (Green and Willhite, 1998). This is useful for generating in-situ emulsions without any external source of energy.

A typical surfactant molecule consists of a polar group and a hydrocarbon (nonpolar) group. The hydrocarbon and polar portions are often referred to as ‘tail’ and ‘head’ respectively. The nonpolar portion can either be a straight chain or a branched chain hydrocarbon. A representative surfactant molecular structure is presented in **Fig. 1.5** below.



**Figure 1.5:** A typical molecular structure of surfactant (Akstinat, 1981)




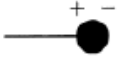
Hydrocarbon components of surfactant interact very weakly with water molecules present in an aqueous solution. The polar group, on the other hand, has strong attraction for water and undergoes solvation. Therefore, the ‘tail’ of surfactant is also termed as hydrophobic or lipophilic group while ionic ‘head’ portion is referred to as hydrophilic group. Because of this dual nature of a surfactant molecule, it is often termed as amphiphile.

Surface active tendency of surfactant molecules arises from the imbalance between hydrophilic and hydrophobic groups. An empirical term known as hydrophilic/lipophilic balance (HLB) is used to characterize surfactants. HLB number of a surfactant determines

type of emulsion it is capable of generating. Surfactant with higher HLB number have more dominant polar group and tends to be more soluble in water, resulting in oil-in-water emulsion.

Surfactants are classified based on the ionic nature of polar head group in aqueous solution. The four categories of surfactants are: (i) anionic (ii) cationic (iii) nonionic, and (iv) amphoteric (zwitterionic). Following **Table 1.1** provides examples and schematics of these four types of surfactants.

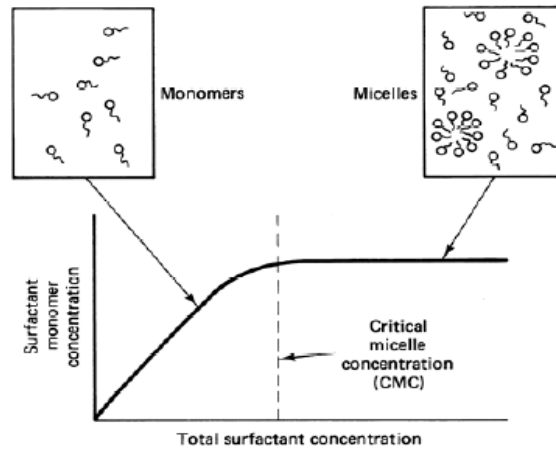
**Table 1.1:** Classification of surfactants (Akstinat, 1981)

			
Anionics	Cationics	Nonionics	Amphoterics
Sulfonates Sulfates Carboxylates Phosphates	Quaternary ammonium organics, pyridinium, imidazolium, piperi- dinium, and sulfonon- ium compounds	Alkyl-, Alkyl- aryl-, acyl-, acylamido-, acyl- aminepolyglycol, and polyol ethers Alkanolamides	Aminocarboxylic acids

As names suggest, polar head groups of cationic and anionic surfactants, when ionize in aqueous solution, exhibit positive and negative charge. Nonionic surfactant does not ionize and is characterized by a head group larger than tail (Green and Willhite, 1998). Amphoterics have two groups of opposite charge.

When surfactant is dissolved in an aqueous solution, it dissociates into an ionic group and a monomer. As concentration of surfactant increases, these monomers groups begin to aggregate and form micelles. Hydrophobic tails are positioned internally within micelles.

Each micelle typically contains 50 to 100 monomers. The concentration at which micelles begin to form is known as critical micelle concentration (CMC). After CMC, increase in surfactant concentration only increases concentration of micelles (see **Fig. 1.6**).



**Figure 1.6:** Graphical representation of critical micelle concentration (Lake, 1989)

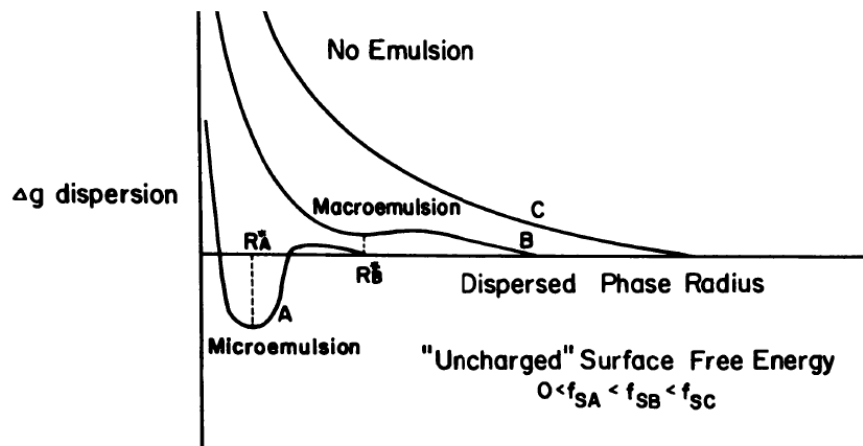
### 1.5 Macro- vs Micro- Emulsions

Understanding the difference between macro- and micro-emulsion and their stability is an important aspect of designing a chemical flooding process. Both of these emulsion types have been studied by several researchers. Sharma and Shah (1985) conducted a comprehensive study of both emulsions and provided detailed description of various factors affecting stability and properties of these emulsions.

Macro-emulsion is a mixture of two immiscible liquids, one of which is dispersed as droplets having size greater than  $0.1 \mu\text{m}$  into a continuous phase of the other liquid. Macro-emulsions are turbid and exhibit milky color. Besides, they are thermodynamically unstable and with time, progressively separate into original phases.



Micro-emulsion differs from macro-emulsion in size of dispersed phase droplets. Typically, average diameter of droplets vary from 100 to 1000 Å. Because of this ultrafine size, they appear transparent. Micro-emulsions are also known as swollen micellar solutions (Sharma and Shah, 1985). **Figure 1.7** presents variation in free energy as a function of dispersed phase radius. This plot clearly confirms that because of smaller size, micro-emulsions exhibit high stability than macro-emulsions. Micro-emulsion are thermodynamically stable while macro-emulsions are kinetically stable.



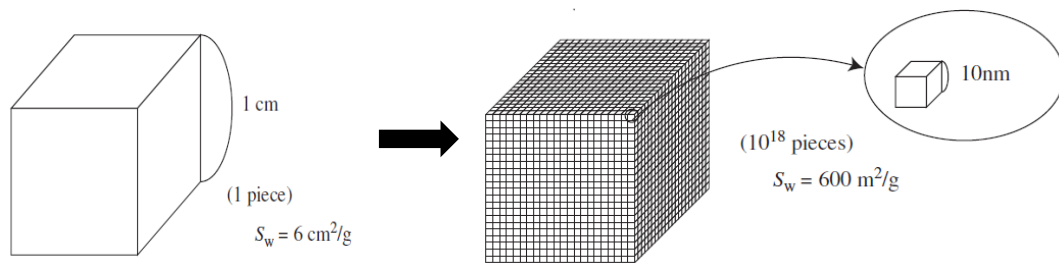
**Figure 1.7:** Change in free energy as a function of droplet size of dispersed medium of emulsions (Sharma and Shah, 1985)

## 1.6 Nanoparticles

Nanoparticles are ultrafine particles that have dimensions in the range of nano ( $10^{-9}$  m) scale. In general, particles in the size range of 1-100 nm are classified as nanoparticles.

These particles are characterized by huge surface area and highly activated particle surface. As shown in **Fig. 1.8**, when a cubic particle having dimension of 1 cm is fragmented into smaller cubes having length of 10 nm, the surface area increases a

million fold. Because of this extremely high surface area to volume ratio, these particles are capable of interacting at atomic or molecular level. As a result, their properties vary significantly from bulk material of the same particles. For example, gold is a stable substance as a bulk but shows unique catalytic characteristics as nanoparticles. It has been documented in literature that nanoparticles not only have different chemical properties but also exhibit unique mechanical, optical, thermal, electrical, magnetic and morphological properties (Yokoyama, 2008). Because of these unique characteristics, nanoparticles have found variety of applications in almost every industry.



**Figure 1.8:** Change in surface area with decreasing particle size (Yokoyama, 2008)

### 1.6.1 Nanotechnology in Oil and Gas Industry

Over the past two decades, several researchers have studied potential applications of nanoparticles across various disciplines of oil and gas industry such as exploration, logging, formation damage, enhanced oil recovery, smart fluids, ex-situ upgrading of oil shales/bitumen etc.

Singh and Bhat (2006) examined application of nano-robots for formation evaluation. They presented potential benefits of using nano-robots that can penetrate deeper into formation. The major advantages being accuracy and real time monitoring of formation

parameters. Berlin et al. (2011) demonstrated use of specially engineered hydrophobic nanoparticles in detecting subsurface hydrocarbon bearing rocks.

Nano-materials are also known to improve properties of drilling fluids. Amanullah et al. (2011) indicated that nanoparticles can improve rheological and filtration properties of fluids and encourage formation of thin and tight mud cake. Nanoparticles can also reduce swelling of clays by restricting water invasion into tiny pores of shales (Sensoy et al., 2009). According to Fakoya and Shah (2013), when silica nanoparticles are added to viscoelastic surfactant-based (VES) fluids, improvement in viscosity and fluid loss properties are observed, even at high temperatures.

Nanotechnology has also found application in minimizing formation damage. Nanoparticles have been employed to improve strength of proppant packing. Because of high surface activity and strong van der Waals force, nanoparticles can create a coating around proppants and restrict migration of fines (Huang et al., 2008). Crews and Huang (2008) discussed the use of nanoparticles with surfactant and brine containing internal breakers, to improve post fracturing cleanup. Maserati et al. (2010) reported use of nano-emulsions as spacers before cementing job, to effectively clean oil-based-mud from the casing or wellbore.

Nanoparticles have been of great interest for EOR applications because of their smaller than pore throat size. Nanoparticles can be transported deep into reservoir rocks with minimum retention at walls of pores (Rodriguez et al., 2009). According to Qui (2010), nanoparticles can also minimize absorption of surfactant on formation walls and improve

overall efficiency of chemical flooding operation. Zhang et al. (2009) examined the effect of silica nanoparticles on viscosity of emulsions through a series of experiments. They observed increment in emulsion viscosity which results in favorable mobility ratio and hence, better displacement efficiency. Studies have also shown that nanoparticles can improve stability of emulsions, foams, and immiscible polymer blends. (Singh and Ahmed, 2010; Fakoya and Shah, 2013).

### **1.7 Research Opportunities**

Heavy oil reservoirs generally yield low-energy and low-productivity wells because of high viscosity, low gas/oil ratio and presence of significant sulfur, asphaltenes and heavy metals. Huge untapped resources of heavy oil and technical challenges associated with producing it economically; indicate a need for extensive research and development activities.

Primary recovery using horizontal and multilateral wells is possible and economical. However, drive mechanism are still not fully understood. As a result, production forecast has often been poor. Moreover, very limited research has been conducted to improve efficiency of these non-thermal recovery techniques.

Waterflooding has largely been dismissed because of adverse mobility ratio. Considering potential future development in offshore heavy oil reservoirs, non-thermal recovery techniques such as water/chemical flooding may serve as the only viable option (Kovscek, 2005).

Thermal recovery techniques especially steam injection and SAGD have exhibited significant improvement in recovery. However, steam is considerably less viscous and denser than heavy oil. High cost associated with steam injection restricts its application to large heavy oil pools located in onshore, shallow, thick and permeable reservoirs. It is imperative to conduct research in the direction of improving efficiency of steam based methods so that favorable economics can be achieved. In-situ combustion has seen limited field application because of technical complexity in designing and controlling in-situ fire front. Unconventional thermal method such as electromagnetic/microwave heating demands more examination and improvement in efficiency before it can be applied commercially.

In summary, even though worldwide production of heavy oil has been increasing, it is just a small fraction of vast oil-in-place. This huge potential can only be realized through development of technologies that are cost effective, efficient, well-understood and have minimum impact on environment.

### **1.8 Scope of Research and Objectives**

The experimental work presented in this document, aimed at examining three different approaches to reduce heavy oil viscosity and improve recovery: (i) nanoparticles, (ii) solvent based emulsion, and (iii) solvent based emulsion containing nanoparticles. This study was conducted with two different heavy oil samples having viscosity of approximately 70,000 cP and 350,000 cP at room temperature. For all test fluids,

rheological measurements were performed at six different temperatures 80, 100, 120, 140, 160, and 180°F.

The objective of first set of experiments, was to investigate effects of nanoparticles on heavy oil viscosity. For this purpose, three different metal oxides - copper (II) oxide, iron (III) oxide and nickel (II) oxide were selected and their effect were examined at three different concentrations - 0.05, 0.1 and 0.5 wt% of oil. This study would improve understanding of nanoparticle interactions at low and high concentration and the resultant effect on rheology.

In second phase of this work, effects of a solvent based micro-emulsion on rheology of heavy oil was examined. Solvent-in-water emulsion (S/W) used in the experiments was prepared using xylene solvent, 2% NaCl brine and Triton™ X-100 (surfactant). Concentration of solvent and surfactant used was 1.8 wt% and 3.2 wt% respectively. This particular composition is known to produce stable micro-emulsion and ultra-low interfacial tension with oil (Qiu, 2010; Srinivasan, 2014). Prepared S/W emulsion was mixed with heavy oil in four different proportions (5, 10, 15 and 20 vol% of oil) and rheology of resultant emulsion was analyzed.

In third set of experiments, combined effect of nanoparticles and S/W emulsion were investigated. Amount of S/W emulsion used was 5 and 10 vol% of oil and nanoparticles concentration was kept constant at 0.002 wt% of oil.

The motivation behind the first experimental set was to examine the possibilities of applying nanoparticles in improving cold production of heavy oil. Understanding

rheological effect of S/W emulsion on heavy oil would provide better understanding of its potential application in chemical flooding. Motivation behind the third set of experiments was to investigate the potential effect of nanoparticles on performance of S/W emulsion and resultant heavy oil emulsion. The data generated would serve as a foundation for future core-flooding studies.

Very few researchers have conducted studies with similar objectives. Hascakir (2008) examined the effects of micro-sized iron particles on heavy oil samples having viscosity of 1132 and 2037 cP at room temperature. Shokrlu et al. (2014) presented the effects of nano and micro sized iron, iron oxide, copper oxide and nickel particles on heavy oil having viscosity of 8492 cP at room temperature. Srinivasan (2014) investigated the effects of copper oxide nanoparticles and S/W emulsion on heavy oil samples having viscosity of approximately 600 cP at room temperature.

This study is unprecedented in terms of viscosity of heavy oil samples investigated. The heavy oil samples used in the present work are 9 to 40 times more viscous than those used in any of the previous studies. Moreover, the idea of combining iron oxide and nickel oxide nanoparticles with S/W emulsion is also new.

## **1.9 Overview of Thesis**

This document is distributed into 8 chapters. Chapter 2 discusses typical rheological behavior of heavy oil. Additionally, unreliability associated with heavy oil viscosity measurement is also examined in detail. Chapter 3 provides theoretical overview of various mechanisms believed to be responsible for viscosity alteration by nanoparticles

in heavy oil. In chapter 4, rheological characteristics and phase behavior of solvent based emulsion are discussed. Moreover, potential benefits of S/W emulsion flooding have also been examined. In chapter 5, potential advantages of combining nanoparticles and solvent based emulsion have been analyzed. Chapter 6 contains information on equipment and materials used, and also summarizes experimental procedure. Experimental results are provided in chapter 7. Conclusions from this work and recommendations for future study are discussed in the final chapter 8. All viscosity data generated throughout this study has been incorporated in appendices.



## **2. Heavy Oil Viscosity**

Heavy oil is characterized by high viscosity values typically ranging from 100 cP to 10,000 cP at reservoir condition. Composition wise, heavy oil can be divided into a non-colloidal liquid, maltenes and asphaltenes. According to Larson (1999), heavy oil can also be characterized as a complex fluid comprising of a liquid phase and a structured phase - mainly asphaltenes.

### **2.1 Rheological Behavior**

Usually heavy oils exhibit Newtonian behavior. However, the presence of yield stress and shear thinning tendency is not uncommon. In a recent study, Dion (2011) presented that composition, deformation rate, and temperature are the three major parameters that determine rheological behavior of heavy oil.

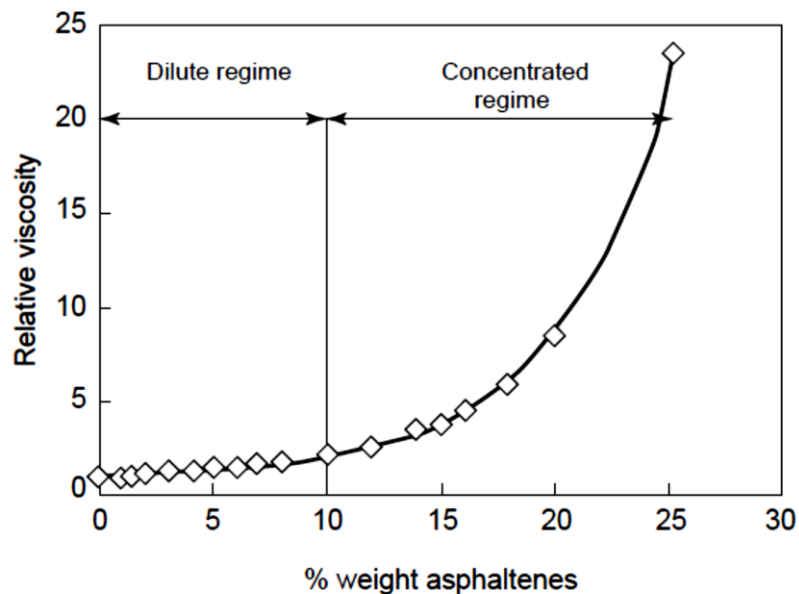
#### **2.1.1 Effect of Shear Rate**

When complex fluid such as heavy oil is subjected to deformation, microstructures developed by asphaltene content is altered. Usually, with increase in shear rate, these structures break down and it is reflected as reduction in apparent viscosity. Microstructure restructuring is not an instantaneous process and hence, heavy oil often exhibits time-dependent rheological behavior, i.e. thixotropy.

#### **2.1.2 Effect of Composition**

Many researchers have established a direct correlation between heavy oil viscosity and asphaltene concentration. Experimental work of Argillier et al. (2002) suggested

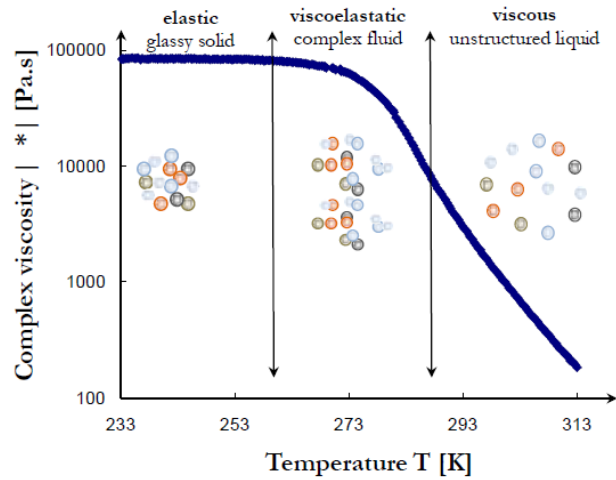
existence of a critical asphaltene concentration beyond which these particles aggregate/entangle and dramatically increase viscosity (see **Fig. 2.1**). Further investigation by Pierre et al. (2004) revealed that presence of resin content also affects resultant viscosity. It was observed that in dilute region (below critical asphaltene concentration), resins increase the viscosity of crude oil while at higher concentrations they minimize the effect of asphaltene and restrict viscosity increment. Asphaltene content of heavy oil samples used in the present study is approximately 22.5 wt% (Sezai, 2015).



**Figure 2.1:** Effect of asphaltene concentration on viscosity of xylene base fluid (Pierre et al., 2004)

### 2.1.3 Effect of Temperature

At very low temperature, heavy oil almost acts as an elastic solid and does not flow. The temperature below which this behavior occurs, is defined as glass transition temperature.



**Figure 2.2:** Effect of temperature on asphaltene structure in a typical heavy oil (Pierre et al., 2004)

At moderate temperatures, solid phase such as asphaltenes are segregated (see **Fig. 2.2**). This promotes shear thinning behavior and development of yield stress. Both of these properties diminish with increasing temperature.

At high temperature (typically higher than 150°F), asphaltene molecules start dissociating and this results in increase in Newtonian behavior. With increasing temperature Newtonian viscosity steadily decreases. At extremely high temperature (> 300°F), thermal cracking of heavier components lead to drastic reduction in viscosity.

## 2.2 Importance of Viscosity Data

Viscosity is an important parameter when it comes to predicting or evaluating fluid flow behavior. This term appears in the Darcy’s equation which governs fluid flow in porous medium. Among all parameters appearing in this equation, apart from reservoir thickness and pressure gradient, viscosity is the only parameter that is easily measurable. It is

routinely used as one of the criteria for selecting appropriate heavy oil extraction method. Additionally, viscosity data also serves as a useful tool for predicting production rates and hence economics of a recovery technique. This is particularly important for cold production techniques where natural drive and oil mobility are the dominant factors responsible for oil recovery. Importance of viscosity data is also manifested by the fact that almost all technical papers related to heavy oil production include discussion on viscosity.

### **2.3 Reliability of Viscosity Data**

Recent studies and field data have suggested that acquisition and use of viscosity data is often over-simplified. On several instances, accuracy of production forecasts based on oil viscosity measurements has been found to be poor (Miller et al., 2003). Yet, very few researchers (Miller et al., 1995, 2003 and Alkandari et al., 2012) have addressed issues of accuracy, reliability and repeatability associated with heavy oil viscosity measurement.

Heavy oil viscosity measurements often exhibit poor reproducibility. It has been found from the literature survey that values of 2 to 10% reproducibility have been observed for repeated runs with the same oil sample (Miller et al., 1995). Moreover, these values were obtained under controlled environment by labs specialized in heavy oil and bitumen analysis. Therefore, it is reasonable to assume that the reproducibility margin of more than 10% would not be unusual.

Poor reliability of heavy oil viscosity measurements can be attributed to various factors associated with sample acquisition, its storage and transportation, and viscosity measurement.

### **2.3.1 Sampling**

Acquiring a representative sample is the most critical aspect of heavy oil viscosity measurement. Unless a careful attention is paid to the method of sampling, viscosity measurements will often mislead than help.

There are various things that can go wrong during sampling process,

- Oil property can undergo notable alteration while transitioning from downhole pressure-temperature to surface condition.
- Properties of heavy oil are known to significantly vary not only with location in the reservoir but also with depth. Hence, place and time of sampling is also very important.
- Sampling from production stream is the cheapest and the most convenient option. However, such sample may contain water, sand or contamination from other drilling/completion/workover chemicals. Bailing is a relatively better method. However, it can be executed safely and continuously only on naturally flowing or non-thermal wells. Core sample is the best available method of sampling if minimum contamination from drilling fluid is ensured.
- Another way to minimize above problems is to acquire as many sample as economically and logistically possible and take average of the viscosity measurements.

### **2.3.2 Handling and Transportation**

Lack of vigilance and planning during storage and transfer can render carefully obtained samples useless. Unless the sample is stored in a pressure sealed and insulated container, property alteration is inevitable. With prolonged exposure to low temperature and pressure, sample loses lighter components and progressively becomes more viscous. Moreover, sample may get contaminated from unclean containers or leaks during transportation.

### **2.3.3 Sample Preparation**

Regardless of sampling method, heavy oil sample usually contains some amount of water and sand. Therefore, it becomes essential to remove these impurities before proceeding for viscosity measurement. Solvent extraction is the most commonly used method for this purpose. Unfortunately, it is usually impossible to remove added solvent without removing some of the lighter fractions of oil as well. Heavy oil viscosity is very sensitive to lighter components and loss of even 1% can result in significant increase in viscosity (Miller et al., 1995). Recently, high speed centrifuge methods have been developed as an alternate to solvent extraction method but they also provide limited removal of contaminants.

### **2.3.4 Viscosity Measurement**

Commercially, many type of viscometers are available that have different working principle. Each type of instrument has unique advantages and limitations, and are prone to different type of errors.

Viscometers based on rotating concentric cylinders can provide rheological behavior over wide range of shear rates. However, they require large sample volumes which makes it difficult to ensure homogeneous properties throughout the sample. High heat losses due to large fluid volume, coupled with viscous heating, lead to mediocre temperature control. This introduces additional errors since heavy oil viscosity is highly sensitive to temperature.

Cone-and-plate type viscometer require very small amount of samples, and temperature control is also relatively accurate. However, they are limited by very narrow range of shear rates. Therefore, to compare low and high shear rheological behavior of heavy oil, different cone-plate configurations need to be employed. This requires to prepare new sample for each test introducing additional error. Moreover, unlike concentric cylinder type, con-and-plate type viscometers are not recommended if solids are present in the fluid sample.

Capillary viscometers are also frequently used by researchers. Usually, fluid sample is placed inside a steel capillary apparatus. This apparatus can be accurately maintained at elevated temperature and pressure; providing more realistic viscosity data at downhole conditions. However, capillary viscometer is based on laminar flow condition and Newtonian fluid behavior. This limits measurement range of individual units.

#### **2.4 Ideal vs Practical Heavy Oil Viscosity**

As defined by Miller et al. (1995), an *ideal heavy oil viscosity* is obtained from uncontaminated sample preserved at or perfectly restored to reservoir conditions, and

using a perfect viscometer having no inherent limitations. While, a *practical heavy oil viscosity* is measured using a dead oil sample acquired and prepared in a cost effective manner and using an affordable apparatus.

In summary, it is almost impossible to measure ideal viscosity of heavy oil. Only thing a researcher can do is minimize errors in practical viscosity measurement by proper planning, employing recommended practices, and testing as many samples as economically and logistically possible.



### **3. Heavy Oil Viscosity Alteration by Nanoparticles**

Effect of nano-sized metal particles on heavy oil viscosity has been studied over the last three decades. However, most of the earlier research was focused on ex-situ upgrading of heavy oil and bitumen. Nano-sized metal particles were evaluated as catalysts to improve efficiency of thermal upgrading or cracking process.

Very limited work has been done to investigate the effects of nanoparticles in improving in-situ recovery of heavy oil. The first comprehensive experiments in this area were conducted by Clark et al. (1990). They examined use of nano-sized metal particles to improve physical properties of heavy oil and enhance production by steam stimulation. They investigated high temperature chemical reactions known as aquathermolysis and its effect on heavy oil viscosity. Over the period of past two decades, researchers (Fan et al., 2002, 2004; Li et al., 2007; Shokrlu et al.; 2010, 2011, 2014; Greff et al., 2011; Farooqui et al., 2015; Muraza et al., 2015) have advocated the use of nanoparticles in conjunction with steam injection to enhance heavy oil recovery.

All of the research work so far was focused on high temperature (>250-300°F) effects of nanoparticles. In high temperature scenarios, catalytic properties of nanoparticles and improved thermo-physical property of heavy oil, play dominant role in viscosity reduction.

Interestingly, few recent works have indicated that viscosity of heavy oil can be reduced even at room temperature by just adding nano/micro-sized metal particles (Hascakir et al., 2008, 2010; Shokrlu et al. 2014, and Srinivasan et al., 2014).

Hascakir et al. (2010) studied the effects of three types of micron-sized iron powders (Fe, Fe<sub>2</sub>O<sub>3</sub>, FeCl<sub>3</sub>) on two different samples of heavy oil. They observed that viscosity alteration not only depends on particle concentration but also on the type of particles and composition of oil. For example, addition of 0.5 wt% Fe<sub>2</sub>O<sub>3</sub> in Bati Raman crude (2037 cP at room temperature) yielded 37 % viscosity reduction. Interestingly, the same amount of nanoparticles had adverse effect on Camurlu oil (1132 cP at room temperature) and increased its viscosity by 15%.

Shokrlu et al. (2014) investigated the effects of copper, iron and nickel particles on a heavy oil sample, having viscosity of 8492 cP at room temperature. They examined nano as well as micron-sized particles. Their results indicated that viscosity alteration is a function of particle size, type, concentration and temperature. Surprisingly, as opposed to the results of Hascakir et al. (2010), they observed maximum viscosity reduction of just 10%. Srinivasan (2014) employed copper oxide nanoparticles and observed viscosity reduction of 20-30%.

These results indicate the presence of some type of physical and/or chemical reactions occurring between nanoparticles and heavy oil. Following section discusses such potential mechanisms.

### **3.1 Low Temperature Viscosity Alteration**

As discussed in previous section, nanoparticles have capability to alter viscosity of heavy oil even at low temperatures. Very limited work has been done to understand and substantiate the mechanisms responsible for it. It is believed that, at low temperatures, molecular level physical and chemical interactions, occurring between nanoparticles and heavy oil, play major role in viscosity alteration. Some of these processes result in viscosity reduction while the rest have negative impact.

#### **3.1.1 Decrease in Viscosity**

It is believed that at low concentration of nanoparticles, dominant physical and chemical reactions are the ones that act in favor of viscosity reduction. Ostwald ripening and exothermic chemical reactions are such processes.

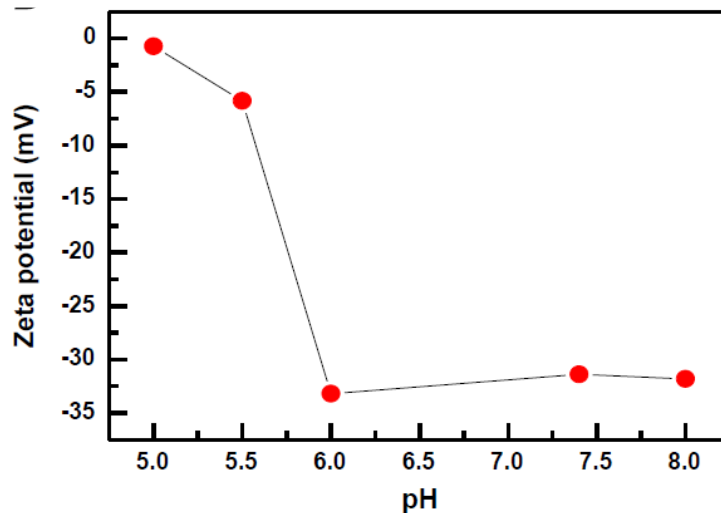
##### ***3.1.1.1 Ostwald Ripening Process***

It is a famous thermodynamically-driven process that describes evolution of inhomogeneity in liquid/solid solutions. In other words, smaller particles/crystals have tendency to coalesce and form increasingly larger structures. This spontaneous process is based on the fact that atoms or molecules lying at surface of a crystal or particle are less stable than the ones located at interior of the structure. Smaller particles have larger surface area and exhibit less stability. Hence, to attain energy stability, these smaller particles display tendency to amalgamate (Karpinski et al., 2002).

It is a well-known fact that asphaltene molecules are responsible for high viscosity in heavy oil. These are complex structures and usually remain positively charged in presence

of external field. When nanoparticles are introduced into oil sample, they encourage electrical attraction with asphaltene molecules. This effect can be scientifically proven by assessing zeta potential of nanoparticles. Zeta potential is a measure of electrostatic forces (attractive or repulsive) between particles and is frequently employed to define stability of colloidal dispersions.

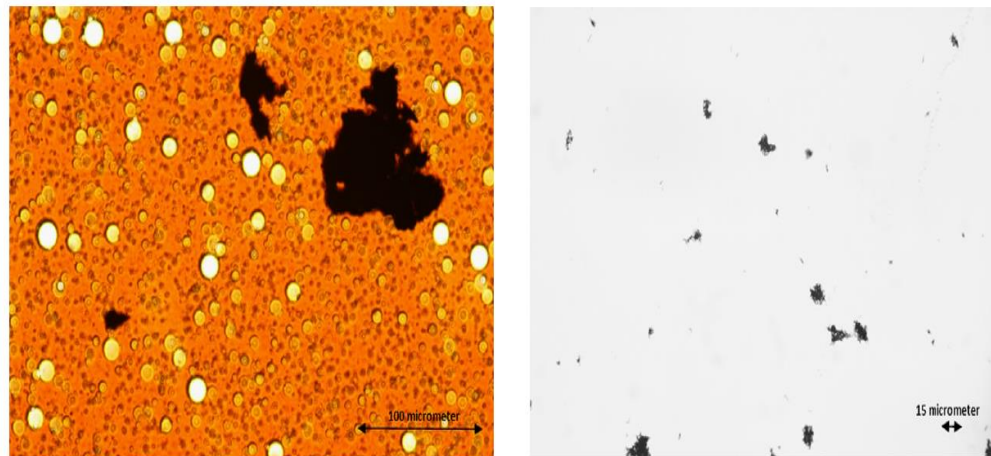
For example, zeta potential analysis shows that copper particles are negatively charged ( $z=-77$  mV at  $\text{pH}=7$ ) and hence, create strong electrical field that attracts asphaltene molecules to their surface. Agglomeration of these structures make bulk oil less viscous (Shokrlu et al., 2014). Similarly, nickel oxide (NiO) also has characteristic negative zeta potential and exhibits the same behavior as copper oxide. **Figure 3.1** displays variation of zeta potential of NiO as a function of pH.



**Figure 3.1:** Zeta potential of NiO nanoparticles as a function of pH (El-Kemary et al., 2013)

Interestingly, iron (III) oxide has zeta potential of +20 mV at pH=7 (Shokrlu et al., 2014). This suggests that the iron particles may actually disperse asphaltenes. This might, in fact, lead to increase in viscosity of heavy oil. This indicates that some other dominant mechanism is responsible for viscosity reduction observed with iron particles. This process is discussed in the next section.

Shokrlu et al. (2014) conducted a study to verify the theory of asphaltene aggregation in the presence of nanoparticles. They studied two different samples under microscope. The first sample contained heavy oil and nickel nanoparticles while the other sample was dispersion of nickel particles in water.



**Figure 3.2:** Microscopic image of nickel nanoparticles dispersed in (a) heavy oil, and (b) water (Shokrlu et al., 2014)

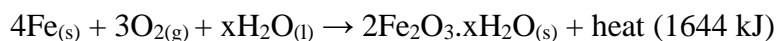
A big cluster of particles can be easily visualized in **Fig. 3.2a**. This cluster is believed to be consisting of nickel particles surrounded by asphaltene aggregates. The microscopic image of nickel particle dispersed in water (**Fig. 3.2b**), shows clusters having average

size of the order of 15 micrometer which is significantly smaller than the clusters observed in the first sample. This confirms the aggregation of asphaltene molecules in presence of nickel nanoparticles.

### ***3.1.1.2 Exothermic Chemical Reactions***

Chemical reactions occurring between nanoparticles and heavy oil at low temperatures have not yet been studied extensively. Hascakir et al. (2008) proposed that the viscosity reduction mechanism observed in case of iron particles, can be explained by a variety of exothermic reactions. These reactions do not occur in bulk and hence do not cause a notable change in temperature of fluid. However, this localized heat generation is capable of weakening chemical bonds. As a result, external energy required to break down heavier components into lighter fractions reduces. This leads to additional viscosity reduction for the same increment in temperature.

Iron may chemically react with some compounds of heavy oil. One such reaction is rusting of iron as shown below



This is a slow process but in presence of saline water, acid compounds or some kind of oxidants, this reaction may speed up. One such compound is carboxylic acid which is known to accelerate rusting (Shokrlu et al., 2014). Additionally, high surface area of nanoparticles also contribute towards increasing rate of reaction.

Besides rusting, formation of iron sulfide (FeS) is also an exothermic process. Heavy oil is known to contain impurities of S, N and O and hence formation of FeS is not impossible. As far as iron (III) oxide particles are concerned, they may lead to formation of magnetite (Fe<sub>3</sub>O<sub>4</sub>), which is also an exothermic process. Heavy oil consists of very complex compounds. Therefore it is reasonable to assume existence of some unknown chemical reactions which may be responsible for viscosity alteration. Further study at a molecular level is necessary to understand and validate these processes.

### **3.1.2 Increase in Viscosity**

As concentration of nanoparticles is increased, processes responsible for viscosity increment become more dominant. Similar to viscosity reduction mechanisms, viscosity increment can also be scientifically explained from physical and chemical point of view.

#### ***3.1.2.1 Nano-Suspensions***

Nano-suspension is a two phase system consisting of a carrier fluid (liquid or gas) and suspension of solid nanoparticles. Rudyak (2013) presented an extensive review work on viscosity of nano-suspensions.

Assuming no inter-molecular interactions, Einstein's correlation proposes that the effective viscosity of suspension increases linearly with increasing solid volume fraction and is always greater than the viscosity of carrier fluid. Mathematically, this correlation is provided as,

$$\eta = \eta_0 [1 + 2.5 \phi]$$

where,  $\eta$  is viscosity of suspension,  $\eta_0$  is viscosity of carrier fluid and  $\phi$  is volume fraction of dispersed particles.

Einstein's equation is not accurate for low solid concentration. Over the years, researchers like Batchelor, Krieger and Dougherty improved the correlation by incorporating the effects of hydrodynamic interactions among particles, packing density, and Brownian motion. All these equations were still inadequate to predict viscosity of nano-suspensions (Fakoya and Shah, 2016).

Recently, some researchers presented correlations to predict viscosity of water based nano- fluids containing CuO and Fe<sub>2</sub>O<sub>3</sub> particles (Rudyak, 2013),

$$\text{For CuO nanoparticles: } \eta = \eta_0 [1.475 - 0.319 \phi + 0.051 \phi^2 + 0.009 \phi^3]$$

$$\text{For Fe}_2\text{O}_3 \text{ nanoparticles: } \eta = \eta_0 [1 + 18.64 \phi + 248.3 \phi^2]$$

These are not universal correlations. Moreover, they also fail to provide accurate predictions for fluid systems other than what they are based on.

At high concentrations, nanoparticles added to heavy oil, may aggregate and behave as Nano-suspension. However, all of the discussed correlations were developed with underlying assumption of physico-chemical inertness. Therefore, they should not be employed to predict the resultant viscosity of heavy oil. Besides, viscosity of heavy oil nano-suspension would not only depend on particle concentration but also on particle size, metal type, degree of aggregation, size of clustered particles, presence of asphaltene molecules etc.

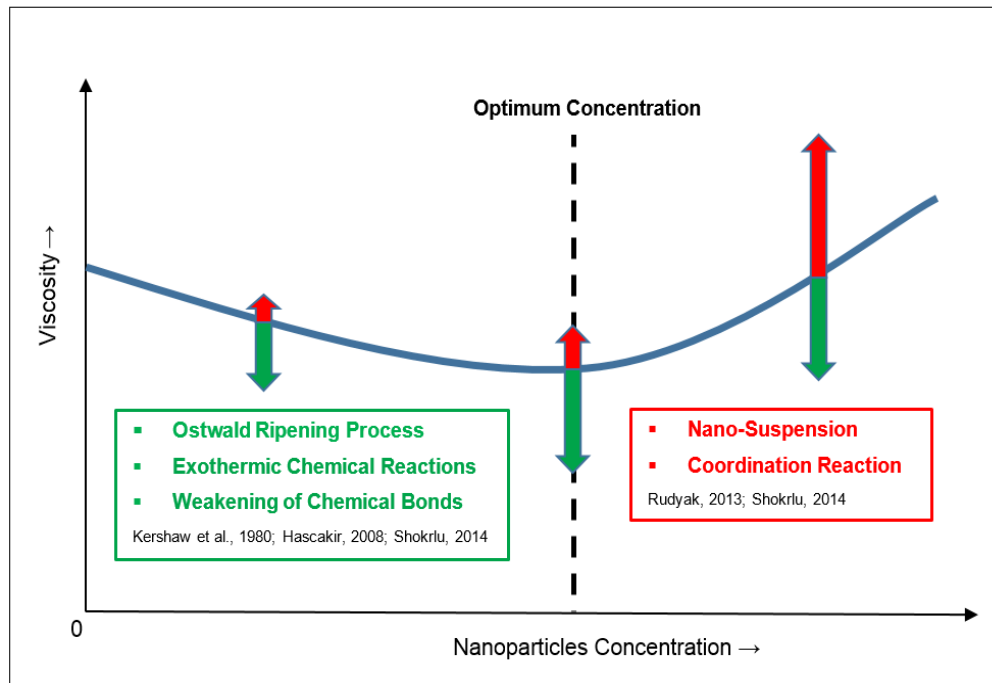


Nonetheless, it is reasonable to assume that at high concentration, aggregation of nanoparticles may become dominant over inter-molecular interactions and results in increased viscosity of heavy oil.

### 3.1.2.2 Coordination Reactions

At high concentrations of transition metal nanoparticles, they may form coordination complexes with asphaltene molecules. This results in even more complex structures within oil and increases viscosity (Shokrlu et al., 2014). Rate of this reaction is not only a function of particle concentration but also increases with increase in temperature.

The low temperature viscosity alteration caused by nanoparticles is summarized in **Fig. 3.3** below.



**Figure 3.3:** Low temperature viscosity alteration by nanoparticles (Not to scale)

## **3.2 High Temperature Viscosity Alteration**

At temperatures greater than 300°F, catalytic properties of nano-sized metal particles become dominant factor in viscosity reduction of heavy oil. Most of the physico-chemical reaction taking place at high temperature tends to reduce viscosity. The only exception is coordination reaction by metal particles which leads to the formation of complex coordinate compounds of asphaltene. However, this process is usually suppressed by more prominent aquathermolysis. Exothermic chemical processes discussed in **section 3.1.1.2** also exist at high temperature and in fact, exhibit higher reaction rate. However, similar to the coordination reaction, their effect is negligible in comparison to thermal cracking and aquathermolysis.

### **3.2.1 Aquathermolysis**

Aquathermolysis is a term used to represent various reactions occurring among steam, sand, and oil components at very high temperatures. Clark et al. (1990) were the first researchers to examine application of nanoparticles as catalysts for aquathermolysis process during steam stimulation. They not only observed improvement in viscosity reduction but also observed improvement in physical properties of produced oil.

The major components that impart high viscosity to heavy oil are asphaltenes, resins and associated derivatives. The main viscosity reduction mechanism provided by aquathermolysis is decomposition of these species. Clark and Hyne (1984) stated that hydrolysis of C-S bonds is the essential step of aquathermolysis and is achieved by

transfer of hydrogen from steam (water) to oil via water gas shift reactions (WGSR). An example reaction is as follows,



It can be observed that water is an essential part of aquathermolysis reactions as it serves as hydrogen donor. Some of the gases produced can also further lower viscosity.

Even without nanoparticles these reactions can occur. However, an important challenge associated with above reactions is viscosity reversal with time. Hydrolysis process produces some additional radical species of S, N and O. These compounds can initiate polymerization reactions and reproduce giant molecules of high viscosity (Muraza et al., 2015). This problem becomes more severe for extra-heavy oil. It has been observed that the addition of nanoparticles can provide non-reversible mechanisms for catalyzing hydrodeoxygenation, hydrodesulfurization and hydrodenitrogenation by cleavage and removal of O, S and N derivatives (Muraza et al., 2015).

Moreover, Shokrlu et al. (2014) indicated that nanoparticles can also improve efficiency of aquathermolysis and provide more conversion of asphaltenes and resins into saturates and aromatics.

### **3.2.2 Improved Thermal Conductivity**

Low heat conductivity of heavy oil is a major restriction in achieving higher efficiency with thermal recovery methods. Enhancement of thermal conductivity and diffusivity of carrier fluid using nano metal particles have been examined for several years. The

Hamilton-Crosser correlation is a classical model used to calculate effective thermal conductivity of nano-fluids as a function of volume fraction of nanoparticles (Shokrlu et al., 2014),

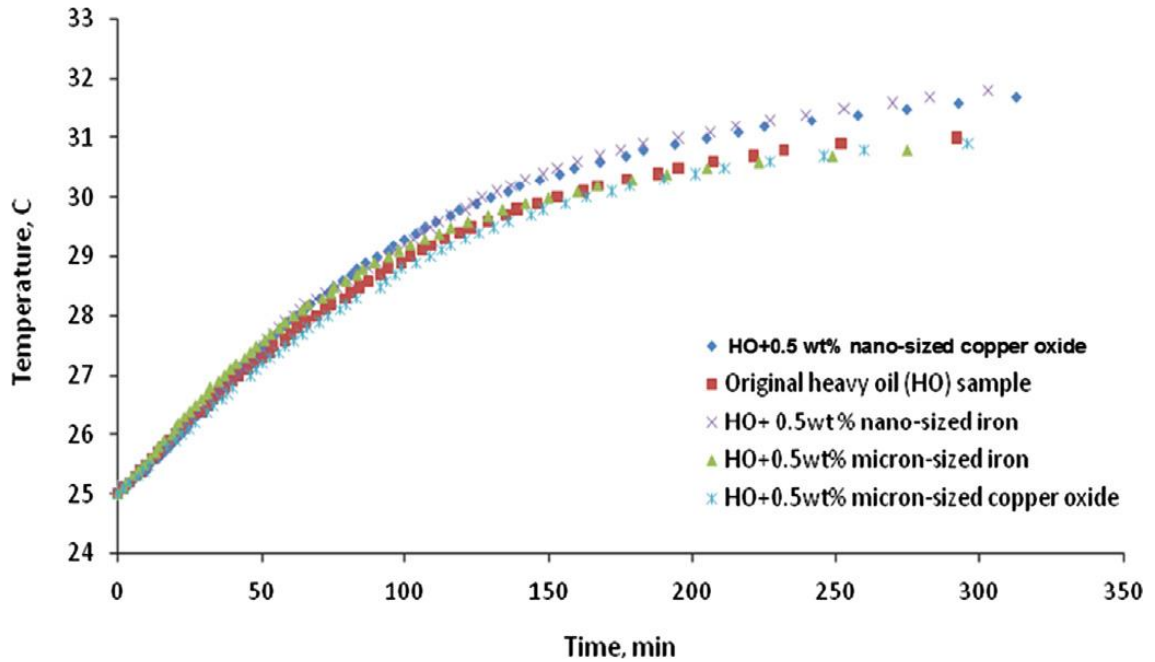
$$\frac{k_{\text{eff}}}{k_f} = \frac{k_p + (s - 1)k_f - (s - 1)\alpha(k_f - k_p)}{k_p + (s - 1)k_f + \alpha(k_f - k_p)}$$

where  $k_p$  and  $k_f$  are thermal conductivity of nanoparticles and carrier fluid respectively.  $\alpha$  is volume fraction of particles and  $n$  is empirical shape factor and is a function of particle sphericity ( $\Psi$ ),

$$s = \frac{3}{\Psi}$$

Shokrlu et al. (2014) performed heat transfer experiments with nano- and micron-sized copper and iron particles. They observed enhancement in thermal conductivity by addition of nanoparticles. For example, time required to heat heavy oil sample from 25°C to 31°C was decreased by 80 min as shown in **Fig. 3.4**. Interestingly, no noticeable improvement in thermal conductivity was observed with micro particles.

Improvement in heat transfer does not directly affect viscosity reduction. However, it indirectly improves heat distribution within the oil. In case of steam stimulation, this can significantly reduce soaking period and hence not only improve economics but also enhance ultimate oil recovery.



**Figure 3.4:** Effect of nano- and micron-sized metal particles on heat transfer rates (Shokrlu et al., 2014)

### 3.3 Optimum Concentration of Nanoparticles

Various mechanisms responsible for viscosity alteration by nanoparticles point toward existence of an optimum concentration at which maximum viscosity reduction is achieved. This optimum concentration depends on various factors such as type of metal, size of particles, composition of oil and temperature.

#### 3.3.1 Effect of Temperature

At low temperatures viscosity alteration by nanoparticles is very sensitive to concentration. As nanoparticles concentration increases, viscosity alteration shifts from reduction (positive) to increment (negative). With increase in nanoparticle concentration, the effects of Ostwald ripening and exothermic chemical reactions become prominent.

However, after a certain point, particles start aggregating and fluid starts behaving as nano-suspension. Additionally, they may form coordination complex with asphaltenes resulting in viscosity increment.

However, at high temperatures, physico-chemical reactions such as aquathermolysis and thermal upgrading dominate over adverse processes, even at high concentrations. This indicates diminishing effect of nanoparticle concentration and increasing sensitivity to temperature. Thus, it can be reasonably stated that with an increase in temperature, the optimum point shifts from lower side to upper concentration side.

### **3.3.2 Effect of Metal Type and Particle Size**

Each metal has its unique properties and react differently with compounds present in oil. For copper and nickel nanoparticles, Ostwald ripening is the dominant mechanism for viscosity reduction while iron particles reduce viscosity through exothermic chemical reactions. This difference clearly suggests that the optimum concentration would be different for each type of particle.

Nano particles have considerably larger surface area than micro-sized particles. Hence at lower concentration, nanoparticles provide notable results. (Shokrlu et al., 2014). However, at higher concentrations, nanoparticles lead to faster aggregation than micron size particles due to collision by Brownian motion. This reduces the advantage of smaller size and hence both size of particles exhibit similar effects.

### **3.3.3 Effect of Oil Composition**

Oil composition also has an impact on optimum concentration point. C-S bond present in asphaltene molecule requires the lowest amount of energy to break. The second in line is carboxylic acid derivatives which have considerably higher dissociation energy. Therefore, heavy oil containing high sulfur content is prone to more viscosity reduction. This reasoning can also be verified from literature. Heavy oil used by Shokrlu et al. (2014) had sulfur content of 0.4% and they observed viscosity reduction of just 10%. On the other hand, heavy oil sample used by Hascakir et al. (2008) had sulfur content of about 4% and it exhibited viscosity reduction as high as 88%.

### **3.4 Field Application**

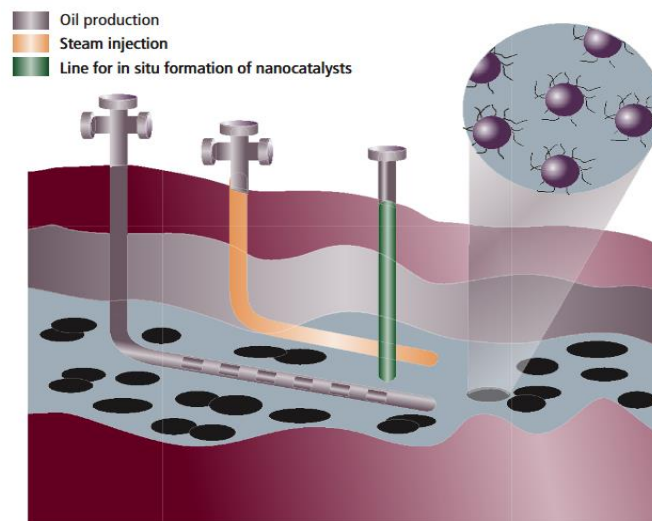
All the discussion so far, advocates efficacy of nano-sized metal particles on reducing heavy oil viscosity. However, applying this knowledge to field is another challenge. Only a couple of researchers have conducted coreflooding studies to explore the possibility of introducing nanoparticles into a reservoir via waterflooding.

Shokrlu et al. conducted experiments in 2011 to study injectivity and transportation of nano- and micron-sized particles. As a substitute for core, they used different size glass beads saturated with heavy oil. They used xanthan gum polymer to stabilize suspension of particles in water. It was observed that the injectivity of nanoparticles was considerably higher than micron size particles. Micro particles had tendency to interact with porous media and got retained at the wall, resulting in shorter penetration.

Greff et al. (2011) studied catalytic effect of nickel nanoparticles under electromagnetic heating. They employed artificial sand packs generated by glass beads and saturated them with heavy oil and catalysts. They observed approximately 57% improvement in ultimate recovery. Nanoparticles also increased efficiency of heating by reducing power requirement and providing faster heat distribution.

Farooqui et al. (2015) studied effects of introducing nano nickel particles at later stages of cyclic steam stimulation. After 5 cycles of steam stimulation, they flooded sand pack with 1 wt% nickel nano particles suspended in water and stabilized by 0.03% xanthan and 0.1% surfactant. They observed additional 10-11% recovery of oil.

**Figure 3.5** provides schematic of a conceptual method of introducing nanoparticles directly into steam being injected. (Nassar et al., 2011)



**Figure 3.5:** Illustration of in-situ injection of nanoparticle to improve heavy oil recovery (Nassar et al., 2011)



## 4. Characteristics of Solvent Based Emulsion

Solvent based emulsion combines benefits of waterflooding, miscible flooding and surfactant flooding. The major mechanisms that make it attractive are: (i) reduction of heavy oil viscosity by solvent dilution, (ii) mobility control, and (iii) in-situ emulsification.

Solvent-in-water emulsion is nothing but an oil-in-water emulsion. It consists of a solvent such as xylene, naphtha, kerosene or light crude oil dispersed in water or brine phase using a surfactant. The idea of using emulsified solvent has been in discussion for few decades now. However, until recently, no systematic study has been conducted to evaluate its field applicability (Sarma et al., 1998).

The idea of using O/W emulsion as a displacing fluid to minimize effect of viscous fingering prominent in waterflooding, was first proposed in 1965 by Binder et al. Later, Van der Knaap et al. (1970) proposed a unique application of solvent. They recommended to achieve water breakthrough as fast as possible. Then, flooding of solvent or a less stable solvent-in-water emulsion can be initiated which would overlies water due to less density and help attain better sweep efficiency. However, very high water cut and difficulty in maintaining sufficient pressure gradient between injection and production wells rendered this method unattractive (Sarma et al., 1998).

McAuliffe (1973) studied mobility control provided by S/W emulsion. He proposed to generate macro-emulsion with droplets diameter larger than pore throats. As a result,

emulsion droplets would block the more permeable path and allow fluid to travel through less permeable zone, providing better sweep efficiency.

Bousaid (1978) suggested to increase the surfactant concentration as emulsion is being flooded into reservoir. This would maintain integrity of emulsion and avoid dilution from subsequent water.

Sarma et al. (1998) conducted comprehensive experiments to determine various variables affecting efficiency of S/W flooding. They investigated effects of solvent volume fraction, surfactant concentration, and flow velocity.

Recently, Qiu (2010) performed a comprehensive phase behavior study of a solvent-in-water emulsion system. He proposed that the use of S/W micro-emulsion provides least interfacial tension with heavy oil and hence more potential recovery.

#### **4.1 Benefits of S/W Emulsion**

There are three main processes involved in emulsified solvent flooding: (i) mobility control, (ii) viscosity reduction, and (iii) in-situ emulsification.

##### **4.1.1 Mobility Control**

A typical solvent-in-water emulsion has water or brine as a continuous phase. Therefore, it does not have viscosity as comparable to that of in-situ heavy oil. However, it would still provide better mobility control than waterflooding. Besides, nanoparticles or polymers can greatly enhance viscosity of S/W emulsion resulting in more favorable

mobility control (Qiu, 2010). Additionally, plugging of more permeable path by emulsion droplets may also improve sweep efficiency (McAuliffe 1973).

The degree of mobility control provided by an emulsion depends on several parameters such as type of emulsion, viscosity of continuous phase, amount of dispersed phase, droplet size etc. Additionally, wettability of porous medium also determines propagation of flood front.

#### **4.1.2 Viscosity Reduction**

Pure miscible solvent injection has been known to greatly reduce oil viscosity but use of pure solvent is very cost intensive. Emulsified solvent flooding does not contain highly concentrated solvent but it is present nonetheless. Injected solvent would dissolve heavier compounds of oil and help in viscosity reduction (Qiu, 2010).

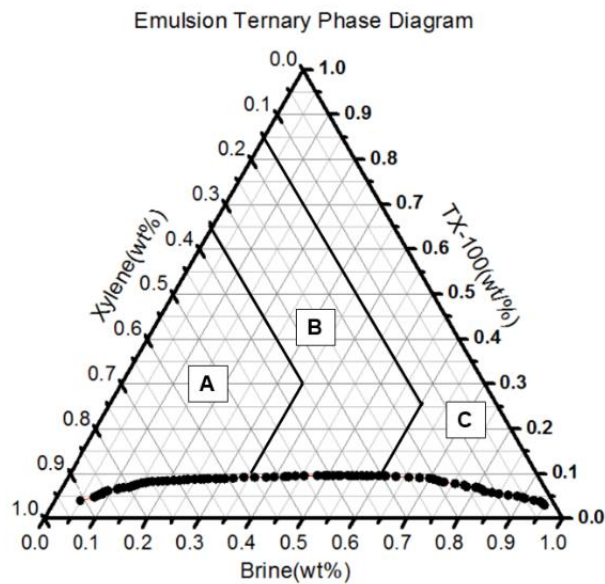
#### **4.1.3 In-Situ Emulsification**

Solvent-in-water emulsion is a tri-component system comprising of solvent, surfactant and water or brine. Injected surfactant with the help of solvent can lower interfacial tension between oil and water phase; hence promoting in-situ emulsification (Bryan et al., 2007; Zhang et al., 2009). A recent study conducted by Qiu (2010) demonstrated that a S/W micro-emulsion system provided ultra-low interfacial tension of 0.08 mN/m with West Sak heavy oil from Alaska.

## 4.2 Phase Behavior of a S/W Emulsion System

It is important to understand the phase behavior of emulsified solvent in order to determine an optimum concentration of solvent, surfactant and water phase which can yield the lowest interfacial tension with oil.

A solvent based emulsion is typically a tri-component system. It is not practical to check all possible combination of these three components for interfacial tension. One way to approach this problem is to determine critical emulsion compositions which separates macro and micro emulsions. As discussed in **Section 1.5**, micro-emulsions are always desirable over macro-emulsion due to higher stability and lower interfacial tension.



**Figure 4.1:** Isothermal ternary diagram for xylene-in-2% NaCl brine emulsion system (Qiu, 2010)

Qiu (2010) examined phase behavior of a solvent based emulsion system consisting of xylene (solvent), Triton X-100 (surfactant) and 2% NaCl brine (continuous phase). He prepared a ternary phase diagram after conducting several emulsion benchmark tests (see **Fig. 4.1**).

The data points in the diagram represent critical composition line that separates macro- and micro-emulsion. The region above this line represents compositions that produce micro-emulsion while the region lying below the line corresponds to macro-emulsions. This critical line is a strong function of surfactant used. Interestingly, for this system, the line does not exceed 10 wt% of surfactant.

### **4.3 Rheology of S/W Emulsion**

Rheology of S/W emulsion is an important parameter that should be carefully examined to understand injectivity, mobility control, and resultant viscosity of heavy oil emulsion. Solvent based micro-emulsion system described by Qiu (2010) was characterized by three different rheological behavior which depended on composition (see **Fig. 4.1**).

*Zone A:* As shown in **Fig. 4.1**, this zone is dominated by xylene (solvent). Emulsions having composition in this zone displayed weak shear thinning behavior and had relatively less viscosity than samples from the other two zones.

*Zone B:* Samples having composition in this range displayed formation of gel. They exhibited moderate shear thinning behavior with higher apparent viscosities than zone A and C.

*Zone C*: Emulsion samples from this zone exhibited higher shear thinning behavior than the other two zones.

#### **4.4 Optimum Composition of S/W Emulsion**

For solvent based emulsion flooding to be economically viable, it is extremely important to optimize concentration of solvent and surfactant. Qiu (2010) performed extensive study of interfacial tension of various emulsion compositions with a north Alaskan crude. Based on the results, he determined the optimum composition of S/W emulsion to be 95 wt% brine, 1.8 wt% solvent and 3.2 wt% surfactant (see **Table 4.1** below). This composition was employed in preparing the S/W emulsion used in the present study.

**Table 4.1:** Interfacial tension of an Alaskan crude oil with brine, air and optimized micro-emulsion (Qiu, 2010)

	<b>2 % NaCl brine</b>	<b>Air</b>	<b>S/W micro-emulsion</b>
<b>West Sak Crude</b>	28.9 mN/m	27.5 mN/m	0.08 mN/m

## **5. Properties of Solvent Based Emulsion Containing Nanoparticles**

In recent years, nanoparticles stabilized emulsions have attracted a lot of attention from researchers. Use of nanoparticles can improve performance of chemical flooding operations up to various extent (Zhang et al., 2010).

Nano-particle dispersed in a carrier fluid, also known as nanofluids, can provide four major benefits: (i) increase in viscosity of carrier fluid, resulting in more favorable mobility ratio (Qui, 2010; Tarek, 2015), (ii) decrease in interfacial/surface tension (wasan et al., 2010; Zhang et al., 2009, Srinivasan, 2014), (iii) high emulsion stability (Zhang et al., 2009, 2010), and (iv) deeper penetration into formation because of small size.

Zhang et al. (2009, 2010) examined various properties of an emulsion stabilized by silica nanoparticles. They studied phase behavior, rheology and droplet size of various emulsions for several months and found notable increase in emulsion stability due to nanoparticles. They determined that stability is also a function of concentration and wettability preference of nanoparticles.

Qiu (2010) investigated effect of copper oxide nanoparticles on xylene-in-brine micro-emulsion. Addition of nanoparticles improved viscosity of emulsion and also reduced its interfacial tension with heavy oil. Crews and Gomaa (2012) employed nanoparticles with a surfactant based fluid and successfully achieved performance similar to cross-linked polymer gel.

Ogolo et al. (2012) conducted various EOR experiments with aluminum, silica, nickel and iron oxide nanoparticles dispersed in water and diesel based carrier fluids. They noted up to 30% increase in oil recovery because of nanoparticles.

Alomair (2014) prepared different nanofluids consisting of silicon oxide, aluminum oxide, nickel oxide and titanium oxide dispersed in brine. They performed core flooding studies and observed reduction in interfacial tension between heavy oil and nanofluids and also achieved viscosity reduction of up to 25% by emulsification.

Pei et al. (2015) examined phase behavior and rheology of emulsions containing various nanoparticles. They not only observed improvement in emulsion stability but also noticed marked increase in emulsion viscosity. Their study also indicated additional oil recovery up to 20-30% because of nanoparticles.

In a recent study, Tarek (2015) conducted core flood experiments with mixture of nanofluids containing aluminum oxide, silicon oxide, and iron oxide. He observed improved performance in comparison to single nanofluid flooding.

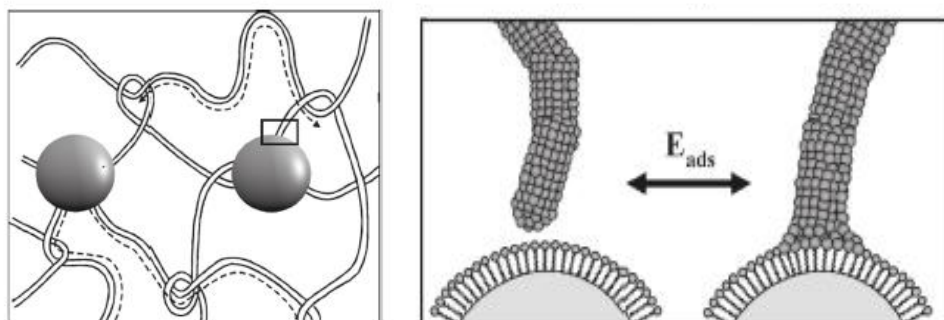
## **5.1 Rheological Behavior**

As discussed in **Section 3.1.2.1**, when nanoparticles are added to a carrier fluid, they tend to increase its viscosity by a factor determined by its concentration. In presence of surfactant based fluid, nanoparticles can interact with micellar structures and can significantly affect its rheology (Crews and Gomaa, 2012).



In 2010, Helgeson et al. presented a systematic study of structural, rheological, and thermodynamic properties of mixtures of wormlike micelles and nanoparticles. They observed notable increase in viscoelastic property of the fluid. They hypothesized two different mechanisms at work: (i) entanglement of micelles, and (ii) generation of micelle-particle junctions.

As shown in **Fig. 5.1**, nanoparticles can join two micelles, resulting in a longer micellar structure. This increment in length will further increase entanglement within these microstructures leading to improved visco-elasticity of fluid. Additionally, if particles generate three or more junctions then, a network of micelles is created which would be similar to a network of polymer chains observed in cross-linked gel.

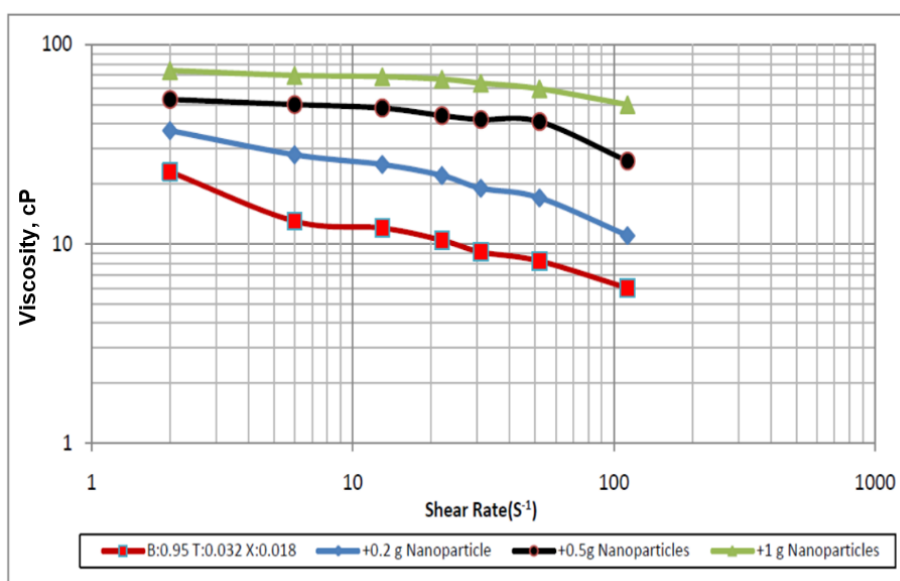


**Figure 5.1:** Double network structure formation in presence of nanoparticles by entanglement of micelles (Helgeson et al., 2010)

Generation of these ‘double network’ structures depends not only on surface chemistry of nanoparticles but also on particle and micelle concentration. At lower concentration, a mild increase in viscosity is expected which can be attributed to lengthening of micelles. At entanglement concentration and beyond, addition of nanoparticles can create visco-elasticity even in a Newtonian base fluid (Helgeson et al., 2010). At very high

concentration, surfactant solution may run out of micelles and further addition of nanoparticles may result in breaking of long micellar chains and hence reduction in viscosity.

Qiu (2010) had investigated effect of copper oxide nanoparticles on rheology of xylene-in-water emulsion. As shown in **Fig. 5.2**, increment in viscosity was observed upon addition of nanoparticles.

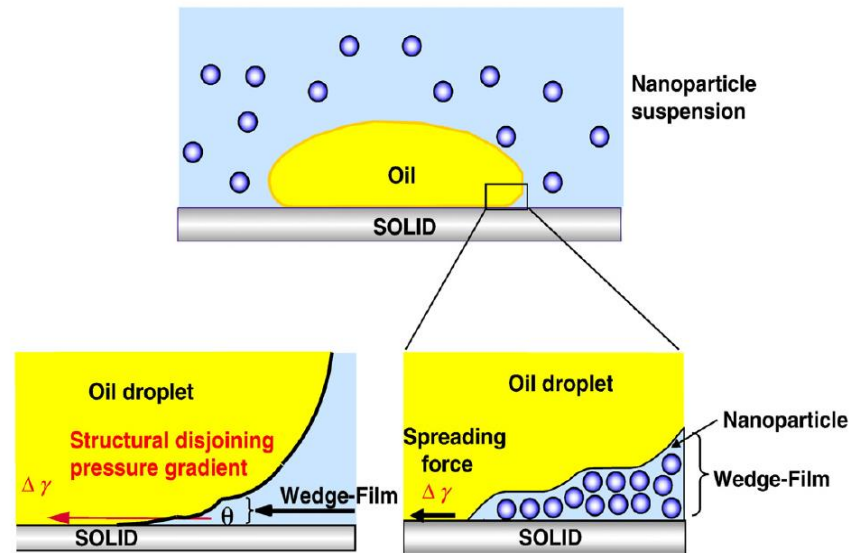


**Figure 5.2:** Effect of copper oxide nanoparticles on viscosity of xylene-in-brine micro emulsion (Qiu, 2010)

## 5.2 Interfacial Tension Alteration

Mechanism by which nanoparticles can reduce interfacial/surface tension, was first examined by Wasan et al. (2010). They found that when an aqueous phase containing nanoparticles is injected into a porous medium, particles form a wedge like structure and try to force themselves between discontinuous phase (oil) and formation wall (see **Fig.**

5.3). The pressure exerted by particles in this confined region is termed as ‘disjoining pressure’ (Wasan et al., 2010; McElfresh et al., 2012).



**Figure 5.3:** Spreading of nanofluids on solids surface through ‘disjoining pressure’ (Wasan et al., 2010)

Brownian motion and electrostatic forces between particles are considered to be responsible for this pressure. A single particle is not capable of exerting sufficient pressure. However, as particle concentration increases, disjoining pressure also increases. Because of smaller size and high surface area, nanoparticles exhibit significant surface forces resulting in relatively high disjoining pressure.

Disjoining pressure directly affects a fluid’s ability to spread on solid surfaces (McElfresh et al., 2012). Interfacial forces between surface, oil and aqueous phase are not similar. This imbalance of forces along with the disjoining pressure allow nanoparticles to spread along the surface and form a monolayer. As shown in **Fig. 5.3**, nanoparticles then self-

assemble and widen the wedge; resulting in increased disjoining pressure. This helps in reducing surface tension and improves efficiency of surfactant micelles to remove oil.

### **5.3 Emulsion Stability**

Nanoparticles are known to improve stability of emulsions. The stability improvement can be explained by the way particles interact at oil-water interface. Surfactant adsorbs and desorbs easily at the interface while particles require relatively high energy for attachment. However, once attached, they are virtually irreversibly adsorbed (Zhang et al., 2009).

Additionally, it has also been observed that nanoparticles can form a compact layer at droplet interface. Nanoparticles have freedom to move laterally or perpendicularly at the interface. Therefore, they align themselves in such a manner that interface between particles is not only flat but also satisfies contact angle condition. The contact angle is determined by wettability preference of particles. Formation of this type of structured layer around emulsion droplets improve stability of emulsion (Zhang et al., 2009).

Stability of emulsion depends on various factors such as nanoparticles surface chemistry, their concentration, electrostatic repulsion, van der Waals attraction etc. For example, Pei et al. (2015) observed that with increasing nanoparticles concentration, droplet size of resultant emulsion decrease, resulting in improved stability.

## **6. Experimental Setup and Methodology**

Experimental work presented in this document is entirely based on rheological measurements of three different type of test fluids: (i) heavy oil containing nanoparticles, (ii) heavy oil emulsion prepared by adding xylene-in-brine emulsion, and (iii) heavy oil nano-emulsion containing both nanoparticles and xylene-in-brine emulsion. Two different heavy oil samples, henceforth referred to as ‘Sample A’ and ‘Sample B’, were used to prepare these test fluids.

This chapter is divided into six sections. Equipment and materials used are described in the first two sections. Third section discusses procedure for preparing test fluids. Various steps undertaken to improve reliability and repeatability of viscosity measurement have been discussed in sections four and five. The last section contains information on rheological models used to characterize the test fluids.

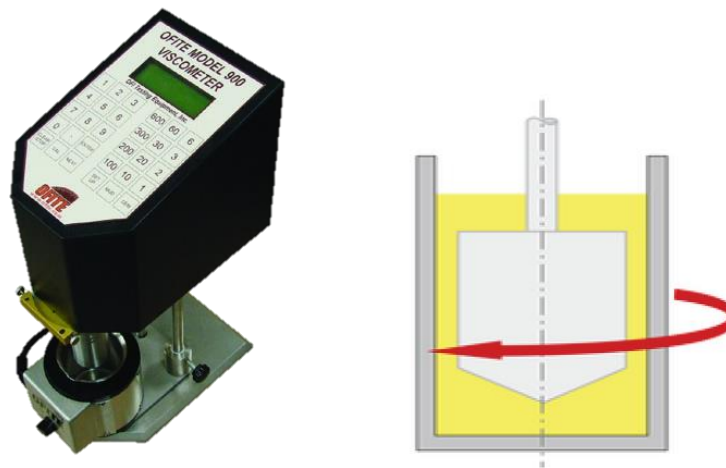
### **6.1 Equipment Used**

The model 900 OFITE viscometer was used for all rheological measurement at ambient and elevated temperatures. OFITE universal heater cup was used for heating fluid samples. To mix solvent-in-water emulsion with heavy oil sample, Waring 700G commercial blender was used.

#### **6.1.1 Viscometer**

Viscometer employed in this study is a Couette type coaxial cylinder viscometer. It comprises of an inner stationary bob and an outer rotating cylinder. The fluid sample is

contained in an annular space (also known as shear gap) between the rotor and the bob. The bob is attached to a torsion spring. The viscous drag force exerted by the fluid generates a torque on the bob causing an angular displacement proportional to viscosity of the fluid. The angular displacement is monitored by a transducer and converted to a shear stress value by a processor. Apparent viscosity along with corresponding shear rate and shear stress values are displayed on output screen located on top of the viscometer.



**Figure 6.1:** (a) Model 900 OFITE viscometer (b) Couette principle (source: viscopedia.com)

By default, the viscometer is setup for stand-alone use. However, it can also be connected to a computer and can be controlled by Windows<sup>®</sup> based ORCADA<sup>®</sup> software. In the present study, the viscometer was controlled via software for the sake of convenience. The software also permits users to run tests automatically - based on user defined templates. However, for better control over temperature changes caused by viscous heating, this option was not opted.

The viscometer is supplied with a stainless steel sample cup. It is recommended to fill the cup with test fluid up to a scribed line which corresponds to approximately 165-170 ml of volume.

**6.1.1.1 Selection of Bob and Spring**

The viscometer usually comes installed with a torsion spring F-1 and bob B1 with which maximum shear stress of 1680 dyne/cm<sup>2</sup> (or 3.5 lbf/ft<sup>2</sup>) can be measured at any shear rate. In other words, maximum apparent viscosity that can be measured decreases with increasing shear rate. For example, at 1 and 100 s<sup>-1</sup> shear rates, it can measure apparent viscosity of up to 167,580 and 1,675.8 cP respectively. The shear stress measurement limit of the instrument can be changed by installing a torsion spring with different spring constant or by changing size of the bob.

**Table 6.1:** Shear stress measurement limit of various spring and bob configuration as provided by the manufacturer

Maximum Shear Stress, (Dyne/cm <sup>2</sup> )	Shear Stress Constant	R1B1	R1B2	R1B3	R1B4
F 0.2 (Green)	77.2	330	651	1320	2644
F 0.5 (Yellow)	193	840	1657	3359	6730
F 1.0 (Blue)	386	1680	3314	6717	13460
F 2.0 (Red)	772	3360	6629	13435	26921
F 3.0 (Purple)	1158	5040	9943	20152	40381
F 4.0 (White)	1544	6720	13257	26870	53841
F 5.0 (Black)	1930	8400	16571	33587	67302
F 10.0 (Orange)	3860	16800	33143	67175	134603

It can be observed from **Table 6.1** that, to facilitate rheological measurement of high viscosity fluids, progressively higher numbered spring or bob should be used. Torsion

spring with higher spring constant requires more torque to cause same amount of angular displacement of bob. Hence, it increases shear stress measurement limit.

**Table 6.2:** Shear rate range for different bobs as provided by the manufacturer

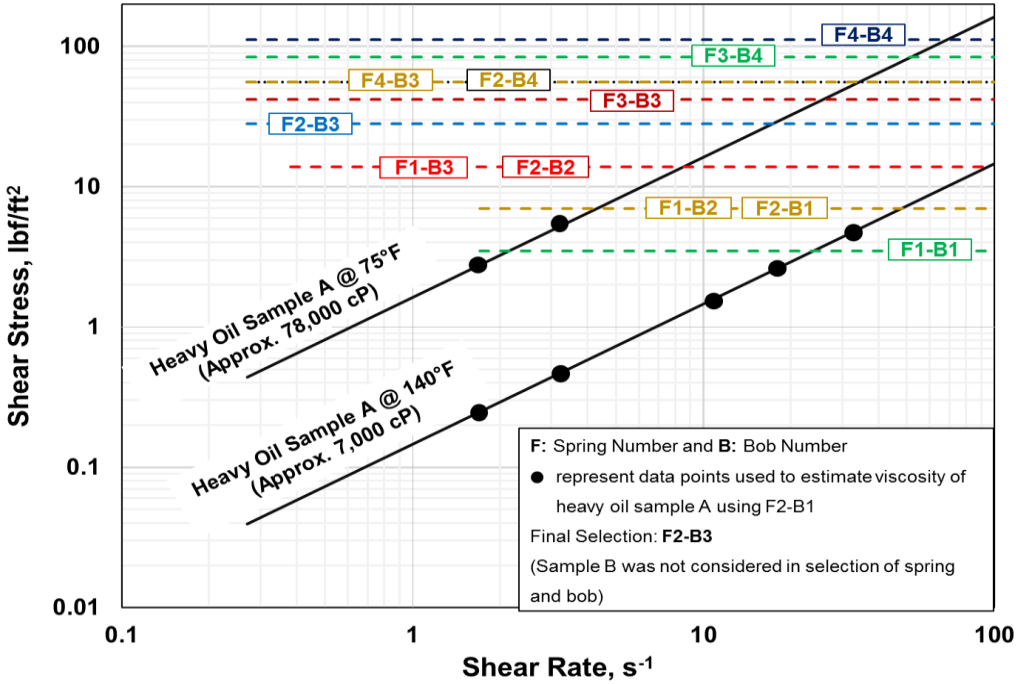
Bob Type	R1B1	R1B2	R1B3	R1B4
Shear Rate Constant (S <sup>-1</sup> /RPM)	1.7023	0.377	0.2682	0.2682
Shear Gap (cm)	0.117	0.6139	0.9793	0.9793
Bob Height (cm)	3.8	3.8	3.8	1.9
Rotation Speed	Shear Rate (s <sup>-1</sup> )			
1 RPM	1.70	0.38	0.27	0.27
2 RPM	3.40	0.75	0.54	0.54
3 RPM	5.11	1.13	0.80	0.80
6 RPM	10.21	2.26	1.61	1.61
10 RPM	17.02	3.77	2.68	2.68
20 RPM	34.05	7.54	5.36	5.36
30 RPM	51.07	11.31	8.05	8.05
60 RPM	102.14	22.62	16.09	16.09
100 RPM	170.23	37.70	26.82	26.82
200 RPM	340.46	75.40	53.64	53.64
300 RPM	510.69	113.10	80.46	80.46
600 RPM	1021.38	226.20	160.92	160.92
1000 RPM	1702.30	377.00	268.20	268.20

Diameter of bob decreases with increasing bob number. This results in progressively more annular gap between bob and rotor. It can be observed from **Table 6.2** that for a constant rotation speed, as shear gap increases, the deformation rate or shear rate experienced by the fluid decreases. This results in increased shear stress measurement capacity of the instrument.

To select appropriate spring and bob for the desired shear rate range, it is essential to know approximately the maximum apparent viscosity of fluids to be tested. Viscosity of both heavy samples used in this experimental work were unknown. Therefore, it was decided to estimate viscosity of one of the samples using already installed F-2 spring and



B1 bob. The viscosity of **Sample A** was estimated to be 78,000 cP and 7000 cP at 75 and 140°F respectively. Assuming Newtonian behavior, shear stress vs shear rate relationship (rheogram) was plotted as shown in **Fig. 6.2**. Maximum shear stress limits of various spring and bob configuration were also plotted on the same graph. To prevent air exposure, Sample B was kept in a sealed container until all tests with Sample A were completed. Therefore, viscosity of Sample B, was not considered while selecting spring and bob configuration for this study.



**Figure 6.2:** Shear stress limit of different spring-bob configuration plotted with the estimated rheogram of both heavy oil samples (at 75 and 140°F)

Shear rate corresponding to subsurface flow is usually considerably low. However, to understand rheological behavior of test fluids over wide range of shear rates; it was decided to evaluate apparent viscosity at shear rates up to 100 s<sup>-1</sup>. The temperature of the

reservoir from which heavy oil samples were acquired, is around 140°F. Hence, at this temperature, the viscometer should be able to measure apparent viscosity of test fluids over desired range of shear rates. **Figure 6.2**, clearly indicates that the combination of spring F2 (or higher) and bob B3 (or higher) would be suitable for this purpose. Out of all options, it was decided to use combination of F2 spring and B3 bob. Detailed specifications of the selected configuration are listed in **Table 6.3**.

**Table 6.3:** Specifications of the spring and bob configuration used in the viscometer

<b>Spring</b>	F 2.0
<b>Bob</b>	B3
<b>Rotor Radius (cm)</b>	1.8415
<b>Bob Radius (cm)</b>	0.8622
<b>Bob Height (cm)</b>	3.8
<b>Shear Gap (cm)</b>	0.9793
<b>Shear Rate Constant (s<sup>-1</sup>/RPM)</b>	0.2682
<b>Max. Shear Stress (lbf/ft<sup>2</sup>)</b>	28.06
<b>Shear Rate Capability</b>	0.27-268.20 s <sup>-1</sup> (1 to 1000 RPM)
<b>Shear Rates Used</b>	0.8-80.40 s <sup>-1</sup> (3 to 300 RPM)
* Complete shear rate capability was not utilized because of high calibration errors observed at shear rates greater than 300 RPM	

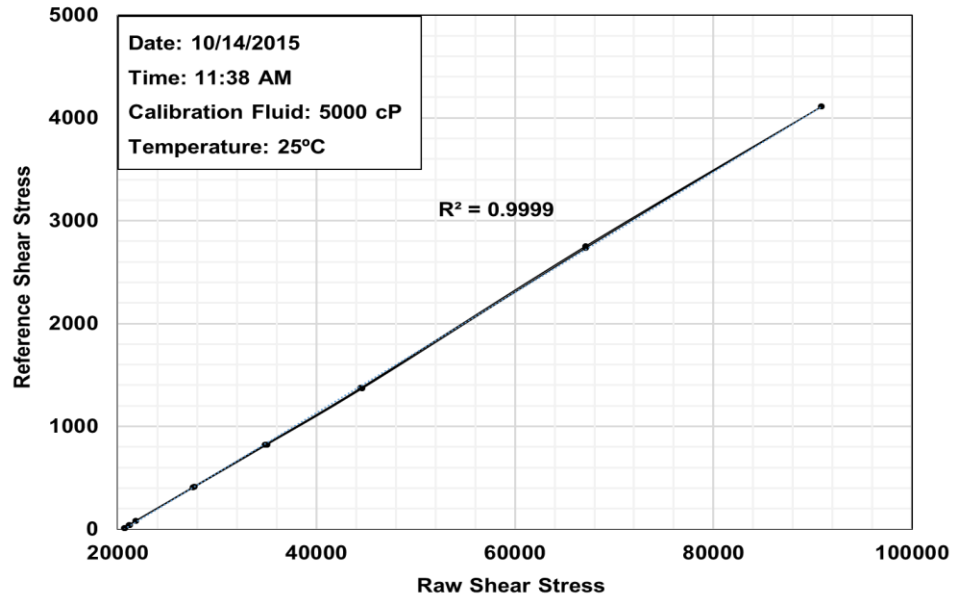
There are two reasons for selecting F2-B3 configuration: (i) spring F3 and higher would have been a special order requiring few weeks to manufacture. Besides, springs are considerably more expensive than bobs and hence, it was decided to use already available F2 spring and purchase a new bob (ii) as annular gap between bob and rotor increases, high shear rate measurements become increasingly less reliable (manufacturer's advice). Therefore, bob B4 and B5 were not considered and it was decided to purchase bob B3.

### **6.1.1.2 Calibration**

After changing spring and bob, it is essential to recalibrate the viscometer. Ideally, a calibration fluid should have viscosity approximately similar to that of fluid to be tested. However, calibration fluid having viscosity in the range of 70,000 cP or more was not commercially available and would have to be specially manufactured. Therefore, Brookfield general purpose silicon fluid, having viscosity of 5000 cP at 25°C, was used as the calibration fluid.

Calibration operation was performed using the software by entering the reference viscosity value and desired shear rate range. Calibration was performed for 0.8 to 80.4s<sup>-1</sup> shear rates. During calibration process, the software checks linear correlation between the raw shear stress measured by the instrument and reference shear stress value (i.e. reference viscosity value). Calibration was repeated until the value of coefficient of determination ( $R^2$ ) calculated, was greater than 0.9990 (Manufacturer's recommendation). **Figure 6.3** displays the final calibration plot.

(Note: Calibration for shear rates higher than 80.4 s<sup>-1</sup> was attempted but  $R^2$  value of more than 0.90 could not be achieved. Manufacturer also suggested not to trust measurement above 80.4 s<sup>-1</sup> because of potential Taylor instability caused by high shear gap corresponding to bob B3.)



**Figure 6.3:** Viscometer calibration plot

### 6.1.2 Heater Cup

The heater cup used to heat test fluids is shown in **Fig. 6.4**. It perfectly accommodates stainless steel viscometer cup inside the heating well. The heater cup can either be connected to the viscometer or a direct power outlet. When connected to viscometer along with thermometer, the temperature is maintained by software or the viscometer itself, depending on the mode of operation. If heater is connected to external power supply then temperature needs to be controlled manually using thermostat knob provided at the front.



**Figure 6.4:** Heater cup used with the viscometer

The test fluids used in the present experimental work were highly viscous. Therefore, shearing of fluid between bob and rotor resulted in notable viscous heating. Temperature spike of 7 to 8°F was not uncommon. The software was unable to account for these temperature variations and hence, throughout the testing, temperature was controlled manually using thermostat knob.

### 6.1.3 Blender

A commercial blender shown in **Fig. 6.5** was used to prepare heavy oil emulsion by mixing solvent-in-water emulsion with the heavy oil sample. A speed controller was used along with the blender to control blending speed.



**Figure 6.5:** Commercial blender used to prepare heavy oil emulsion

## 6.2 Materials Used

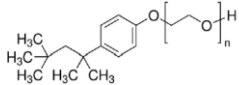
Detailed specification of all these materials are as follows.

### 6.2.1 Triton™ X-100 Surfactant

It is a non-ionic type surfactant. It is also known as 4-(1,1,3,3-Tetramethylbutyl)phenyl-polyethyleneglycol, polyethylene glycol *tert*-octylphenyl ether, and t-

Octylphenoxy polyethoxy ethanol. It has very good thermal stability up to 250°C. It is a clear viscous fluid owing to the hydrogen bonding of its hydrophilic polyethylene oxide parts. It is a widely used surfactant with several applications. It is mainly used as a laboratory grade detergent and an ingredient of the influenza vaccine. It has HLB value of 13.4 which makes it a water soluble surfactant and favors oil-in-water emulsion (Dow Chemical Co., 2014). Other specifications are listed in **Table 6.4**.

**Table 6.4:** Specifications of the surfactant used

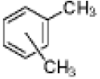
<b>Chemical Formula</b>	
<b>Appearance (Color)</b>	Colorless to Light Yellow
<b>Appearance (Turbidity)</b>	Clear to Slightly Hazy
<b>Appearance (Form)</b>	Liquid
<b>Solubility (Color)</b>	Colorless to Faint Yellow
<b>Solubility (Turbidity) (0.1 mL/mL of H<sub>2</sub>O)</b>	Clear to Slightly Hazy
<b>Density</b>	1.07 g/cm <sup>3</sup>
<b>Brookfield Viscosity</b>	243 - 291 cps
<b>Hydrophile Lipophile Balance (HLB)</b>	13.4

### 6.2.2 Xylene

Xylene is an aromatic hydrocarbon comprising of a benzene ring and two methyl groups attached to it. It has three isomers defined by position of methyl groups on benzene ring-ortho-, meta- and para-xylene. It is practically insoluble in water and easily dissolves in non-polar compounds such as hydrocarbon. Therefore it is mainly used as solvent or

cleaning agent in various industries. Relevant specifications of xylene used in this study are provided in **Table 6.5**.

**Table 6.5:** Specifications of xylene

<b>Chemical Formula</b>	
<b>Molecular Weight</b>	106.17 g/mol
<b>Appearance (Color)</b>	Colorless
<b>Appearance (Form)</b>	Liquid
<b>GC purity</b>	≥ 98.5 %A xylene isomer plus ethylbenzene
<b>Water (by Karl Fischer)</b>	≤ 0.05 %
<b>Sulfur compounds (as S)</b>	≤ 0.003 %
<b>Density</b>	0.86 g/cm <sup>3</sup>

### 6.2.3 NaCl Brine

Anhydrous sodium chloride (90-96% pure) and distilled water were used to prepare the 2 wt% NaCl brine solution. This brine was used as a continuous phase of solvent based emulsion.

### 6.2.4 Copper (II) Oxide Nanoparticles

Copper (II) oxide or cupric oxide (CuO) nanoparticles have found application in various fields such as catalysis, superconducting materials, thermoelectric materials, sensing materials, glass, ceramics etc. Additionally, because of its toxicity, it is also used as anti-micro-bacterial agent. Major physical properties of CuO nanopowder used in this study are listed in **Table 6.6**.

**Table 6.6:** Properties of copper (II) oxide nanopowder

<b>Chemical Formula</b>	CuO
<b>Molecular Weight</b>	79.55 g/mol
<b>Appearance (Color)</b>	Black
<b>Appearance (Form)</b>	Powder
<b>Average particle size</b>	≤ 50 nm
<b>Surface are (m<sup>2</sup>/g)</b>	25-40

### 6.2.5 Iron (III) Oxide Nanoparticles

Iron (III) oxide (Fe<sub>2</sub>O<sub>3</sub>) has attracted a lot of attention due to its super-magnetic property. Its major applications are magnetic storage, catalysis, sensors, development of highly sensitive magnetic resonance imaging (MRI) etc. Unlike CuO, iron oxide is not toxic, and hence, it is also being investigated for potential use in therapeutics. Some of the major physical properties of Fe<sub>2</sub>O<sub>3</sub> nanoparticles are presented in **Table 6.7**.

**Table 6.7:** Properties of iron (III) oxide nanopowder

<b>Chemical Formula</b>	Fe <sub>2</sub> O <sub>3</sub>
<b>Molecular Weight</b>	159.69 g/mol
<b>Appearance (Color)</b>	Red brown to brown
<b>Appearance (Form)</b>	Powder
<b>Average particle size</b>	≤ 50 nm
<b>Surface are (m<sup>2</sup>/g)</b>	40-60 (for 20-40 nm size)

### 6.2.6 Nickel (II) Oxide Nanoparticles

Nickel oxide (NiO) nanopowder has nearly similar applications as copper oxide. It is widely used as catalyst, cathode material for batteries, pigment for ceramics and glasses,



optical filters, and development of electro-chromic materials. Its main physical characteristics are summarized in **Table 6.8**.

**Table 6.8:** Properties of nickel (II) oxide nanopowder

<b>Chemical Formula</b>	NiO
<b>Molecular Weight</b>	74.69 g/mol
<b>Appearance (Color)</b>	Dark green to very dark green/black/green-black
<b>Appearance (Form)</b>	Powder
<b>Average particle size</b>	≤ 50 nm
<b>Surface are (m<sup>2</sup>/g)</b>	50-100 (for 10-20 nm size range)
<b>Purity</b>	99.8% (based on trace metal analysis)

### 6.3 Fluid Preparation

The test matrix for each heavy oil sample is listed in **Table 6.9**. Total of 40 test fluids (20 with each heavy oil sample) were prepared. In addition to measuring rheology of heavy oil samples, three types of test fluids were prepared: (i) heavy oil containing nanoparticles, (ii) heavy oil emulsion (heavy oil mixed with solvent-in-water emulsion), and (iii) heavy oil nano-emulsion (heavy oil mixed with solvent-in-water emulsion containing nanoparticles).

Procedures employed for preparing above mentioned test fluids are as follows.

#### 6.3.1 Heavy Oil Containing Nanoparticles

Manufacturer recommended test fluid volume for the viscometer cup is 165 to 170 ml. Weight of 165 ml of heavy oil sample was 159.5 gm (Sample A) and 162.3 gm (Sample B). Based on the weight of 165 ml of oil, desired amount of nanoparticles (0.05, 0.1 or

0.5 wt%) was weighed and kept aside. Then, the oil was gradually poured into the viscometer cup while simultaneously sprinkling nanopowder to ensure proper mixing, The cup was filled up to the scribed line marked on it.

**Table 6.9:** Test matrix for each heavy oil sample

Serial Number	Nanoparticles Type	Nanoparticle Concentration (wt% of oil)	S/W Emulsion to Heavy Oil Ratio (vol% of oil)	Temperatures for Rheological Measurement (°F)	
1	-	-	-	80, 100, 120, 140, 160, and 180	
2	<b>Copper Oxide (CuO)</b>	0.50	-		
3		0.10	-		
4		0.05	-		
5		0.002	5		5
6			10		10
7		<b>Iron Oxide (Fe<sub>2</sub>O<sub>3</sub>)</b>	0.50		-
8	0.10		-		
9	0.05		-		
10	0.002		5		5
11			10		10
12	<b>Nickel Oxide (NiO)</b>		0.50		-
13		0.10	-		
14		0.05	-		
15		0.002	5		5
16			10		10
17		-	-		5
18	-	-	10		
19	-	-	15		
20	-	-	20		

\* For most of the test fluids, temperature of 80°F could not be achieved because of variable room temperature and heat generated during fluid mixing.

\* Viscometer’s operating temperature limit is 190°F and hence, heater cup is configured to override manual control at about 180°F. Therefore, extremely poor temperature control was observed at 180°F.

\* Due to lack of data and its reliability, viscosity measurements at 80 and 180°F have not been used for comparative analysis.

\* Effect of 0.002 wt% nanoparticles alone has not been investigated because viscosity alteration is not expected to exceed reproducibility error.

An attempt was made to mix nanoparticles with oil using the blender. However, because of extremely high viscosity of oil, it tended to adhere to the wall of blender jar and the blades. Hence, some amount of oil would be lost while transferring it from the jar to the viscometer cup. Moreover, a fraction of nanopowder may get stuck to the blades or the wall of the jar. These risks would make it difficult to maintain precise concentration of nanoparticles. Therefore, it was decided to mix nanoparticles directly into the viscometer cup as described in **Section 6.3.1**.

### **6.3.2 Solvent-in-Water (S/W) Micro-Emulsion**

The optimum composition of solvent-in-water micro-emulsion was established by Qiu (2010) as 95 wt% brine, 1.8 wt% solvent and 3.2 wt% surfactant (refer to **Section 4.4**). This solvent based emulsion was prepared using the blender. First, 200 ml of 2% NaCl brine was prepared and poured into the blender jar. Then, 3.84 gm of xylene (solvent) and 6.82 gm of Triton<sup>TM</sup> X-100 (surfactant) were slowly added while continuously stirring at moderate speed. The fluid was stirred at high speed for 15 minutes while avoiding air entrapment. The fluid was then allowed to stabilize for additional 15 minutes.

### **6.3.3 Heavy Oil Emulsion**

Heavy oil emulsion was prepared by mixing S/W emulsion with heavy oil. First, 170 ml of oil was poured into the blender jar. Then, appropriate amount of (5, 10, 15 or 20 vol%) S/W emulsion was measured and slowly added to the oil. Fluid was stirred at moderate speed for 20-30 minutes until homogeneous emulsion was observed.

### **6.3.4 Heavy Oil Nano-Emulsion**

Heavy oil nano-emulsions were prepared by mixing S/W emulsion and nanoparticles with heavy oil. First, 170 ml of oil was poured into the blender jar. Then, appropriate amount of (5 or 10 vol% of oil) S/W emulsion containing nanoparticles (0.002 wt% of oil) were slowly added. Fluid was stirred at moderate speed for 20-30 minutes until homogeneous emulsion was observed.

## **6.4 Challenges in Viscosity Measurement**

Viscosity measurement of heavy oil is a challenging task and generated data is often unreliable. Various factors that affect reliability of viscosity data are discussed in **Section 2.3**. For the present experimental work, sample acquisition method, storage and transportation process could not be monitored. However, viscosity measurement procedure was carefully planned and executed to improve accuracy, repeatability and reliability of the data. The biggest challenges were maintaining temperature and minimizing effect of shear degradation and viscous heating.

### **6.4.1 Temperature Control**

Because of extremely high viscosity of oil sample, viscous heating was prominent and its intensity varied with change in shear rate. Temperature spike of as high as 8-10°F was observed while stepping up from the lowest shear rate ( $0.8 \text{ s}^{-1}$ ) to the highest shear rate ( $80 \text{ s}^{-1}$ ).

One of the major disadvantages of concentric cylinder type viscometer is large sample volume. This increases rate of heat loss as larger fluid surface is exposed to atmosphere.

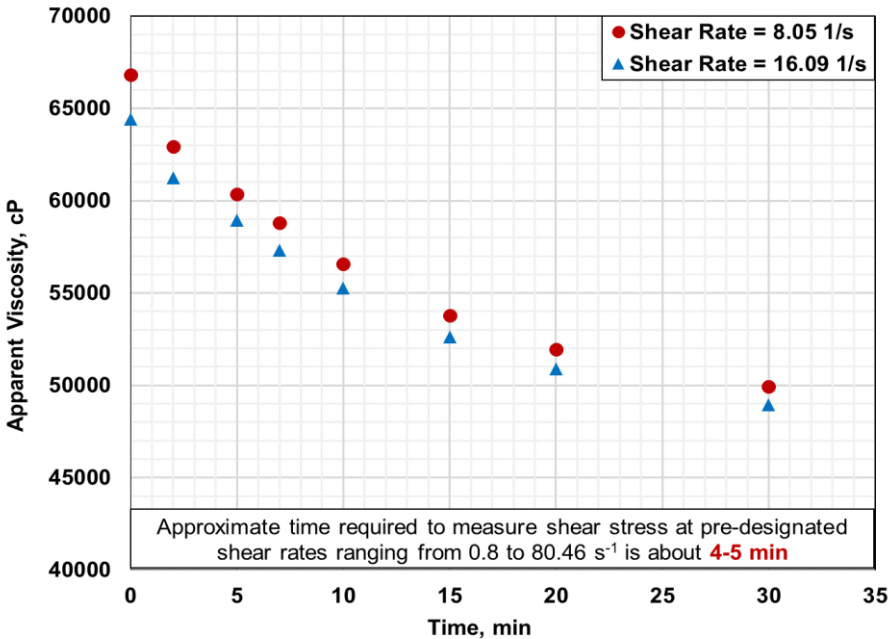
In addition to that, the heater cup used does not have a chiller or cooling system. These issues combined with viscous heating, were responsible for significant temperature fluctuation.

For better temperature control, heating was controlled manually, using thermostat knob on the heater cup. Heating would be stopped before reaching the desired temperature. Then, shear rate would be increased to the highest possible rate (not exceeding 300 rpm). Shearing the fluid for few seconds would increase the temperature because of viscous heating. Shearing would be stopped when temperature reaches slightly higher than the desired temperature. Then, the fluid would be allowed to stabilize for 1 minute so that homogenous temperature distribution is achieved. During this, the temperature would decrease to the desired temperature with accuracy of  $\pm 1^\circ\text{F}$ . Now, shear stress measurements can be initiated from the lowest shear rate towards the high shear rate.

#### **6.4.2 Viscosity Measurement Approach**

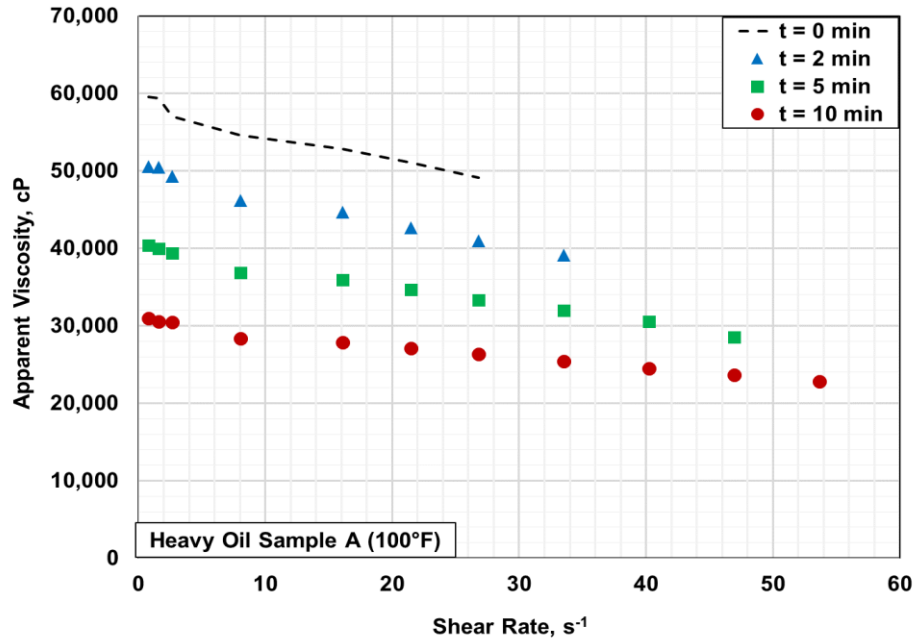
Pilot tests were run in order to investigate the effect of viscous heating. First of all, variation in shear stress as a function of time was observed at a constant shear rate in the absence of external heat supply. As expected, because of viscous heating caused by shearing, the shear stress value decreased with time (see **Fig. 6.6**). Typical time required to cover all shear rates from 3 to 300 rpm, is approximately 4-5 minutes. It can be clearly visualized from **Fig. 6.6** that in 5 minutes, apparent viscosity reduced by 5000-6000 cP. Moreover, temperature increment of 1-2 $^\circ\text{F}$  was observed even though no external heat

was supplied to the fluid sample. These two observations confirm time dependence of shear stress measurement and presence of viscous heating.



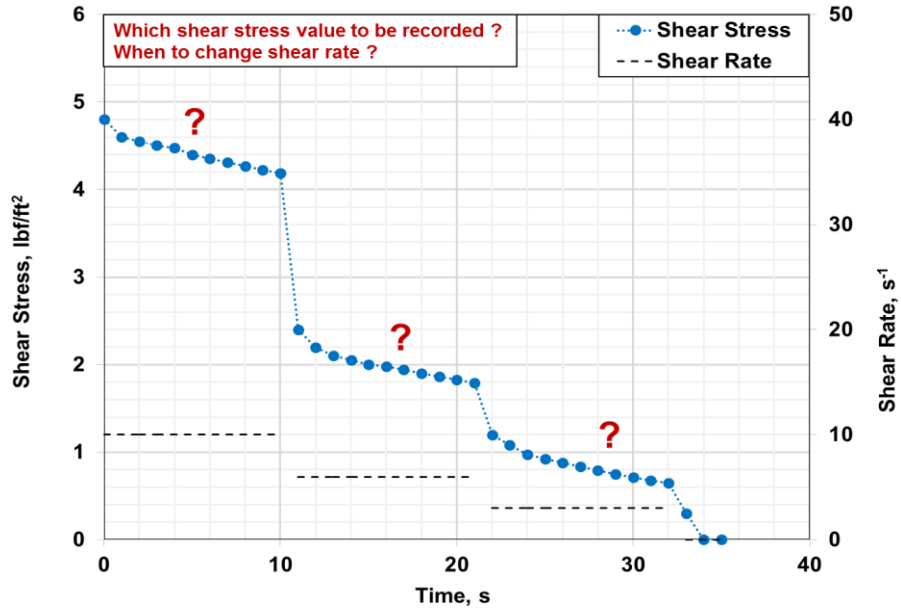
**Figure 6.6:** Effect of viscous heating on apparent viscosity (at a constant shear rate and in absence of external heat energy)

Shear stress measurements can either be performed along increasing shear rate or decreasing shear rate. Ideally, both approaches are employed to check the hysteresis effect which is often absent in case of low viscosity fluids. Usually, when a shear rate is increased or decreased, shear stress changes accordingly and then stabilizes after few seconds. However, in the present case, because of shear degradation and viscous heating, shear stress would never stabilize and will continue to decrease with time. As shown in **Fig. 6.7**, even in the absence of external heat source, apparent viscosity depends on shear history.

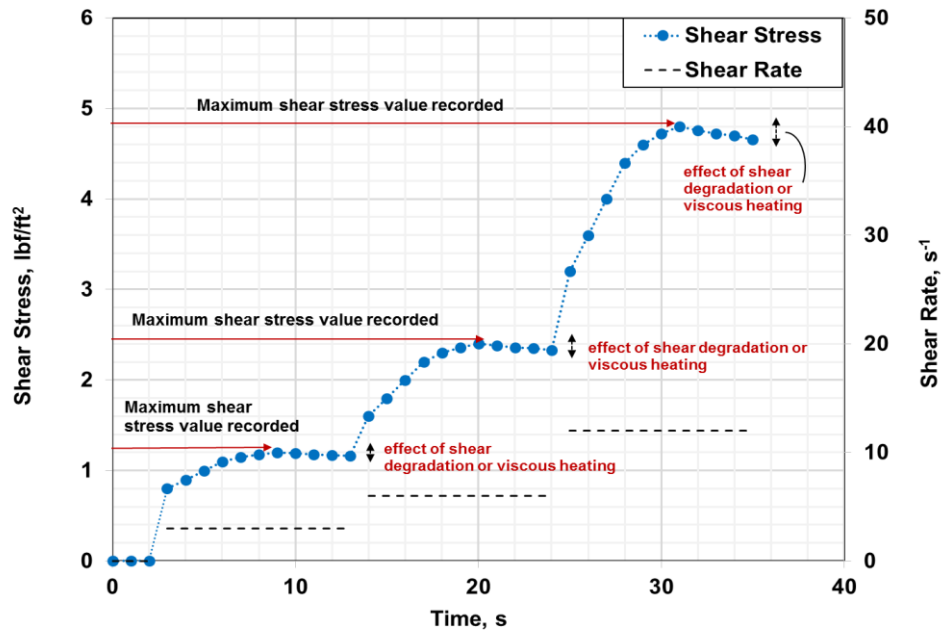


**Figure 6.7:** Hysteresis effect (absence of external heat source)

As shown in **Fig. 6.8**, if step-down shear rate approach is used then, shear stress value will always have a decreasing trend leading to the confusion of which value to be recorded. In other words, shear stress value recorded would also depend on time. However, as presented in **Fig. 6.9**, in step-up shear rate approach, shear stress would increase, reach a peak and then start decreasing. In this case, maximum shear stress value can be recorded ensuring a consistent measurement approach which is independent of time. Therefore, step-up shear rate approach was employed for all the tests conducted in the present study.



**Figure 6.8:** Graphical representation of shear stress variation during step-down shear rate approach

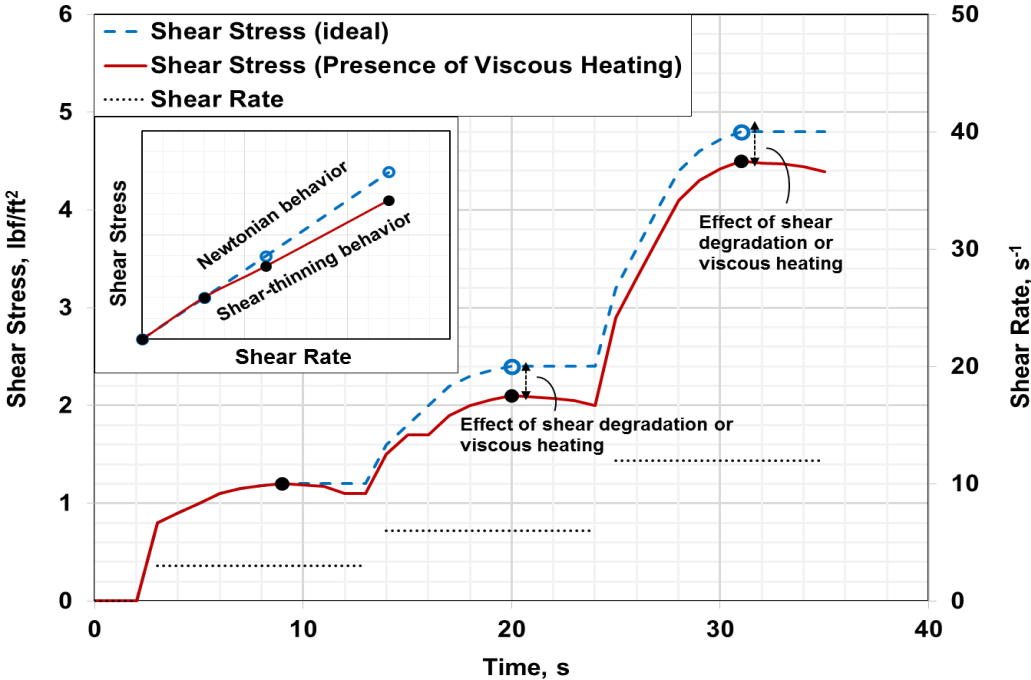


**Figure 6.9:** Graphical representation of shear stress variation during step-up shear rate approach



### 6.4.3 Artificial Shear-Thinning Behavior

Ideally, as soon as shear stress reaches a peak and begins to decrease, shear rate should be changed. However, in reality, it takes few seconds to write down the value and change the shear rate; during which, shear stress might have decreased slightly. Because of this, as shown in **Fig. 6.10**, shear stress peaks would be slightly less than what would have been obtained in absence of shear degradation. This error progressively increases with increase in shear rate. Therefore, the rheogram of the fluid would exhibit slightly shear-thinning behavior even though, in reality, it might actually be Newtonian (see inset graph in **Fig. 6.10**).



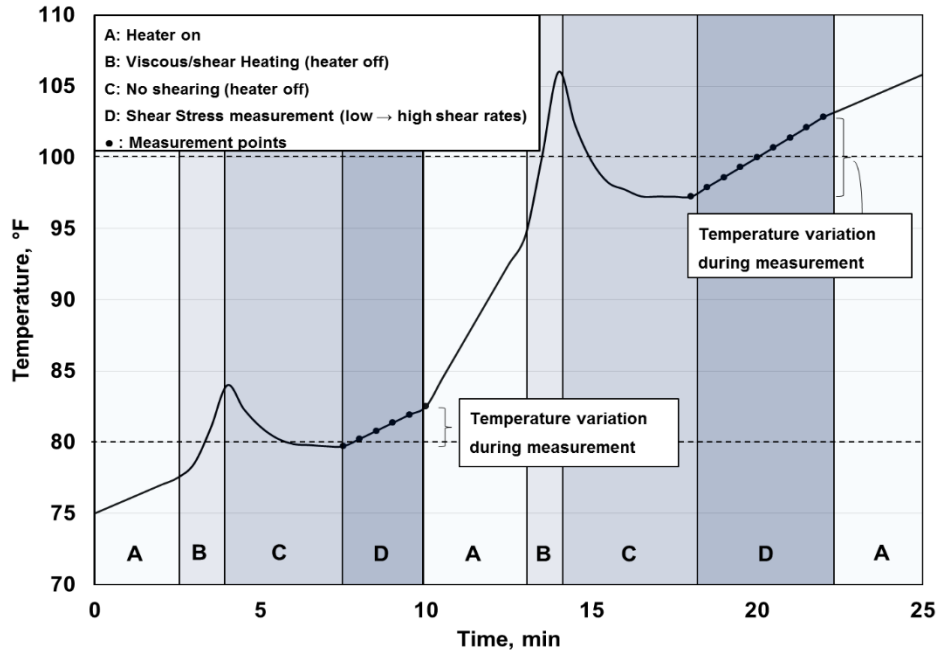
**Figure 6.10:** Graphical representation of artificial shear-thinning behavior introduced by shear degradation and viscous heating

## 6.5 Procedure of Viscosity Measurement

Based on the challenges discussed so far, following standard procedure of viscosity measurement was established.

- Take 165 ml of test fluid into the viscometer cup.
- Insert the cup into the heating-well of the heater. Submerge temperature sensor into the fluid.
- Measure the shear stress values at shear rates of 3, 6, 10, 30, 60, 80, 100, 125, 150, 175, 200, 225, 250, 275, and 300 rpm; moving from low to high shear rate. (1 RPM =  $0.266 \text{ s}^{-1}$ )
- Next step is to measure the rheology at 80°F. As discussed in **Section 6.4.1**, turn off the heater at 77-78°F. Increase the temperature to 82-83°F by shear heating. Then, stop shearing and allow the fluid to achieve homogeneous temperature. The temperature would decrease and stabilize around 79-80°F. Now, initiate the shear stress measurements.
- Follow the same procedure and measure rheology of the fluid at 100, 120, 140, 160 and 180°F.

It was observed that temperature control becomes increasingly challenging at progressively higher temperatures. Throughout this document, 80, 100, 120, 140, 160, and 180°F corresponds to approximate temperature range of 80-83, 100-104, 120-125, 140-145, 160-166, and 180-190°F respectively. **Figure 6.11** provides graphical representation of typical temperature variation during tests.



**Figure 6.11:** Graphical representation of typical temperature variation during test

## 6.6 Models Employed for Rheological Characterization of Fluids

As discussed in **Section 2.1**, heavy oil typically exhibits Newtonian behavior. However, at higher shear rates, shear thinning behavior is not uncommon. Therefore, all fluids prepared in this study were characterized using not only Newtonian model but also Ostwald-de Waele power law model.

### 6.6.1 Newtonian Model

Fluids that display linear relationship between shear stress and shear rate, can be represented by this model. This type of fluid is called Newtonian fluid and is characterized by shear independent viscosity. Mathematically it is written as,

$$\tau = (\mu\dot{\gamma})/47880 \quad \dots\dots\dots (6.1)$$

where  $\tau$  is shear stress in lbf/ft<sup>2</sup>,  $\mu$  is Newtonian viscosity in cP,  $\gamma$  is shear rate in s<sup>-1</sup> and 47880 is the unit conversion factor.

### 6.6.2 Ostwald-de Waele Power Law Model

This model is suitable for describing pseudoplastic or shear thinning fluid behavior. Mathematical description of this model is as follows,

$$\tau = K_v \gamma^n \dots\dots\dots (6.2)$$

where  $\tau$  is shear stress in lbf/ft<sup>2</sup>,  $K_v$  is consistency index in lbf.s<sup>n</sup>/ft<sup>2</sup>,  $\gamma$  is shear rate in s<sup>-1</sup> and n is a dimensionless parameter known as fluid behavior index.

Apparent viscosity is a function of shear rate and is defined as,

$$\mu_a = \tau / \gamma = K_v \gamma^{(n-1)} \dots\dots\dots(6.3)$$

where  $\mu_a$  is apparent viscosity in lbf-s/ft<sup>2</sup>. In conventional units, above equation can be written as,

$$\mu_a = \tau / \gamma = 47880 K_v \gamma^{(n-1)} \dots\dots\dots(6.4)$$

where  $\mu_a$  is apparent viscosity at a particular shear rate in cP unit.

Equation (6.2) can be written in logarithmic form as,

$$\log(\tau) = \log(K_v) + n \log(\gamma) \dots\dots\dots (6.5)$$

Shear stress and shear rate values, measured using the viscometer, were plotted on a log-log chart. A straight line was fitted to the data points and using slope and intercept of this line, fluid behavior index (n) and consistency index ( $K_v$ ) were calculated.

$$\text{Fluid behavior index (n) = slope of } \log(\tau) \text{ vs } \log(\dot{\gamma}) \text{ curve} \quad \dots\dots\dots(6.6)$$

and

$$\text{Consistency index (K}_v\text{) = } 10^{\text{intercept of } \log(\tau) \text{ vs } \log(\dot{\gamma}) \text{ curve}} \quad \dots\dots\dots(6.7)$$

where n is a dimensionless and  $K_v$  is in  $\text{lbf}\cdot\text{s}^n/\text{ft}^2$ ,

Ostwald-de-Waele model is based on the assumption of absence of yield stress i.e. fluid starts flowing as soon as shear rate is applied. Heavy oil sometimes exhibits yield stress (Hascakir, 2008). Heavy oil samples used in this study may also possess characteristic yield stress. In that case, Herschel Bulkley or yield power law model would be more suitable for characterizing the fluids used in this work. However, the usefulness of this model depends on determination of correct yield stress value which is either measured or calculated by extrapolating low shear rate data to zero shear rate. As discussed in **Section 6.4.3**, presence of viscous heating may have been responsible for introducing artificial shear thinning behavior. Therefore, extrapolation of these affected shear stress data, may not provide an accurate yield stress value. Hence, it was decided to use the power law model considering only measured data without any extrapolation. Moreover, power law model was successfully able to describe shear stress vs shear rate trend with  $R^2$  value of more than 0.99.

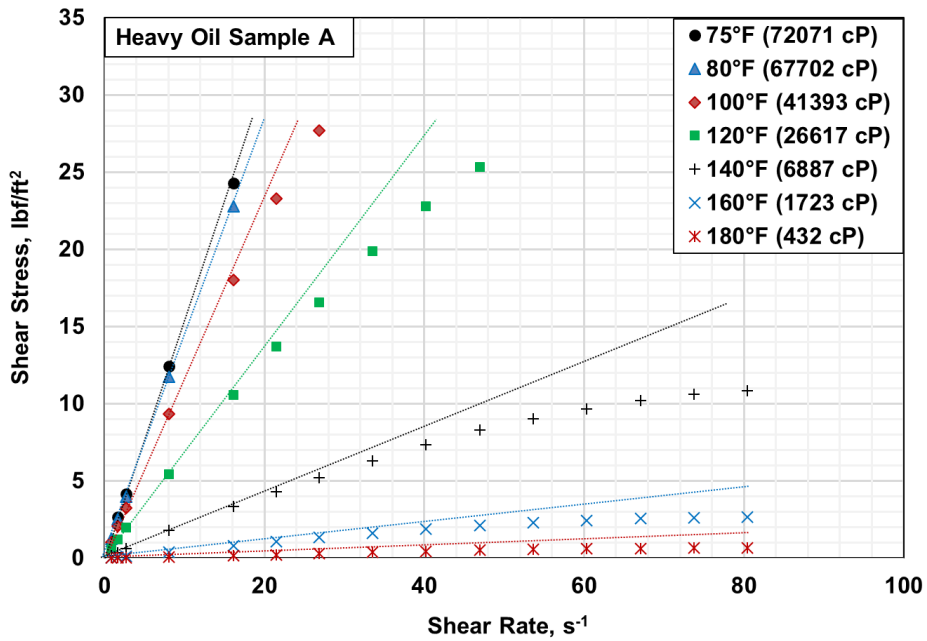
## 7. Results and Discussion

This chapter is divided into five sections. In the first section, the rheological characteristics of heavy oil **Sample A** and **Sample B** are discussed. Viscosity alteration by nano-sized metal particles is discussed in the second section. Rheological behavior of heavy oil emulsion prepared by mixing various amount of solvent-in-water (S/W) emulsion, is presented in the third section. Combined effect of nanoparticles and S/W emulsion on viscosity of both heavy oil samples is described in fourth section. The last section discusses usefulness of viscosity data generated.

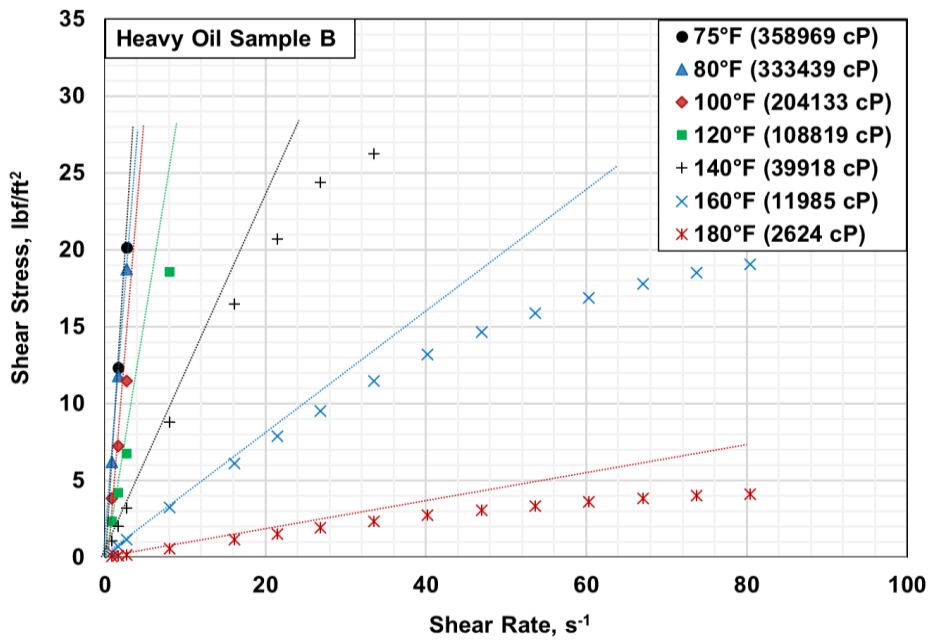
### 7.1 Rheology of Heavy Oil Samples

As expected, both heavy oil samples exhibited Newtonian behavior at low shear rates and shear thinning behavior at high shear rates. Shear stress versus shear rate plots, i.e. rheograms for both samples, are shown in **Figs. 7.1 and 7.2**. It is apparent that at low shear rates all data points fall on a straight line. As shear rate increases, the shear stress starts deviating from the Newtonian model and follows a trend of a shear thinning fluid.

As discussed in **Section 2.1**, increase in shear rate results in restructuring of asphaltene microstructure which is reflected as a reduction in apparent viscosity. Moreover, this process does not occur instantaneously and hence, even at a constant shear rate, the apparent viscosity gradually decreases. Additionally, as discussed in **Section 6.4**, viscous heating and shear degradation may also have been responsible for the reduction in apparent viscosity (see **Fig. 6.10**).



**Figure 7.1:** Rheogram for heavy oil sample A at various temperatures



**Figure 7.2:** Rheogram for heavy oil sample B at various temperatures

\* Viscosity mentioned in parenthesis corresponds to Newtonian viscosity

It is extremely challenging to isolate the shear restructuring and viscous heating effect. Therefore, either of the mechanisms or both, could have been responsible for the shear thinning behavior observed.

Considering the apparent shear thinning behavior, power law fluid model was fitted to the rheological data. Power law parameters - fluid behavior index ( $n$ ) and consistency index ( $K_v$ ) calculated for both samples at various temperatures, are presented in **Table 7.1**. Fluid behavior indices of approximately 0.9 (and more) confirm highly Newtonian behavior. Comparing ‘ $n$ ’ values calculated for the same shear rate range, it was observed that increase in temperature results in increase in ‘ $n$ ’ values i.e. fluid becomes more Newtonian. This is an expected trend as increase in temperature causes dissociation of asphaltene molecules into small fragments, diminishing the effect of shear stretching (Dion, 2011). Power law parameter ‘ $K_v$ ’ follows the same trend as apparent viscosity and hence, it has not been included in results discussion.

**Table 7.1:** Power law parameters of heavy oil samples at various temperatures

Temperature, °F	Heavy Oil Sample A			Heavy Oil Sample B		
	$n$	$K_v$	Shear Rate Range, $s^{-1}$	$n$	$K_v$	Shear Rate Range, $s^{-1}$
80	0.963	1.5686	0.8 to 16.09	0.921	7.5669	0.8 to 2.68
100	0.942	1.2907	0.8 to 26.82	0.910	4.6866	0.8 to 2.68
120	0.926	0.7699	0.8 to 46.94	0.906	2.7784	0.8 to 8.05
140	0.910	0.2401	0.8 to 80.46	0.885	1.3241	0.8 to 33.53
160	0.949	0.0516	0.8 to 80.46	0.881	0.4765	0.8 to 80.46
180	1.041	0.0086	0.8 to 80.46	0.962	0.0726	0.8 to 80.46

\*  $n$  is fluid behavior index (dimensionless) and  $K_v$  is consistency index ( $lbf \cdot s^n / ft^2$ )  
 \*\* At low temperatures, because of high viscosity, current spring-bob configuration did not permit shear stress measurements over the desired shear rate range of 0.8 to 80.46  $s^{-1}$



Shear thinning observed in this study was not significant with the lowest fluid behavior index calculated to be 0.88. Therefore, during comparative analysis, it is reasonable and convenient to represent both samples with Newtonian viscosity instead of shear dependent apparent viscosity.

**Table 7.2:** Newtonian viscosity of heavy oil samples as a function of temperature

Temperature, °F	Heavy Oil Sample A (cP)	% Reduction from Viscosity at 75°F	Heavy Oil Sample B (cP)	% Reduction from Viscosity at 75°F
75	72,071	0.00	358,969	0.00
80	67,702	-6.06	333,439	-7.11
100	41,393	-42.57	204,133	-43.13
120	26,617	-63.07	108,819	-69.69
140	6887	-90.44	39,918	-88.88
160	432	-99.40	2624	-99.27

At room temperature (approximately 75°F) Newtonian viscosity of heavy oil samples A and B were determined to be 72,071 cP and 358,969 cP respectively. Newtonian viscosity of both samples as a function of temperature is listed in **Table 7.2** and also graphically presented in **Fig. 7.3**. It can be seen that temperature plays significant role in viscosity reduction. Even though viscosity of Sample B is almost five times as high as that of Sample A; percentage reduction in viscosity with temperature was practically the same for both of them. As discussed in **Section 2.1.3**, dissociation of asphaltene molecules and thermal upgrading of heavier compounds are believed to be the major reasons for this significant reduction in viscosity.

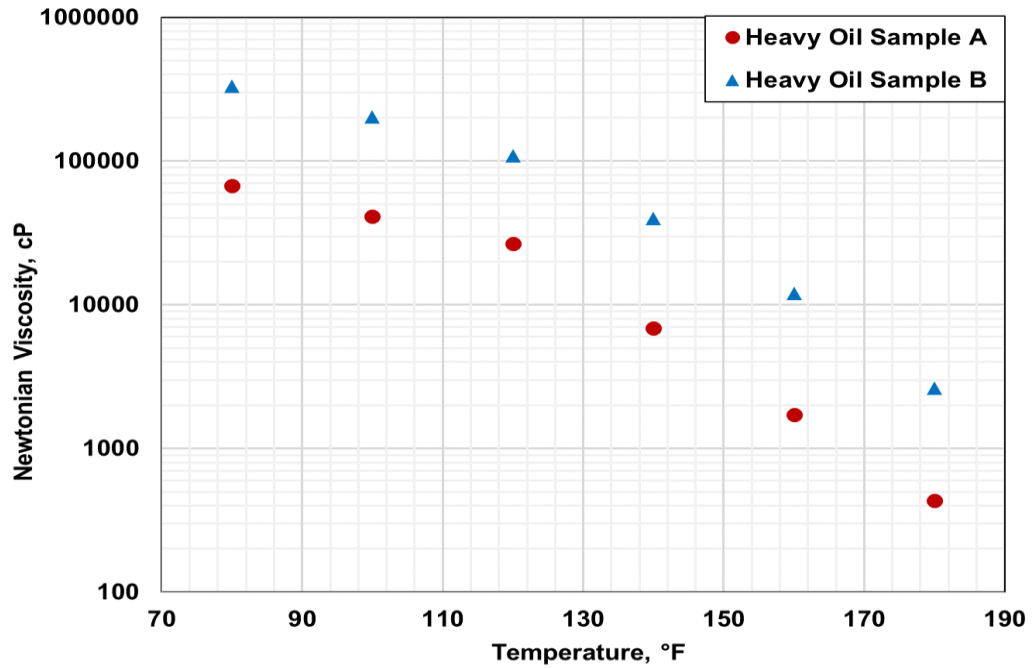


Figure 7.3: Newtonian viscosity of heavy oil samples as a function of temperature

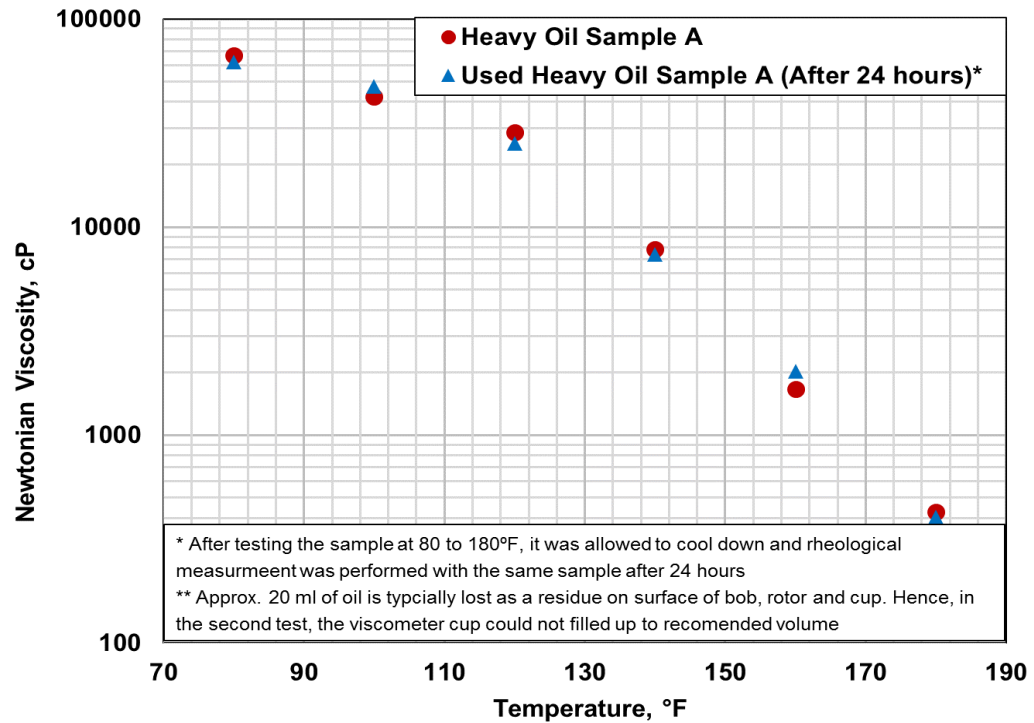


Figure 7.4: Newtonian viscosity of used heavy oil samples as a function of temperature

**Figure 7.4** represents Newtonian viscosity of an already tested heavy oil sample as a function of temperature. The sample had been heated up to 180°F and then kept at ambient condition for 24 hours. It can be clearly observed that, the viscosity of used heavy oil sample does not differ significantly from the original sample. This confirms that while heating up to 180 °F, escape of lighter fractions from the oil is insignificant. If great amount of lighter fractions were being removed during heating process then, the used oil sample would have exhibited higher viscosity than the original sample.

### **7.1.1 Reproducibility**

As discussed in **Section 2.3**, heavy oil viscosity data often exhibits poor reliability. It is practically impossible to acquire an ideal heavy oil sample which is uncontaminated and representative of whole reservoir. Moreover, heavy oil viscosity is highly sensitive to temperature, shear history, composition variation, ambient condition, sample preparation method etc. It is extremely challenging to keep all these conditions the same for all tests. Therefore, only way to improve reliability of viscosity data is to repeat tests as many times as possible and statistically minimize error.

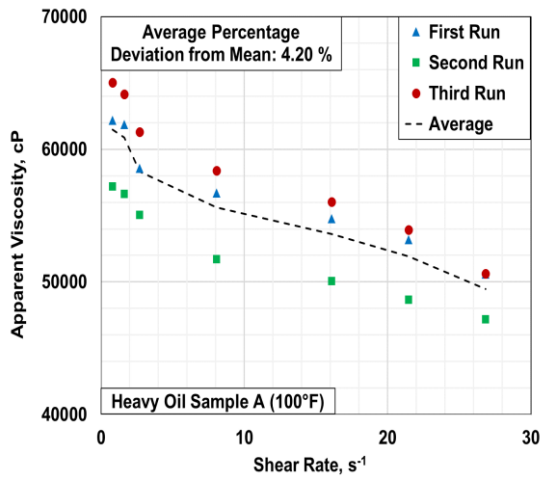
Because of limited volume of oil samples and time constraint, majority of the tests presented in this study could not be repeated. To tackle this problem, for each heavy oil sample, three independent viscosity measurements were performed on random days. From this data, the mean viscosity values were determined for both samples at each temperature. Then, average absolute percentage deviation from the mean was calculated.

A sample calculation is provided in **Table 7.3**. Apparent viscosity plots for these repeatability tests are graphically presented in **Figs. 7.5 and 7.6**.

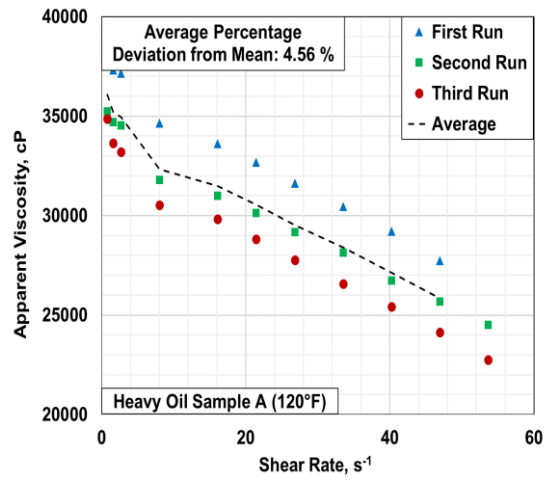
**Table 7.3:** Sample calculation of reproducibility error

Average Shear Stress, lbf/ft <sup>2</sup>	Run 1		Run 2		Run 3		Average of Absolute Deviation, %
	Shear Stress, lbf/ft <sup>2</sup>	Deviation from Average Shear Stress, %	Shear Stress, lbf/ft <sup>2</sup>	Deviation from Average Shear Stress, %	Shear Stress, lbf/ft <sup>2</sup>	Deviation from Average Shear Stress, %	
(S)	(S <sub>1</sub> )	(D <sub>1</sub> )	(S <sub>2</sub> )	(D <sub>2</sub> )	(S <sub>3</sub> )	(D <sub>3</sub> )	$E_i = ( D_1  +  D_2  +  D_3 ) / 3$
0.61	0.64	5.72	0.59	-2.36	0.59	-3.35	3.81
1.18	1.25	5.94	1.17	-1.49	1.13	-4.45	3.96
1.96	2.08	6.25	1.94	-1.21	1.86	-5.04	4.16
5.43	5.82	7.19	5.34	-1.67	5.13	-5.52	4.79
10.58	11.30	6.80	10.42	-1.52	10.02	-5.28	4.53
13.69	14.65	7.03	13.50	-1.37	12.92	-5.65	4.69
16.54	17.72	7.14	16.34	-1.20	15.56	-5.95	4.76
19.88	21.33	7.31	19.71	-0.86	18.60	-6.45	4.87
22.79	24.55	7.71	22.46	-1.44	21.36	-6.28	5.14
25.34	27.19	7.31	25.16	-0.69	23.66	-6.61	4.87
<b>Average of E<sub>i</sub></b>							<b>4.56 %</b>

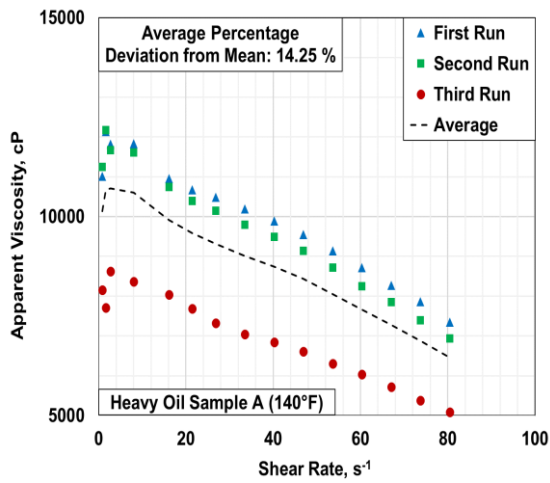
Considering the maximum absolute percentage deviation is another way to represent reproducibility error. However, in that case, an outlier data point might compromise the result. Therefore, it was decided to use the average deviation so that the effect of random errors can also be minimized.



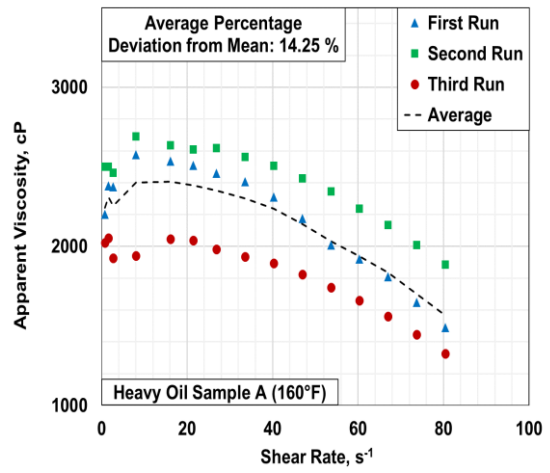
(a)



(b)

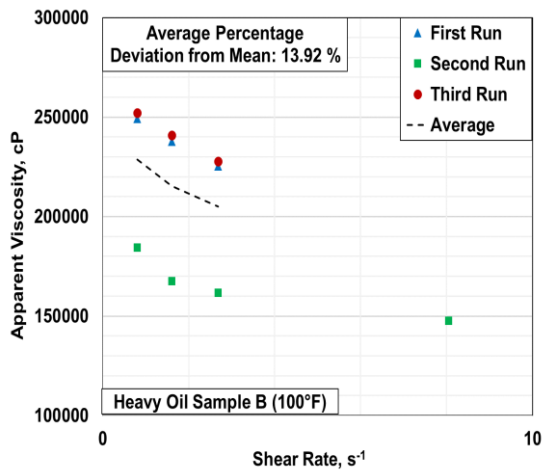


(c)

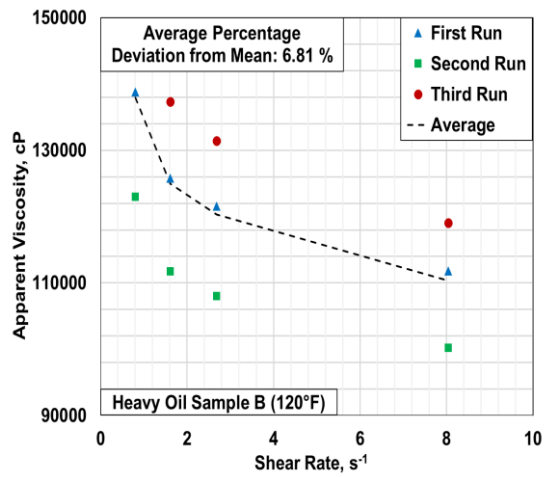


(d)

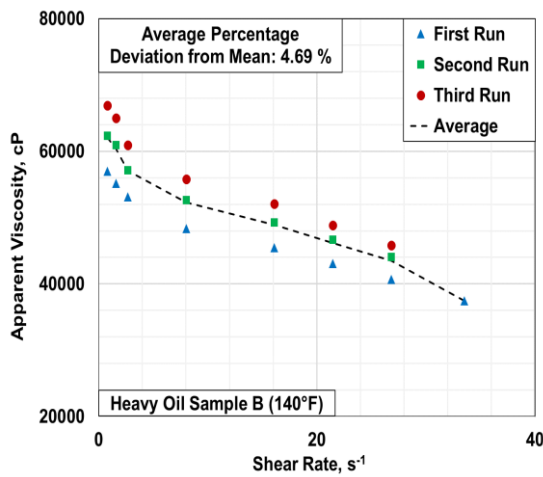
**Figure 7.5:** Graphical representation of reproducibility tests for Sample A at (a) 100°F, (b) 120°F, (c) 140°F, and (d) 160°F



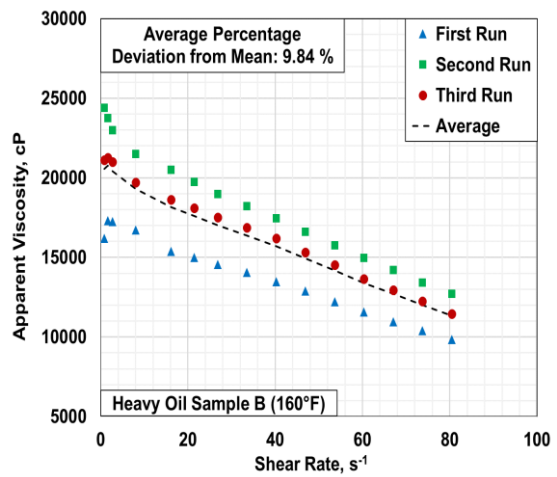
(a)



(b)



(c)



(d)

**Figure 7.6:** Graphical representation of reproducibility tests for Sample B at (a) 100°F, (b) 120°F, (c) 140°F, and (d) 160°F

Summary of reproducibility error calculated for both samples is provided in **Table 7.4**. Reproducibility values ranged from 4.2 to 14.25% for Sample A and 4.69% to 13.92% for Sample B. As discussed in **Section 2.3**, values of 2 to 10% reproducibility is very common even for labs specialized in heavy oil and bitumen analysis (Miller et al., 1995).

**Table 7.4:** Reproducibility of viscosity measurement for heavy oil samples

Temperature, °F	Average % Deviation from Averaged Apparent Viscosity	
	Heavy Oil Sample A	Heavy Oil Sample B
100	4.20	13.92
120	4.56	6.81
140	14.25	4.69
160	10.36	9.84

Reproducibility data presented in the above table was employed as a guideline to validate viscosity alteration caused by nanoparticles or S/W emulsion. If viscosity decreases exceeded reproducibility error, then only it was considered as conclusive evidence of viscosity reduction.

## 7.2 Effect of Nanoparticles

To investigate the effect of nano-sized particles, three different metal oxides – copper (II) oxide, iron (III) oxide and nickel (II) oxide were employed. For each type of particle, three different concentrations (0.05, 0.1 and 0.5 wt%) were examined.

### 7.2.1 Copper Oxide (CuO)

Addition of copper oxide yielded notable reduction in viscosity of both heavy oil samples. The reduction in viscosity was a function of not only particle concentration but also temperature. Addition of nanoparticles did not lead to any significant change in fluid

behavior index and thus fluids' rheological behavior remained the same as that of the original oil samples.

Newtonian viscosity of heavy oil samples in presence of copper oxide nanoparticles is displayed in **Figs. 7.7 and 7.8**. Average percentage reduction in apparent viscosity achieved by addition of these particles is graphically presented in **Figs. 7.9 and 7.10** and is also listed in **Table 7.5**. Apparent viscosity plots for test fluids containing copper oxide nanoparticles are provided in **Appendix A**. It should be noted that an average viscosity reduction displayed in the table, was not determined based on Newtonian viscosity. It was calculated by averaging percentage reduction in apparent viscosity measured at each shear rate.

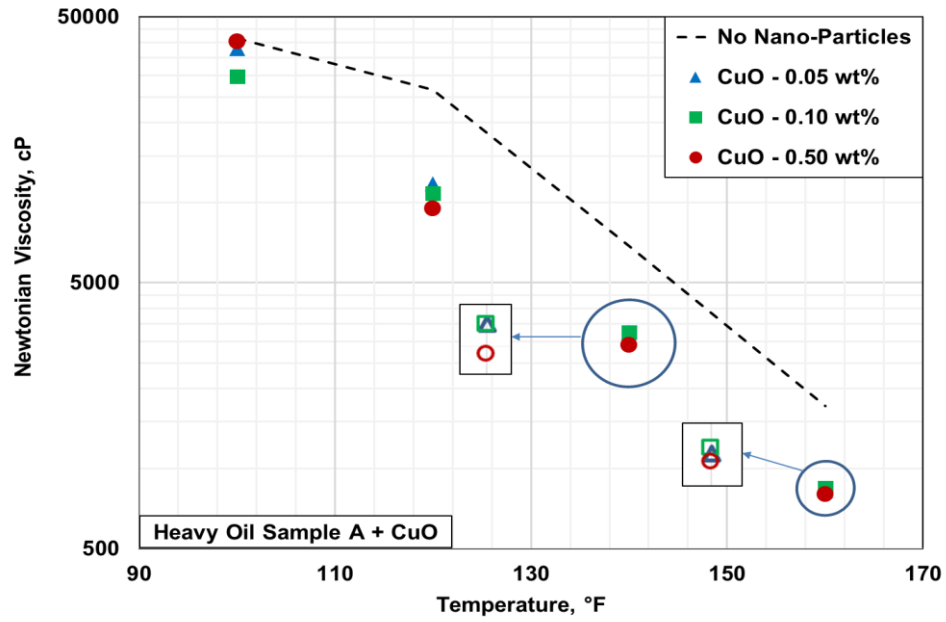
**Table 7.5:** Summary of viscosity alteration by copper oxide nanoparticles

No	Heavy Oil Sample	Copper Oxide Concentration (%wt)	Average Change in Apparent Viscosity (%) **			
			100°F	120°F	140°F	160°F
1	A	0.05	<b>-17</b>	<b>-41</b>	-50	-56
2		0.10	<b>-28</b>	<b>-46</b>	-51	-56
3		0.50	<b>-13</b>	<b>-56</b>	-56	-59
4	B	0.05	<b>-9</b>	<b>-9</b>	<b>-14</b>	-25
5		0.10	<b>-19</b>	<b>-24</b>	<b>-20</b>	-30
6		0.50	<b>-8</b>	<b>-18</b>	<b>-23</b>	-36

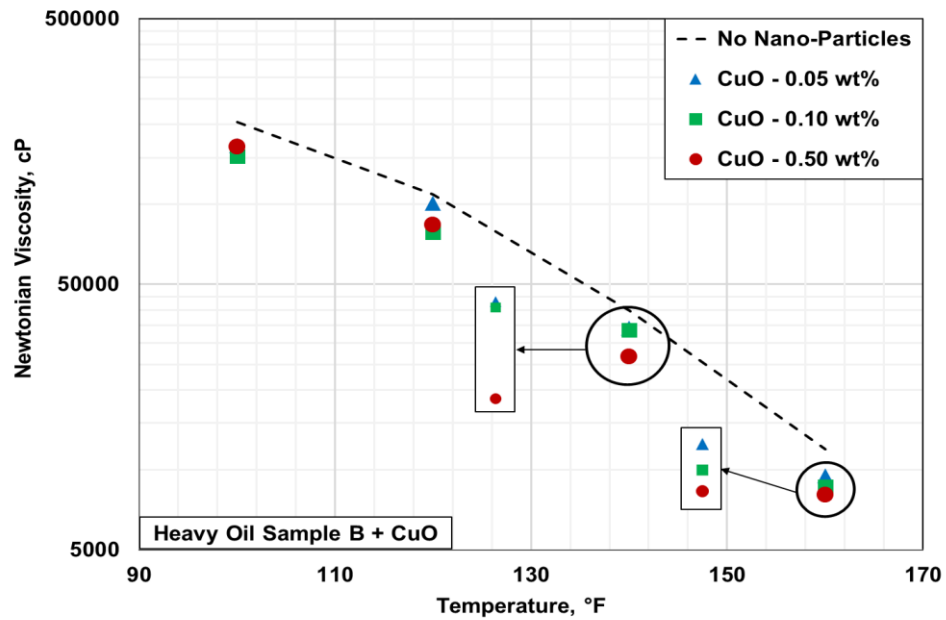
\* Negative change represents viscosity reduction  
 \*\* % change in apparent viscosity observed at each shear rate were averaged to obtain a single representative value  
 \*\*\* Bold faced data are beyond error of reproducibility and hence, can be entrusted to establish viscosity trend

For heavy oil Sample A, the viscosity reduction ranged from 13-17% at 100°F to as high as 56-59% at 160°F. In case of Sample B, comparatively less reduction in viscosity was observed i.e. 8 to 19% at 100°F and 25 to 36% at 160°F.

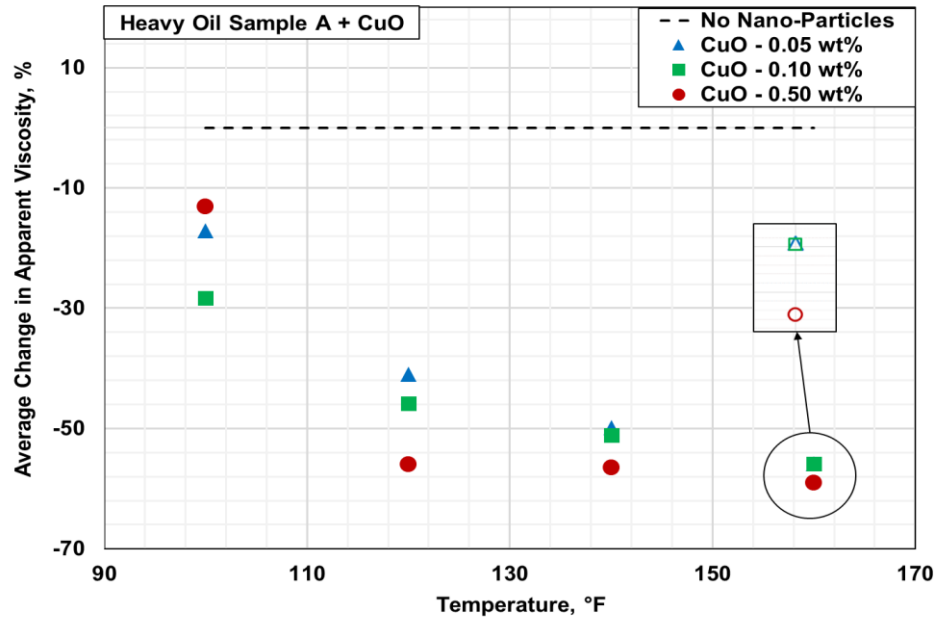




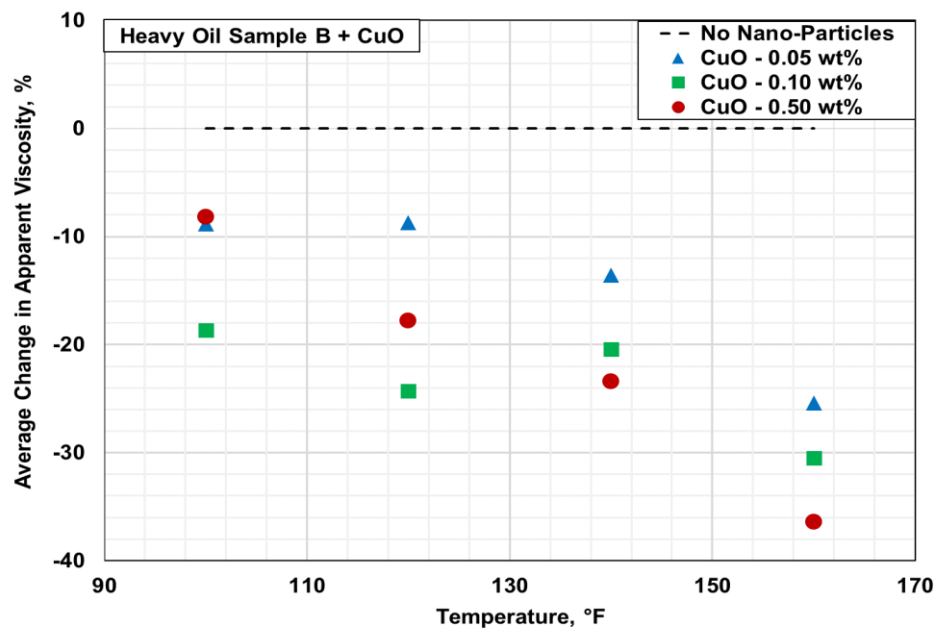
**Figure 7.7:** Newtonian viscosity of heavy oil sample A in presence of copper oxide nanoparticles at various temperatures



**Figure 7.8:** Newtonian viscosity of heavy oil sample B in presence of copper oxide nanoparticles at various temperatures



**Figure 7.9:** Percentage change in apparent viscosity of heavy oil sample A caused by copper oxide nanoparticles at various temperatures



**Figure 7.10:** Percentage change in apparent viscosity of heavy oil sample B caused by copper oxide nanoparticles at various temperatures

At low temperatures, the viscosity reduction can be attributed to Ostwald ripening process discussed in **Section 3.1.1.1**. Zeta potential analysis shows that copper particles are negatively charged ( $z=-77$  mV at pH=7) and hence create strong electrical field that attracts asphaltene molecules to their surface. Agglomeration of these structures make bulk oil less viscous (Shokrlu et al., 2014).

It is also interesting to note that the viscosity reduction improved with increase in temperature. This can be attributed to weakening of hydrogen bond within heavier compounds of oil (Kershaw et al., 1980). Weakening of hydrogen bond combined with improved thermal conductivity increase efficiency of thermal upgrading of heavy oil. This leads to further reduction in viscosity.

The amount of viscosity reduction achieved in this study is unprecedented. Very high amount of asphaltene content seems to be the most likely cause. Only two studies have been conducted wherein the effect of nano- and micro- copper oxide particles on heavy oil viscosity was investigated. Shokrlu et al. (2014) had employed micron size copper oxide particles with Canadian heavy crude oil (8492 cP at 77°F) and observed viscosity reduction of approximately 10%. Srinivasan (2014) observed 10-27% reduction in viscosity by adding nano-sized copper oxide particles to less viscous crude oil (600 cP at 70°F). Comparatively low viscosity reduction achieved in these two studies may be attributed to lack of sufficient asphaltene content for notable Ostwald ripening effect.

It should be noted that the viscosity reduction is also a function of particle concentration. Existence of an optimum concentration was observed at which a maximum viscosity reduction was achieved. Effect of particle concentration and determination of optimum concentration is discussed in upcoming **Section 7.2.4**.

### 7.2.2 Iron Oxide (Fe<sub>2</sub>O<sub>3</sub>)

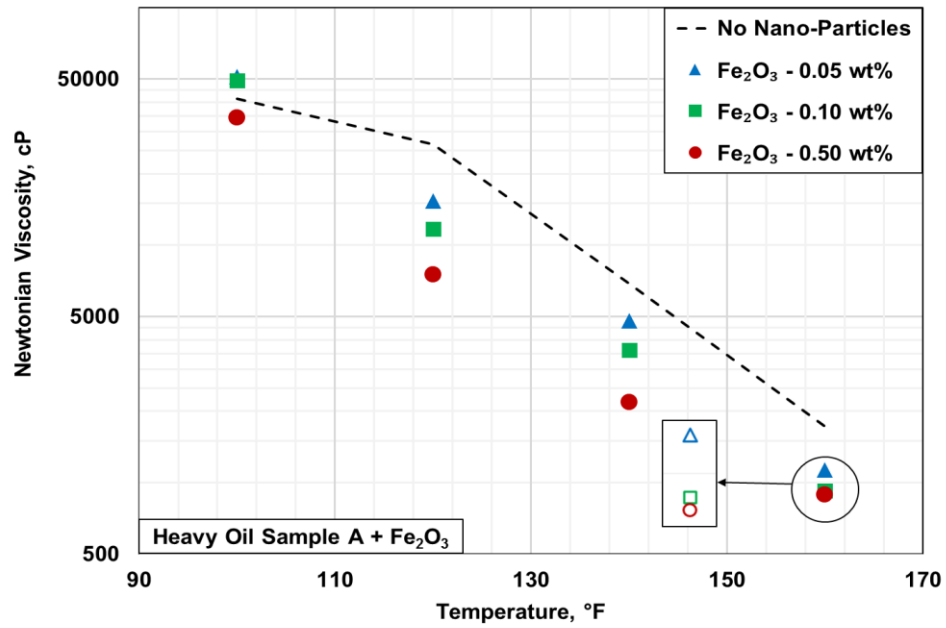
Similar to copper oxide, addition of iron oxide nanoparticles also resulted in marked reduction in viscosity of both heavy oil samples. As far as rheological behavior is concerned, practically no change was indicated. Fluid behavior indices of more than 0.9 were observed in all fluid samples confirming highly Newtonian behavior.

Newtonian viscosity of heavy oil samples in presence of iron oxide nanoparticles is displayed in **Figs. 7.11 and 7.12**. Average percentage reduction observed in apparent viscosity, is presented in **Figs. 7.13 and 7.14** and has also been listed in **Table 7.6**.

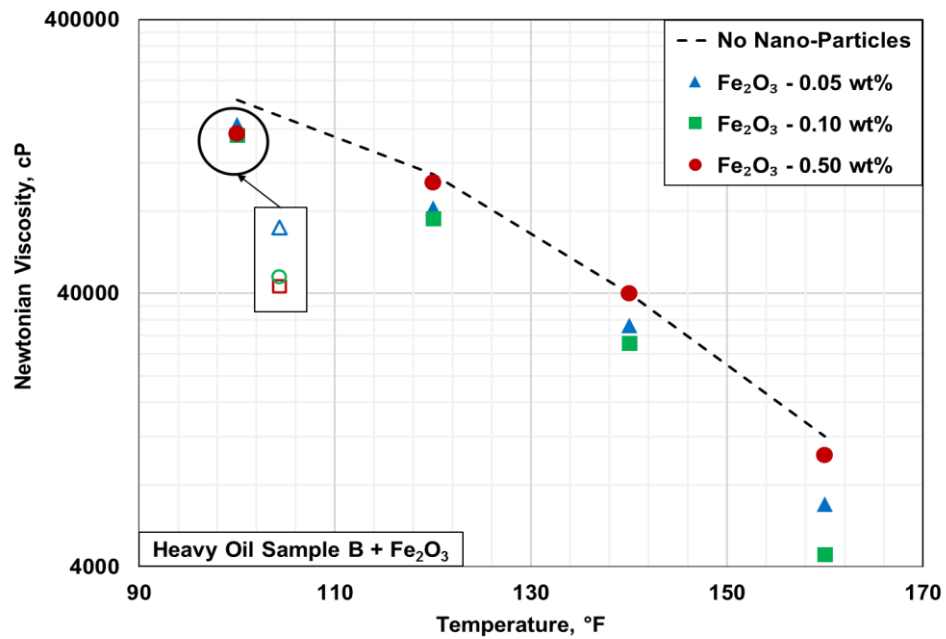
**Table 7.6:** Summary of viscosity alteration by iron oxide nanoparticles

No	Heavy Oil Sample	Iron Oxide Nanoparticles Concentration (%wt)	Average Change in Apparent Viscosity (%)**			
			100°F	120°F	140°F	160°F
1	A	0.05	+4	-22	-30	-35
2		0.10	-2	-48	-50	-48
3		0.50	-22	-62	-65	-52
4	B	0.05	-9	-20	-19	-48
5		0.10	-18	-28	-28	-65
6		0.50	-16	-8	-3	-17

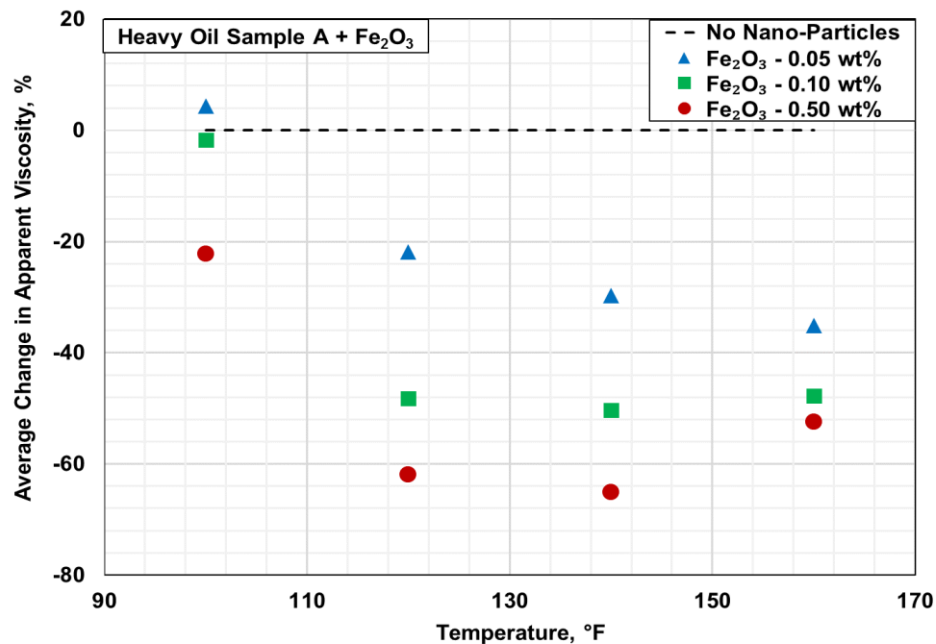
\* Negative change represents viscosity reduction  
 \*\* % change in apparent viscosity observed at each shear rate were averaged to obtain representative value  
 \*\*\* Bold faced data are beyond error of reproducibility and hence, can be entrusted to establish viscosity trend



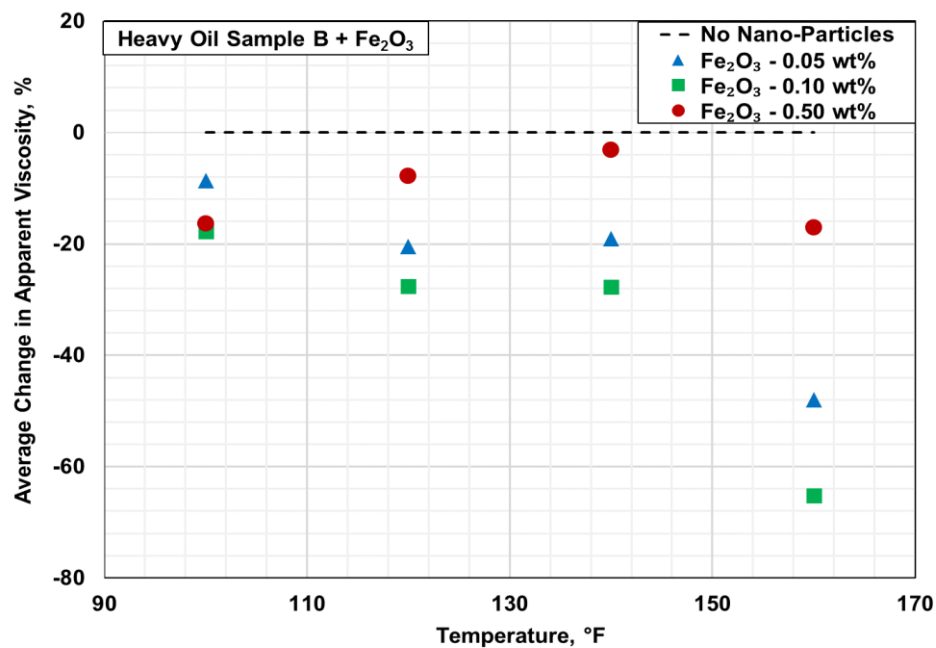
**Figure 7.11:** Newtonian viscosity of heavy oil sample A in presence of iron oxide nanoparticles at various temperatures



**Figure 7.12:** Newtonian viscosity of heavy oil sample B in presence of iron oxide nanoparticles at various temperatures



**Figure 7.13:** Percentage change in apparent viscosity of heavy oil sample A caused by iron oxide nanoparticles at various temperatures



**Figure 7.14:** Percentage change in apparent viscosity of heavy oil sample B caused by iron oxide nanoparticles at various temperatures

For heavy oil Sample A, the viscosity reduction ranged from 2 to 22% at 100°F to as high as 35 to 52% at 160°F. In case of Sample B, comparatively less viscosity reduction was observed that is 9 to 16% at 100°F and 17 to 48% at 160°F. Since viscosity reduction also depends on oil composition (**Section 3.3.3**), dissimilar viscosity reduction at the same particle concentration is expected. This behavior is in line with the results of two previous studies conducted with iron particles. Hascakir (2008) tested micron size iron and iron oxide particles with two moderately viscous oil samples (592 and 700 cP at 75°F) and achieved viscosity reduction of 34 to 88% respectively. Shokrlu et al. (2014) observed reduction of only 8-10% using the micro- and nano-sized iron particles.

Iron oxide particles are characterized by positive zeta potential values. Therefore, unlike copper oxide, iron oxide would disperse asphaltene. Therefore, instead of Ostwald ripening effect, exothermic chemical reactions are believed to play dominant role in viscosity reduction (see **Section 3.1.1.2**). Examples of such reactions are rusting, and formation of magnetite ( $\text{Fe}_3\text{O}_4$ ) and iron sulfide ( $\text{FeS}$ ). These reactions are usually very slow. However, high specific area of nanoparticles combined with presence of saline water, acid compounds or oxidants such as carboxylic acid in oil sample can significantly accelerate these reactions.

Similar to copper oxide, iron oxide also exhibited improvement in viscosity reduction with increase in temperature. Weakening of hydrogen bond, improved thermal conductivity and accelerated chemical reactions can be considered to be the major causes for this behavior.

Interestingly, unlike copper oxide, the effect of concentration on resultant viscosity was more distinct in the presence of iron oxide. More detailed discussion on optimum particle concentration is provided in upcoming **Section 7.2.4**.

### 7.2.3 Nickel Oxide (NiO)

Among three type of nanoparticles, nickel oxide exhibited slightly more viscosity reduction than copper oxide and iron oxide. Moreover, variation in viscosity alteration with concentration was significant. As expected, oil sample retained their original rheological behavior upon addition of nickel oxide.

Newtonian viscosity of heavy oil samples in presence of nickel oxide nanoparticles is graphically presented in **Figs. 7.15 and 7.16**. Average percentage change in apparent viscosity achieved is presented in **Figs. 7.17 and 7.18** and has also been listed in **Table 7.7**. Apparent viscosity plots at various temperatures are provided in **Appendix A**.

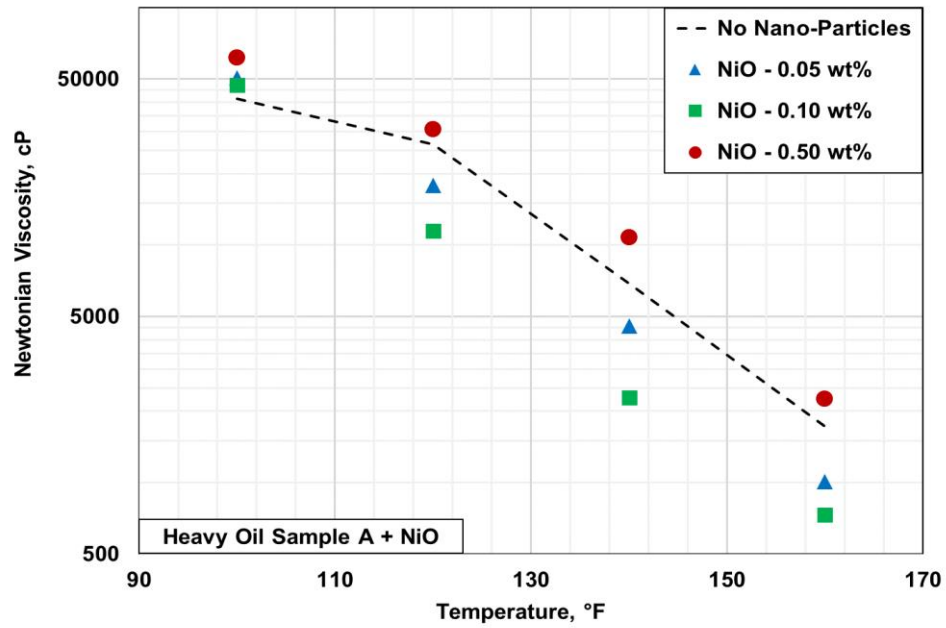
**Table 7.7:** Summary of viscosity alteration by nickel oxide nanoparticles

No	Heavy Oil Sample	Nickel Oxide Nanoparticles Concentration (%wt)	Average Change in Apparent Viscosity (%) **			
			100°F	120°F	140°F	160°F
1	A	0.05	<b>+1</b>	<b>-12</b>	<b>-35</b>	<b>-46</b>
2		0.10	<b>-7</b>	<b>-51</b>	<b>-70</b>	<b>-65</b>
3		0.50	<b>17</b>	<b>17</b>	<b>59</b>	<b>38</b>
4	B	0.05	<b>-29</b>	<b>-30</b>	<b>-32</b>	<b>-53</b>
5		0.10	<b>-36</b>	<b>-50</b>	<b>-53</b>	<b>-64</b>
6		0.50	<b>-17</b>	<b>-24</b>	<b>-13</b>	<b>-17</b>

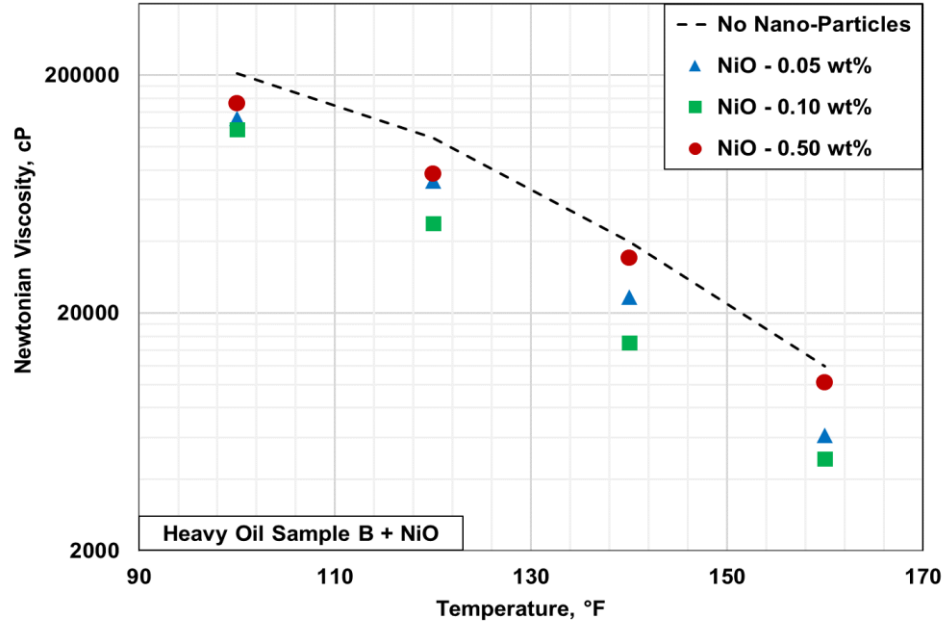
\* Negative change represents viscosity reduction  
 \*\* % change in apparent viscosity observed at each shear rate were averaged to obtain representative value  
 \*\*\* Bold faced data are beyond error of reproducibility and hence, can be entrusted to establish viscosity trend

For heavy oil Sample A, the viscosity reduction ranged from 7 to 70% depending on the concentration and temperature. In case of Sample B, the reduction varying from 13 to 64% was achieved. This behavior is further discussed in **Section 7.2.4**.

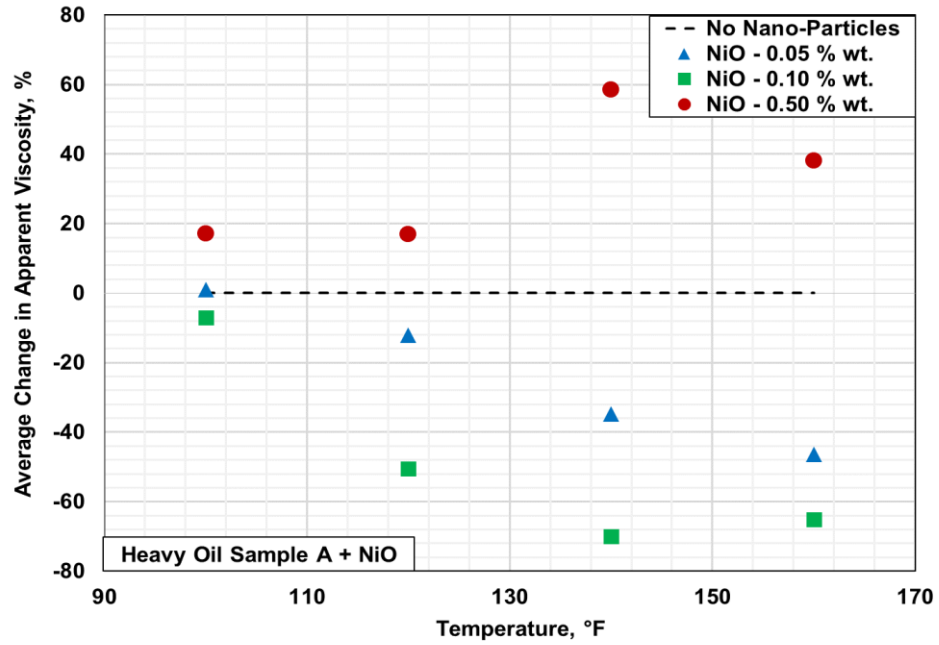




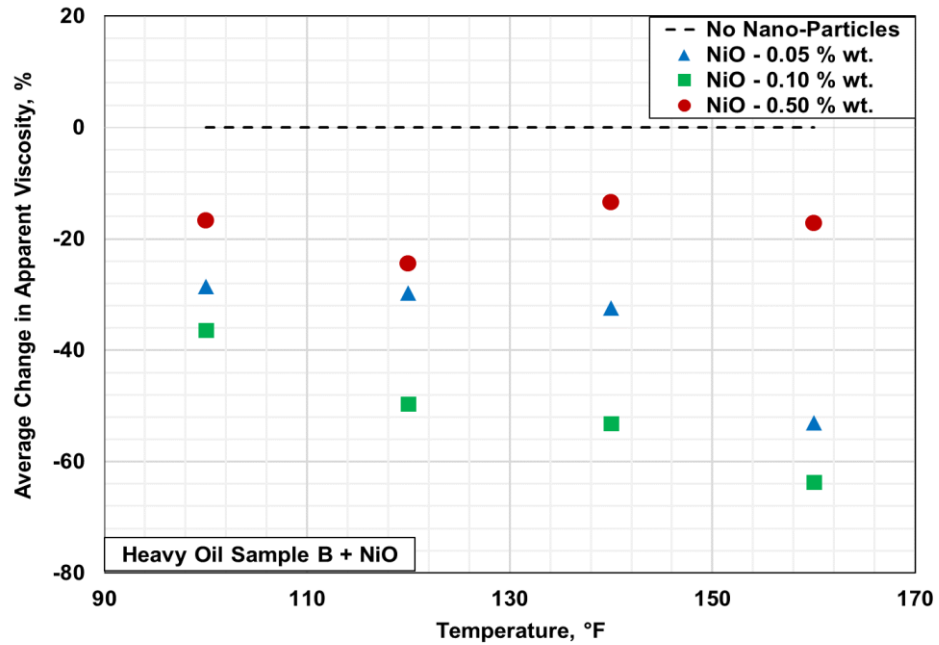
**Figure 7.15:** Newtonian viscosity of heavy oil sample A in presence of nickel oxide nanoparticles at various temperatures



**Figure 7.16:** Newtonian viscosity of heavy oil sample B in presence of nickel oxide nanoparticles at various temperatures



**Figure 7.17:** Percentage change in apparent viscosity of heavy oil sample A caused by nickel oxide nanoparticles at various temperatures



**Figure 7.18:** Percentage change in apparent viscosity of heavy oil sample B caused by nickel oxide nanoparticles at various temperatures

Similar to copper oxide, Ostwald ripening process is the dominant mechanism leading to viscosity reduction in Nickel oxide. Zeta potential of NiO is -32 mV at pH of 7. This negative charge attracts positively charged asphaltene molecules resulting in the reduction of viscosity of bulk fluid. Shokrlu et al. (2014) provided a visual confirmation of asphaltene aggregation around nickel oxide. (see **Fig. 3.2** and **Section 3.1.1.1**).

Similar to copper oxide and iron oxide, nickel oxide also exhibited an improvement in viscosity reduction with increase in temperature. This trend can be attributed to weakening of hydrogen bond.

Shokrlu et al. (2014) had examined the effect of nickel nanoparticles and noted a maximum of 8% reduction as opposed to 70% observed in the present study. Compositional difference in the oil samples may have been responsible for this notable variation in performance. Viscosity of two oil samples used in this study are 8 and 40 times of that was used by Shokrlu et al. Therefore, a significant viscosity alteration achieved in the present work can be reasonably attributed to high asphaltene content of oil. Besides, Shokrlu et al. used nickel particle while in the present investigation, nickel oxide particles were used. This suggests that intermolecular physico-chemical interactions may have also been different in both cases.

#### **7.2.4 Optimum Concentration**

Results obtained with nanoparticles indicate existence of an optimum concentration at which maximum viscosity reduction was achieved. This optimum concentration depends not only on particle concentration but also on metal type, temperature and oil composition (see **Section 3.3**).

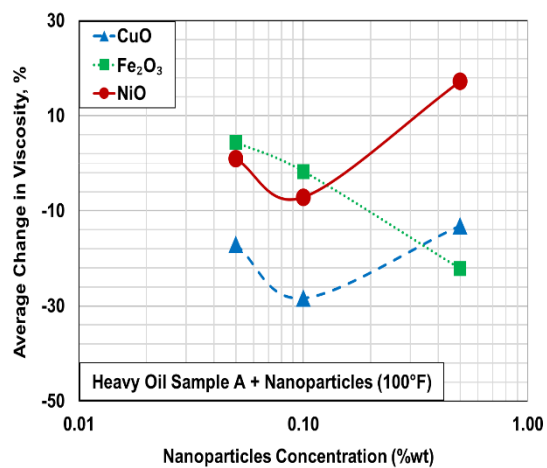
**Table 7.8:** Optimum concentration (% wt.) of nanoparticles at different temperatures

Heavy Oil Sample	Nanoparticles Type	100°F	120°F	140°F	160°F
<b>A</b>	Copper oxide (CuO)	0.10	≥ 0.50	Undetermined*	Undetermined*
	Iron Oxide (Fe <sub>2</sub> O <sub>3</sub> )	≥ 0.50	≥ 0.50	≥ 0.50	Undetermined*
	Nickel Oxide (NiO)	0.10	0.10	0.10	0.10
<b>B</b>	Copper oxide (CuO)	Undetermined*	0.10	≥ 0.50	≥ 0.50
	Iron Oxide (Fe <sub>2</sub> O <sub>3</sub> )	0.10	0.10	0.10	0.10
	Nickel Oxide (NiO)	0.10	0.10	0.10	0.10

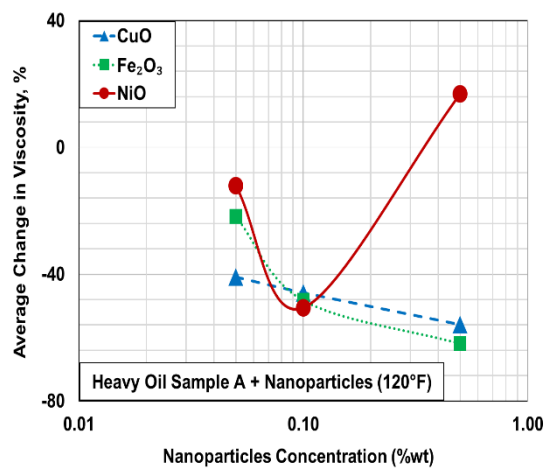
\* Variation in viscosity with change in concentration was less than reproducibility error

Summary of optimum concentration determined in the present study are listed in **Table 7.8**. Optimum concentration was determined by plotting an average percentage change in viscosity as a function of particle concentration (see **Figs. 7.19 and 7.20**).

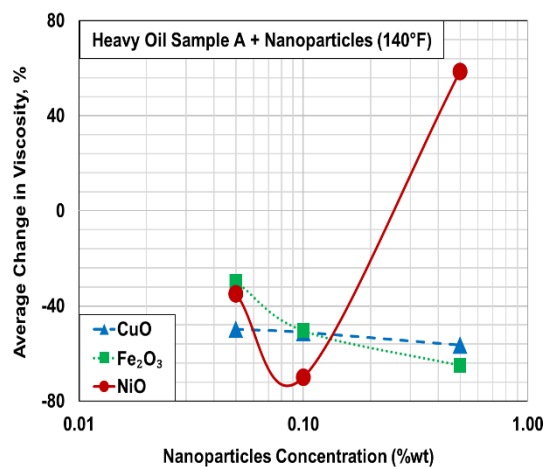
Results obtained confirm the dependence of optimum concentration on metal type, temperature and oil composition. Moreover, it was observed that the optimum point moves toward higher concentration as temperature is increased. With increase in temperature, the thermal upgradation of heavier compounds becomes more dominant. Additionally, rate of exothermic chemical reaction also increases. These two mechanisms suppress viscosity increment caused by particle suspension. At high temperature (>200-300°F), aquathermolysis becomes the most dominant process and hence, the effect of particle concentration diminishes.



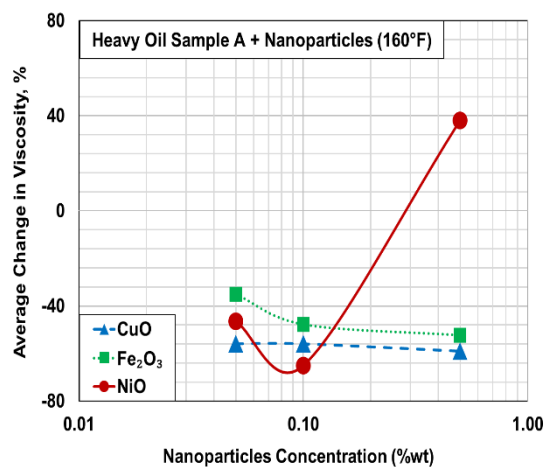
(a)



(b)

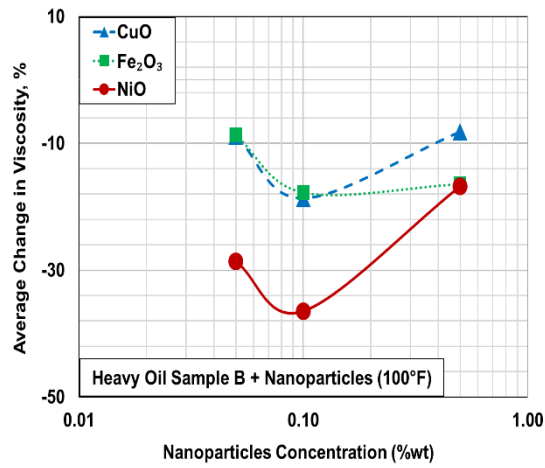


(c)

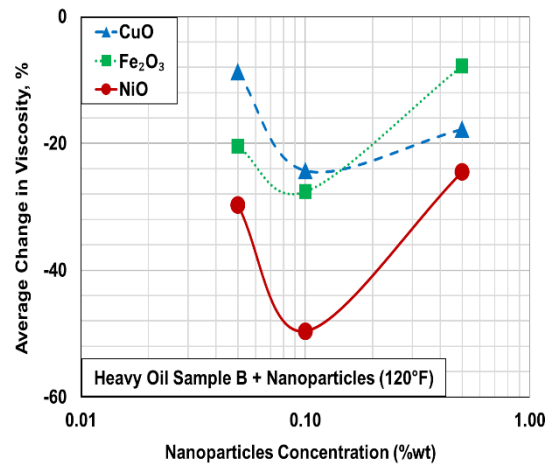


(d)

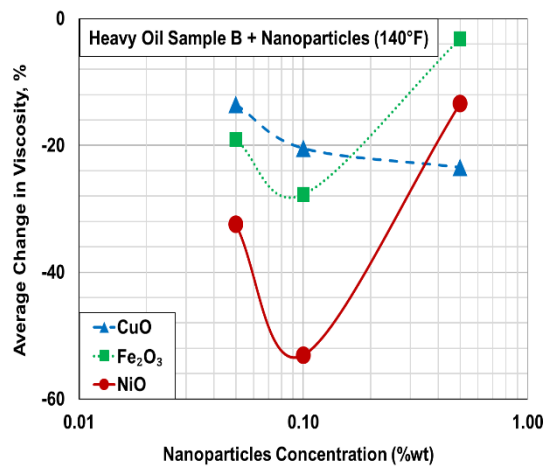
**Figure 7.19:** Percentage change in viscosity of heavy oil Sample A as a function of nanoparticle concentration at (a) 100°F, (b) 120°F, (c) 140°F, and (d) 160°F



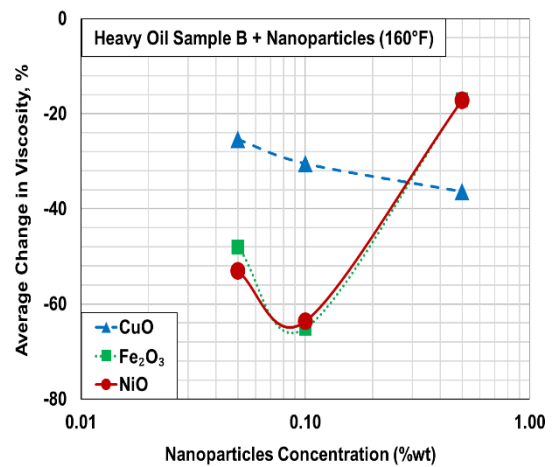
(a)



(b)



(c)



(d)

**Figure 7.20:** Percentage change in viscosity of heavy oil Sample B as a function of nanoparticle concentration at (a) 100°F, (b) 120°F, (c) 140°F, and (d) 160°F

Interestingly, unlike copper oxide and iron oxide; nickel oxide particles exhibited a marked difference in performance of all three concentrations. For example, in case of Sample A, at 120°F, 0.05 wt% concentration led to slight decrease in viscosity (12%). Concentration of 0.1 wt% yielded viscosity reduction of 51%, and high concentration of 0.5 wt% had adverse effect and increased the viscosity by 17%. This remarkable trend observed with nickel oxide indicates presence of some unknown molecular level reactions other than those discussed so far. Further research at molecular level from chemistry point of view is essential to understand the mechanisms responsible for this behavior.

As can be observed from **Table 7.8**, concentration of 0.1 wt% was the most common optimum point. This results match with those observed by Shokrlu et al. (2014). In some cases, such as with iron oxide in Sample A and copper oxide in Sample B; decreasing trend in viscosity was observed with increase in concentration. Since, concentration higher than 0.5 wt% has not been investigated in the present work, it is reasonable to assume that the optimum point lies at or beyond 0.5 wt% concentration.

### **7.3 Effect of S/W Emulsion**

In this section, viscosity reduction achieved with solvent-in-water (S/W) emulsion is discussed. Composition of S/W emulsion used and procedure for preparing it, is provided in **Section 6.3.2**. S/W emulsion was mixed with heavy oil sample in four different volumetric ratios (5, 10, 15, and 20%) and rheology of resultant emulsion was examined.

### **7.3.1 Rheological Behavior**

Power law parameter - fluid behavior index ( $n$ ), was employed to characterize rheological behavior of resultant heavy oil emulsion. Because of experimental error and artificial shear-thinning induced by viscous heating; ' $n$ ' values of 0.9 to 1.1 were considered to be an indicative of Newtonian behavior. Presence of shear-thinning was acknowledged only if ' $n$ ' value was less than 0.9. Fluid behavior indices for various volume fraction of S/W emulsion and temperature are presented in **Tables 7.9 to 7.12**.

#### ***7.3.1.1 5 and 10 vol% Emulsion***

At these low volume fractions of S/W emulsion, practically no change was observed in original rheological behavior of oil samples. Most of the samples exhibited ' $n$ ' values greater than 0.9 at all temperatures indicating highly Newtonian behavior. It can be clearly observed in the **Tables 7.9 and 7.10** that in general, increase in temperature resulted in strengthening of Newtonian behavior.

#### ***7.3.1.2 15 vol% Emulsion***

Addition of 15 vol% S/W emulsion had different effect on both heavy oil samples. As shown in **Table 7.11**, in case of heavy oil sample A, slight shear thinning property was observed at low temperature of 100 and 120°F. With increase in temperature, Newtonian behavior progressively became more prominent.

Unlike Sample A, addition of 15 vol% S/W emulsion in Sample B resulted in significant change in rheological behavior. ' $n$ ' values dropped below 0.5 and the fluid displayed



highly shear thinning behavior. Interestingly, unlike 5 and 10 vol% emulsions, increase in temperature resulted in further increase in pseudo-plastic behavior.

**Table 7.9:** Power law parameters of heavy oil emulsions containing 5 vol% S/W emulsion

Temperature, °F	Heavy Oil Sample A + 5 vol% S/W Emulsion			Heavy Oil Sample B + 5 vol% S/W Emulsion		
	n	K <sub>v</sub>	Shear Rate Range, s <sup>-1</sup>	n	K <sub>v</sub>	Shear Rate Range, s <sup>-1</sup>
100	0.9013	1.2215	0.8 to 33.53	0.8788	2.7306	0.8 to 8.05
120	0.857	0.7168	0.8 to 80.46	0.8777	1.5548	0.8 to 26.82
140	0.8994	0.205	0.8 to 80.46	0.8338	0.8764	0.8 to 80.46
160	0.9715	0.0328	0.8 to 80.46	0.9167	0.2101	0.8 to 80.46

\* n is fluid behavior index (dimensionless) and K<sub>v</sub> is consistency index (lbf.s<sup>n</sup>/ft<sup>2</sup>)  
 \*\* At low temperatures, because of high viscosity, current spring-bob configuration did not permit shear stress measurements over the desired shear rate range of 0.8 to 80.46 s<sup>-1</sup>

**Table 7.10:** Power law parameters of heavy oil emulsions containing 10 vol% S/W emulsion

Temperature, °F	Heavy Oil Sample A + 10 vol% S/W Emulsion			Heavy Oil Sample B + 10 vol% S/W Emulsion		
	n	K <sub>v</sub>	Shear Rate Range, s <sup>-1</sup>	n	K <sub>v</sub>	Shear Rate Range, s <sup>-1</sup>
100	0.8505	1.1257	0.8 to 53.64	0.8528	2.7487	0.8 to 8.05
120	0.8409	0.6163	0.8 to 80.46	0.8477	1.711	0.8 to 21.46
140	0.9181	0.1662	0.8 to 80.46	0.8121	0.8327	0.8 to 80.46
160	0.9543	0.033	0.8 to 80.46	0.9335	0.1307	0.8 to 80.46

\* n is fluid behavior index (dimensionless) and K<sub>v</sub> is consistency index (lbf.s<sup>n</sup>/ft<sup>2</sup>)  
 \*\* At low temperatures, because of high viscosity, current spring-bob configuration did not permit shear stress measurements over the desired shear rate range of 0.8 to 80.46 s<sup>-1</sup>

**Table 7.11:** Power law parameters of heavy oil emulsions containing 15 vol% S/W emulsion

Temperature, °F	Heavy Oil Sample A + 15 vol% S/W Emulsion			Heavy Oil Sample B + 15 vol% S/W Emulsion		
	n	K <sub>v</sub>	Shear Rate Range, s <sup>-1</sup>	n	K <sub>v</sub>	Shear Rate Range, s <sup>-1</sup>
100	0.806	1.1824	0.8 to 60.35	0.4406	0.8976	0.8 to 8.05
120	0.8653	0.4375	0.8 to 80.46	0.4439	0.6598	0.8 to 21.46
140	0.9208	0.1367	0.8 to 80.46	0.3658	0.679	0.8 to 80.46
160	0.9866	0.0266	0.8 to 80.46	0.3399	0.4198	0.8 to 80.46

\* n is fluid behavior index (dimensionless) and K<sub>v</sub> is consistency index (lbf.s<sup>n</sup>/ft<sup>2</sup>)  
 \*\* At low temperatures, because of high viscosity, current spring-bob configuration did not permit shear stress measurements over the desired shear rate range of 0.8 to 80.46 s<sup>-1</sup>

**Table 7.12:** Power law parameters of heavy oil emulsions containing 20 vol% S/W emulsion

Temperature, °F	Heavy Oil Sample A + 20 vol% S/W Emulsion			Heavy Oil Sample B + 20 vol% S/W Emulsion		
	n	K <sub>v</sub>	Shear Rate Range, s <sup>-1</sup>	n	K <sub>v</sub>	Shear Rate Range, s <sup>-1</sup>
100	0.5606	0.2751	0.8 to 80.46	0.5640	0.3858	0.8 to 8.05
120	0.5638	0.1726	0.8 to 80.46	0.5374	0.3396	0.8 to 21.46
140	0.5115	0.132	0.8 to 80.46	0.5533	0.2047	0.8 to 80.46
160	0.5672	0.0435	0.8 to 80.46	0.5476	0.0865	0.8 to 80.46

\* n is fluid behavior index (dimensionless) and K<sub>v</sub> is consistency index (lbf.s<sup>n</sup>/ft<sup>2</sup>)  
 \*\* At low temperatures, because of high viscosity, current spring-bob configuration did not permit shear stress measurements over the desired shear rate range of 0.8 to 80.46 s<sup>-1</sup>

### 7.3.1.3 20 vol% Emulsion

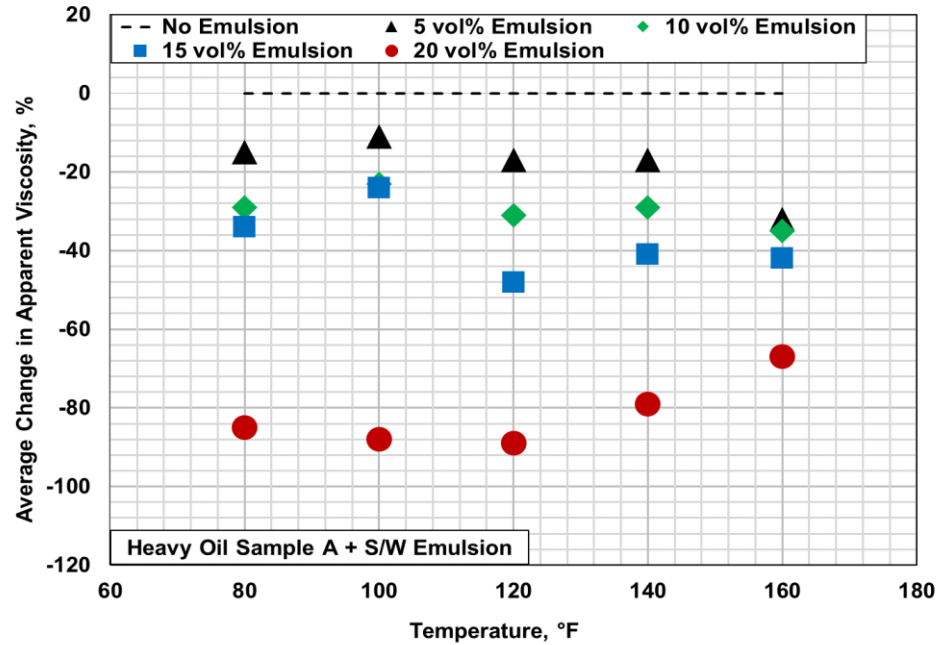
As shown in **Table 7.12**, addition of 20 vol% S/W emulsion yielded identical results in both heavy oil samples. Because of high water fraction, the fluid samples demonstrated high shear thinning behavior. In case of Sample A, the data was not clear enough to make conclusive comment on trends. However, in case of Sample B, increasing non-Newtonian behavior was observed with increase in temperature.

### 7.3.2 Viscosity Reduction

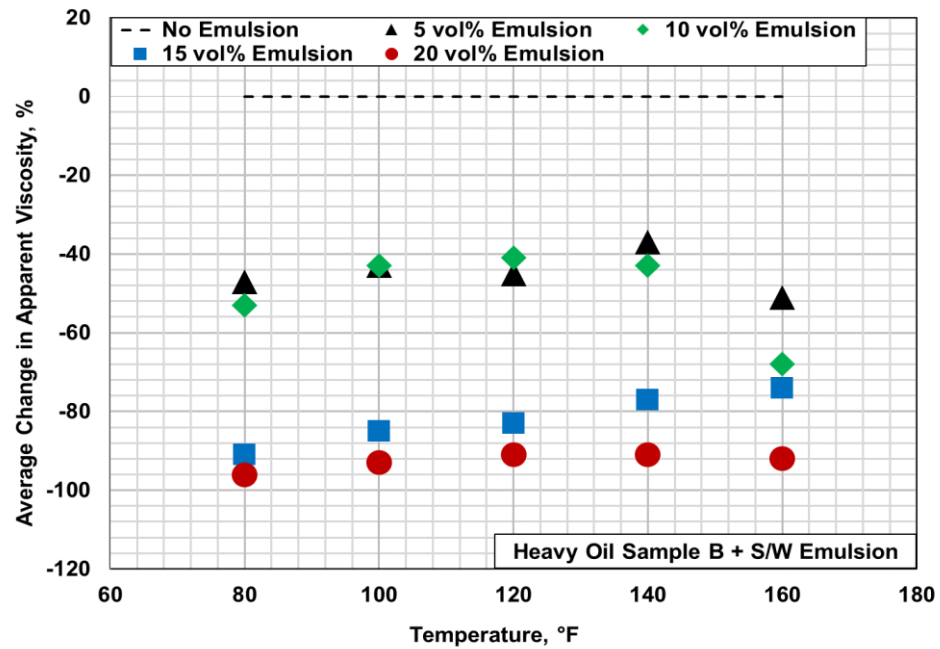
Because of non-Newtonian behavior exhibited by 15 and 20 vol% emulsions, the apparent viscosity of fluid varies significantly with shear rate. Therefore, Newtonian viscosity term cannot be employed to compare performance of different volume fractions of S/W emulsion. Interestingly, it was observed that the percentage reduction in apparent viscosity remained practically constant regardless of shear rate. Viscosity alteration achieved with S/W emulsion is summarized in **Table 7.13**.

**Table 7.13:** Summary of average viscosity reduction caused by S/W emulsion

Heavy Oil Sample	S/W Emulsion to Oil Volume Ratio (%vol)	Average Change in Apparent Viscosity (%)			
		100°F	120°F	140°F	160°F
A	5.00	-10.96	-17.02	-17.06	-31.78
	10.00	-22.64	-30.82	-28.93	-35.01
	15.00	-24.25	-48.10	-41.06	-42.26
	20.00	-88.21	-88.95	-79.16	-67.44
B	5.00	-42.52	-44.96	-37.12	-50.84
	10.00	-42.67	-40.84	-42.92	-67.79
	15.00	-84.90	-83.19	-76.80	-73.98
	20.00	-93.43	-90.89	-91.14	-92.18



**Figure 7.21:** Average reduction in apparent viscosity of heavy oil sample A caused by varying volume fraction of S/W emulsion as a function of temperature



**Figure 7.22:** Average reduction in apparent viscosity of heavy oil sample B caused by varying volume fraction of S/W emulsion as a function of temperature

As expected, increasing volume fraction of S/W emulsion also improves viscosity reduction. The trend can be clearly visualized in **Figs. 7.21 and 7.22**. By observing the comparison provided in **Table 7.13**, it can be observed that, for the same volume fraction of base emulsion, viscosity reduction was more significant in case of heavy oil Sample B than Sample A. For 5, 10 and 15 vol%, approximately 3 to 4 times more reduction was observed with Sample B in comparison to Sample A. With 20 vol% emulsion, remarkable viscosity reduction of 88% and 93% was achieved for both samples, even at room temperature.

The viscosity reduction achieved can be attributed to two mechanisms: (i) dissolution of heavier components by xylene solvent present in S/W emulsion, and (ii) presence of surfactant helps lower interfacial tension, and generate emulsion by dispersing water droplets within oil sample, resulting in decreased bulk viscosity. Unlike nanoparticles, the performance of emulsion did not vary significantly with temperature. Since, Sample B is about 5 times more viscous than Sample A, it is reasonable to assume that its asphaltene content is considerably higher. Therefore, the effect of above two mechanisms would be more prominent and hence more viscosity reduction.

Considering small volume fraction of water in comparison to oil, it is reasonable to assume that the resultant heavy oil emulsion is water-in-oil type emulsion. It was confirmed by dilution test as well. Had it been oil-in-water type emulsion, an addition of extra water would not remain immiscible. Emulsion samples were visually observed over the period of 15 days. As expected, no sign of water and oil phase separation was

observed, confirming good stability of emulsion. Furthermore, emulsion samples were also visually checked for viscosity.

Ideally, to monitor changes in viscosity of emulsion samples with time, the viscometer should have been employed. However, once a rheology test was conducted, out of 165 ml of sample, only about 130-140 ml sample could be recovered. The rest would remain adhered to rotor, bob, temperature sensor and walls of viscometer cup. The amount of oil recovered would not be sufficient enough to run another viscometry test. Besides, a total volume of heavy oil samples available for this study was also limited and hence, only 170 ml of fluid samples were prepared for each test. Because of these reasons, the viscosity was visually inspected.

#### **7.4 Effect of S/W Emulsion Containing Nanoparticles**

This section discusses the effects observed upon mixing S/W emulsion containing nanoparticles with heavy oil. Amount of S/W emulsion used was 5 and 10 vol% of oil while nanoparticle concentration used was 0.002 wt% of oil. Selection of these concentration was purely based on economic point of view. More detailed discussion on the cost analysis for all test fluids, is provided in **Section 7.5**.

##### **7.4.1 Heavy Oil Nano-Emulsion Containing Copper Oxide Nanoparticles**

Effect of S/W emulsion containing copper oxide nanoparticles on fluid behavior indices of both heavy oil samples, is presented in **Tables 7.14 and 7.15**. Addition of copper oxide to base emulsion did not lead to significant changes in rheological behavior of resultant heavy oil emulsion. In almost all instances, the calculated values of ‘n’ were above 0.9,

indicating Newtonian behavior. Except for few aberrant data points, in general, Newtonian behavior increased with increasing temperature and decreased with increasing shear rate.

Average percentage change in apparent viscosity observed for heavy oil nano-emulsions in comparison to original oil samples and heavy oil emulsions is presented in **Figs. 7.23 and 7.24**. In general, the apparent viscosity of these heavy oil nano-emulsions were 20 to 60% less than the original oil samples.

Interestingly, in case of Sample A, addition of CuO nanoparticles helped further reduced viscosity of heavy oil emulsions. With the exception of one data point, 5% nano-emulsion exhibited 5 to 20 % less viscosity than 5% emulsion. In case of 10% nano-emulsion this reduction was as high as 30%. In case of sample B, the results appear to follow the same trend. However, data points are not distinct enough to make any conclusive remark.

This marked improvement in viscosity reduction may be attributed to a combination of three independent processes: (i) because of nonionic nature of surfactant molecules, it is reasonable to assume that CuO particles do not interact with them. Hence, CuO particles may have worked independently. Because of strongly negative zeta potential (-72 mV at pH of 7), CuO particles attract positively charged asphaltene molecules. Aggregation of these heavier compounds reduces bulk viscosity (ii) dissolution of heavier components by xylene solvent, and (iii) reduction in interfacial tension and emulsification caused by surfactant molecules. Further investigation at molecular level is necessary to confirm

above hypothesis or to understand exact nature of mechanisms responsible for this compound effect of nanoparticles and S/W emulsion on heavy oil viscosity.

**Table 7.14:** Power law parameters of heavy oil nano-emulsions containing 5 vol% S/W emulsion and 0.002 wt% copper oxide nanoparticles

Temperature, °F	Heavy Oil Sample A + 5 vol% S/W Emulsion + 0.002 wt% CuO			Heavy Oil Sample A + 5 vol% S/W Emulsion + 0.002 wt% CuO		
	n	K <sub>v</sub>	Shear Rate Range, s <sup>-1</sup>	n	K <sub>v</sub>	Shear Rate Range, s <sup>-1</sup>
100	0.806	1.1824	0.8 to 60.35	0.4406	0.8976	0.8 to 8.05
120	0.8653	0.4375	0.8 to 80.46	0.4439	0.6598	0.8 to 21.46
140	0.9208	0.1367	0.8 to 80.46	0.3658	0.679	0.8 to 80.46
160	0.9866	0.0266	0.8 to 80.46	0.3399	0.4198	0.8 to 80.46

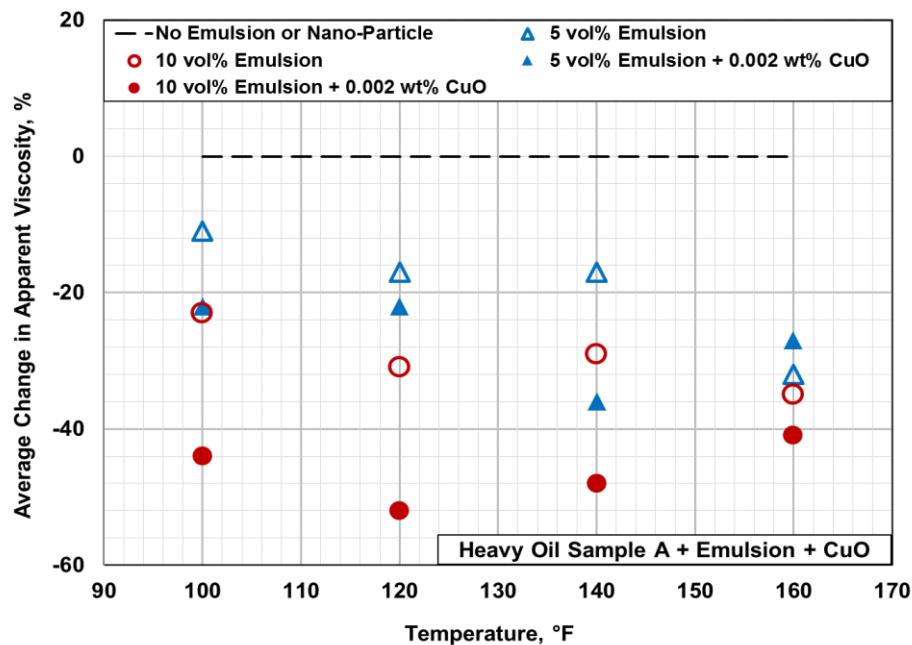
\* n is fluid behavior index (dimensionless) and K<sub>v</sub> is consistency index (lbf.s<sup>n</sup>/ft<sup>2</sup>)  
 \*\* At low temperatures, because of high viscosity, current spring-bob configuration did not permit shear stress measurements over the desired shear rate range of 0.8 to 80.46 s<sup>-1</sup>

**Table 7.15:** Power law parameters of heavy oil nano-emulsions containing 10 vol% S/W emulsion and 0.002 wt% copper oxide nanoparticles

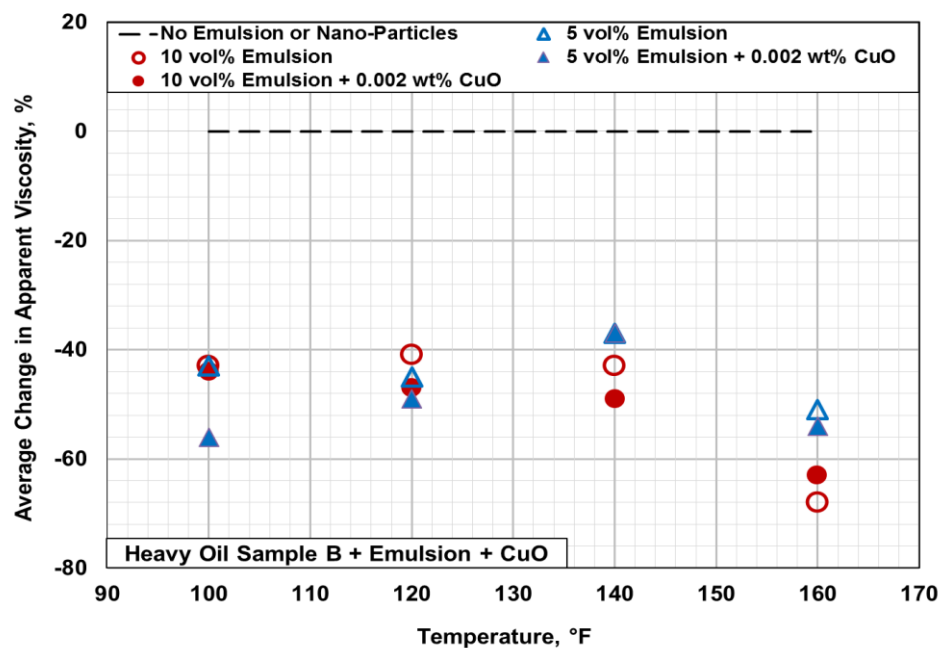
Temperature, °F	Heavy Oil Sample A + 10 vol% S/W Emulsion + 0.002 wt% CuO			Heavy Oil Sample A + 10 vol% S/W Emulsion + 0.002 wt% CuO		
	n	K <sub>v</sub>	Shear Rate Range, s <sup>-1</sup>	n	K <sub>v</sub>	Shear Rate Range, s <sup>-1</sup>
100	0.8442	0.8194	0.8 to 40.23	0.8321	2.7309	0.8 to 16.09
120	0.8858	0.3823	0.8 to 80.46	0.8385	1.5498	0.8 to 33.53
140	0.9166	0.122	0.8 to 80.46	0.8285	0.7274	0.8 to 80.46
160	0.9745	0.0281	0.8 to 80.46	0.9181	0.1582	0.8 to 80.46

\* n is fluid behavior index (dimensionless) and K<sub>v</sub> is consistency index (lbf.s<sup>n</sup>/ft<sup>2</sup>)  
 \*\* At low temperatures, because of high viscosity, current spring-bob configuration did not permit shear stress measurements over the desired shear rate range of 0.8 to 80.46 s<sup>-1</sup>





**Figure 7.23:** Effect of S/W emulsion containing copper oxide nanoparticles on viscosity of heavy oil sample A



**Figure 7.24:** Effect of S/W emulsion containing copper oxide nanoparticles on viscosity of heavy oil sample B

#### 7.4.2 Heavy Oil Nano-Emulsion Containing Iron Oxide Nanoparticles

Rheological behavior of heavy oil nano-emulsion containing iron oxide particles was observed to be the same as that of original oil samples. The trends and values of fluid behavior index 'n' were similar to that obtained with nano-emulsion containing copper oxide. As can be observed from **Tables 7.16 and 7.17**, Newtonian characteristic of the fluid samples improved with increase in temperature.

As far as viscosity alteration is concerned, an addition of iron oxide nanoparticles to the base emulsion did not improve viscosity reduction. As can be observed from **Fig. 7.25**, in case of heavy oil sample A, 10 vol% nano-emulsion provided a similar performance as 10 vol% emulsion. In case of 5 vol% emulsion, an addition of  $\text{Fe}_2\text{O}_3$  had adverse effect and resulted in increment in viscosity. As shown in **Fig. 7.26**, in the case of sample B, viscosity reduction observed with nano-emulsion was almost similar to that of emulsion having no nanoparticles. In short, iron oxide particles had adverse effects if any at all, on performance of S/W emulsion.

It is challenging to comment on exact mechanisms responsible for this interesting behavior just based on rheology tests, without studying molecular level interactions. Nevertheless, based on the limited information available, three possible explanations can be presented: (i) iron oxide particles are characterized by mildly positive zeta potential (+20 mV at pH of 7). Hence, they have tendency to repel positively charged asphaltene molecules and hence, negate Ostwald ripening effect. In this case, S/W emulsion would perform better in absence of  $\text{Fe}_2\text{O}_3$ , (ii) phenomena of micellar entanglement (see **Section**

5.1), can be another possible reason for increase in viscosity, and (iii) in S/W emulsion, iron oxide particles may have interacted at the interface of xylene and water. This might have restricted xylene droplets from interacting with and dissolving heavier compounds.

**Table 7.16:** Power law parameters of heavy oil nano-emulsions containing 5 vol% S/W emulsion and 0.002 wt% iron oxide nanoparticles

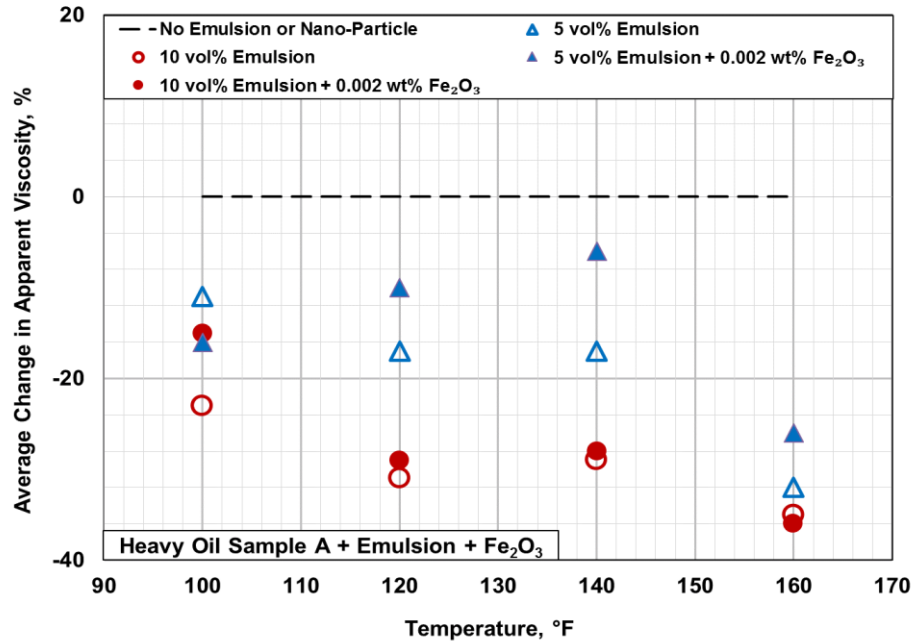
Temperature, °F	Heavy Oil Sample A + 5 vol% S/W Emulsion + 0.002 wt% Fe <sub>2</sub> O <sub>3</sub>			Heavy Oil Sample A + 5 vol% S/W Emulsion + 0.002 wt% Fe <sub>2</sub> O <sub>3</sub>		
	n	K <sub>v</sub>	Shear Rate Range, s <sup>-1</sup>	n	K <sub>v</sub>	Shear Rate Range, s <sup>-1</sup>
100	0.8442	0.8194	0.8 to 40.23	0.8321	2.7309	0.8 to 16.09
120	0.8858	0.3823	0.8 to 80.46	0.8385	1.5498	0.8 to 33.53
140	0.9166	0.122	0.8 to 80.46	0.8285	0.7274	0.8 to 80.46
160	0.9745	0.0281	0.8 to 80.46	0.9181	0.1582	0.8 to 80.46

\* n is fluid behavior index (dimensionless) and K<sub>v</sub> is consistency index (lbf.s<sup>n</sup>/ft<sup>2</sup>)  
 \*\* At low temperatures, because of high viscosity, current spring-bob configuration did not permit shear stress measurements over the desired shear rate range of 0.8 to 80.46 s<sup>-1</sup>

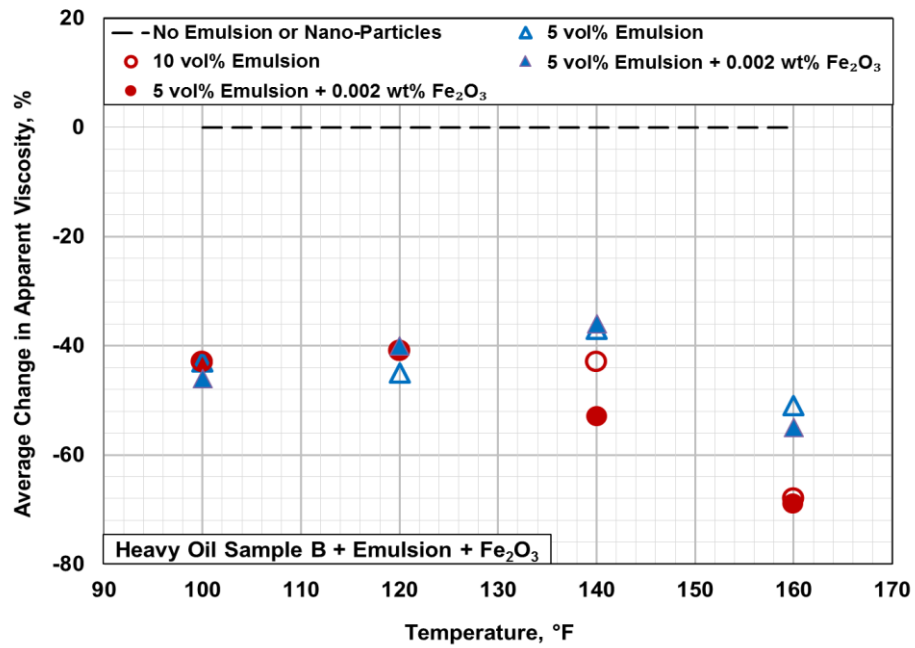
**Table 7.17:** Power law parameters of heavy oil nano-emulsions containing 10 vol% S/W emulsion and 0.002 wt% iron oxide nanoparticles

Temperature, °F	Heavy Oil Sample A + 10 vol% S/W Emulsion + 0.002 wt% Fe <sub>2</sub> O <sub>3</sub>			Heavy Oil Sample A + 10 vol% S/W Emulsion + 0.002 wt% Fe <sub>2</sub> O <sub>3</sub>		
	n	K <sub>v</sub>	Shear Rate Range, s <sup>-1</sup>	n	K <sub>v</sub>	Shear Rate Range, s <sup>-1</sup>
100	0.7951	1.3326	0.8 to 60.35	0.842	2.7573	0.8 to 16.09
120	0.8256	0.6512	0.8 to 80.46	0.8212	1.7503	0.8 to 33.53
140	0.904	0.1752	0.8 to 80.46	0.8278	0.6602	0.8 to 80.46
160	0.9714	0.0313	0.8 to 80.46	0.9294	0.1293	0.8 to 80.46

\* n is fluid behavior index (dimensionless) and K<sub>v</sub> is consistency index (lbf.s<sup>n</sup>/ft<sup>2</sup>)  
 \*\* At low temperatures, because of high viscosity, current spring-bob configuration did not permit shear stress measurements over the desired shear rate range of 0.8 to 80.46 s<sup>-1</sup>



**Figure 7.25:** Effect of S/W emulsion containing iron oxide nanoparticles on viscosity of heavy oil sample A



**Figure 7.26:** Effect of S/W emulsion containing iron oxide nanoparticles on viscosity of heavy oil sample B

### 7.4.3 Heavy Oil Nano-Emulsion Containing Nickel Oxide Nanoparticles

Mixing S/W emulsion containing nickel oxide nanoparticles with the heavy oil samples did not cause any significant change in rheological behavior as indicated by variation in fluid behavior index 'n' (see **Tables 7.18 and 7.19**). In general, the trends are similar to those obtained in case of heavy oil nano-emulsions containing copper oxide or iron oxide. For the same shear rate range, values of 'n' increased with increase in temperature.

Viscosity alteration caused by S/W emulsion containing nickel oxide nanoparticles is graphically presented in **Figs. 7.27 and 7.28**. Interestingly, adding NiO nanoparticles to the S/W emulsion produced different results than those observed with CuO and Fe<sub>2</sub>O<sub>3</sub>. With 5 vol% emulsion, an addition of NiO resulted in increased viscosity while adding the same amount of particles in 10 vol% emulsion resulted in decreased viscosity.

Exact processes behind this interesting behavior can only be hypothesized. While preparing nano-emulsions, nanoparticles were mixed in S/W emulsion first and then added to the oil. Overall amount of nanoparticles added was the same in both 5 and 10 vol% heavy oil nano-emulsion i.e. 0.002 wt% of oil. However, it should be noted that the concentration of NiO in 5 vol% S/W emulsion was twice of that in 10 vol% emulsion, i.e. 0.06 and 0.03 wt% of emulsion respectively. This difference in concentration might have been responsible for opposite effect on viscosity.

In case of 5 vol% S/W emulsion, due to high concentration, van der Waals attraction forces might have overcome electrostatic repulsive forces; resulting in an increased probability of micellar entanglement. This would explain an increase in viscosity. The same amount

of NiO particles, when added to 10 vol% might be more dispersed and would not cause micellar structure to twine together. Moreover, nanoparticles would remain free and cause asphaltene molecules to aggregate, resulting in a reduced bulk viscosity.

**Table 7.18:** Power law parameters of heavy oil nano-emulsions containing 5 vol% S/W emulsion and 0.002 wt% nickel oxide nanoparticles

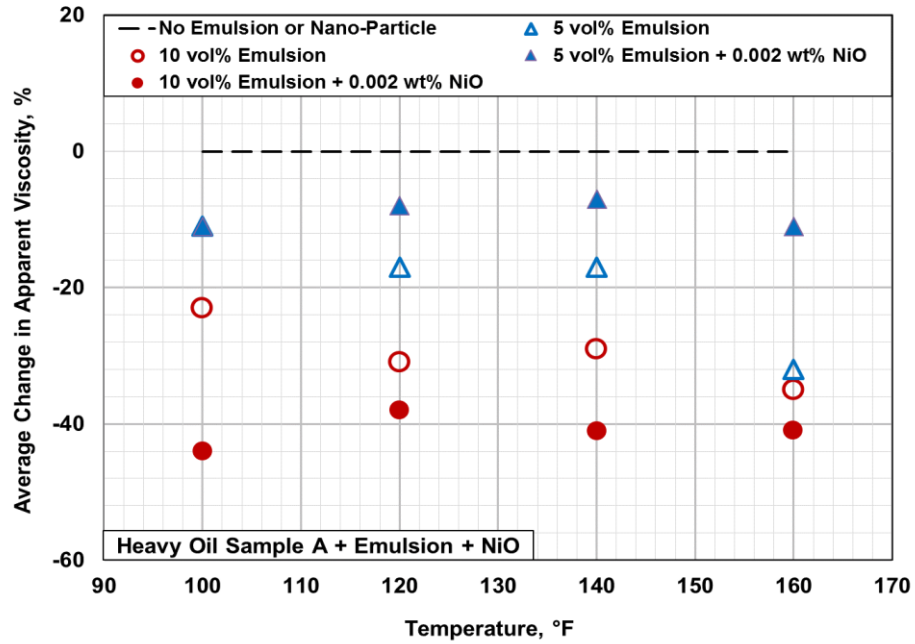
Temperature, °F	Heavy Oil Sample A + 5 vol% S/W Emulsion + 0.002 wt% NiO			Heavy Oil Sample A + 5 vol% S/W Emulsion + 0.002 wt% NiO		
	n	K <sub>v</sub>	Shear Rate Range, s <sup>-1</sup>	n	K <sub>v</sub>	Shear Rate Range, s <sup>-1</sup>
100	0.9148	1.1949	0.8 to 33.53	0.888	2.8689	0.8 to 8.05
120	0.8929	0.743	0.8 to 67.05	0.8674	1.8949	0.8 to 21.46
140	0.9166	0.2193	0.8 to 80.46	0.8278	1.0286	0.8 to 67.05
160	0.9776	0.042	0.8 to 80.46	0.9281	0.1773	0.8 to 80.46

\* n is fluid behavior index (dimensionless) and K<sub>v</sub> is consistency index (lbf.s<sup>n</sup>/ft<sup>2</sup>)  
 \*\* At low temperatures, because of high viscosity, current spring-bob configuration did not permit shear stress measurements over the desired shear rate range of 0.8 to 80.46 s<sup>-1</sup>

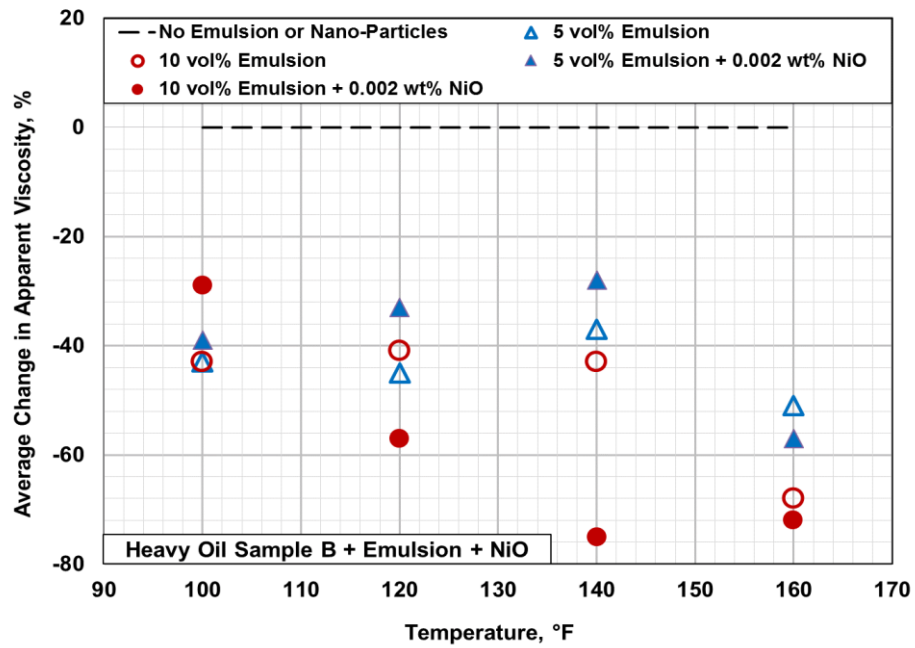
**Table 7.19:** Power law parameters of heavy oil nano-emulsions containing 10 vol% S/W emulsion and 0.002 wt% nickel oxide nanoparticles

Temperature, °F	Heavy Oil Sample A + 10 vol% S/W Emulsion + 0.002 wt% NiO			Heavy Oil Sample A + 10 vol% S/W Emulsion + 0.002 wt% NiO		
	n	K <sub>v</sub>	Shear Rate Range, s <sup>-1</sup>	n	K <sub>v</sub>	Shear Rate Range, s <sup>-1</sup>
100	0.853	0.8036	0.8 to 73.76	0.8441	3.4197	0.8 to 8.05
120	0.8577	0.5288	0.8 to 80.46	0.7885	1.3013	0.8 to 53.64
140	0.9228	0.1363	0.8 to 80.46	0.9052	0.2995	0.8 to 80.46
160	1.0096	0.0251	0.8 to 80.46	0.9305	0.1129	0.8 to 80.46

\* n is fluid behavior index (dimensionless) and K<sub>v</sub> is consistency index (lbf.s<sup>n</sup>/ft<sup>2</sup>)  
 \*\* At low temperatures, because of high viscosity, current spring-bob configuration did not permit shear stress measurements over the desired shear rate range of 0.8 to 80.46 s<sup>-1</sup>



**Figure 7.27:** Effect of S/W emulsion containing nickel oxide nanoparticles on viscosity of heavy oil sample A



**Figure 7.28:** Effect of S/W emulsion containing nickel oxide nanoparticles on viscosity of heavy oil sample B

## 7.5 Economic Analysis

This section provides a simple cost-based economic analysis of test fluids prepared in the present study. Cost of nano-sized particles depends on various factors such as manufacturer, manufacturing process, purity, particle size distribution, particle shape, etc.

**Table 7.20** summarizes the cost of three nano metal oxide particles used in the present work. It can be observed that products with smaller particles, stringent size distribution and high chemical purity exhibit higher cost. Nanoparticles are, in general, highly expensive especially nickel oxide is relatively more expensive than copper oxide and iron oxide. It should be noted that with increase in quantity of order, the cost reduces drastically.

**Table 7.20:** Cost of nano-sized metal oxide particles

Type of nanoparticles	Purity and particles size	Per gram cost in USD for various amount of purchase order				
		5 g	25 g	100 g	500 g	1 kg
<b>Copper (II) Oxide</b>	99%, <80nm	-	1.40	0.55	0.24	0.17
	99%, 40 nm	-	1.40	0.55	0.36	0.25
	99.95%, 25-55nm	10.60	3.44	1.89	0.92	0.80
<b>Iron (III) Oxide</b>	99.5%, 30nm	9.80	3.16	1.59	0.85	0.76
	>98%, 20-40 nm	6.60	2.12	0.73	0.29	0.21
	99%, 20-40nm	5.00	1.80	0.86	0.47	0.36
<b>Nickel (III) Oxide</b>	99.5+%, 15-35 nm	7.60	2.72	1.29	0.66	0.59
	99%, 10-20 nm	7.80	2.48	1.08	0.50	0.49

\* Source: <http://www.us-nano.com/nanopowders>  
 \*\* Nanoparticles used in the present study had size distribution of <50 nm



Cost of chemicals used in preparing solvent-in-brine base emulsion is listed in **Table 7.21**. The cost of preparing one barrel of S/W emulsion is calculated to be \$118. Surfactant is the most expensive chemical that contributes to about 95.5 % of the total cost. The cost of surfactant and xylene used, were based on 1 barrel of purchase quote. For a field application, bulk order would significantly reduce the cost.

**Table 7.21:** Cost of chemicals used in preparing S/W emulsion

<b>Material</b>	<b>Cost</b>
Triton X-100 Surfactant	\$ 3772/bbl
Xylene Solvent	\$ 200/bbl
NaCl	\$ 0.1 / lb
<b>Xylene-in-Brine (S/W) Emulsion</b>	<b>\$ 118/bbl</b>
* Composition of S/W emulsion: 1.8 wt% xylene, 3.2 wt% surfactant and the rest 2% NaCl brine	
** Surfactant makes up 95.5% of total cost	

Estimated cost of all test fluids prepared in this experimental work, along with their viscosity performance, are provided in **Tables 7.22 and 7.23**. Interestingly, for heavy oil Sample A, presence of only nanoparticles provided better viscosity reduction than S/W emulsions or nano-emulsions. However, in case of heavy oil Sample B, S/W emulsion and nano-emulsion exhibited better performance than only nanoparticles.

In the tables, the highlighted rows represent the test fluids that yielded at least 30% viscosity reduction at a cost less than \$25. Value of \$25 may seem high but it should be noted that the cost presented were estimated based on purchase quote of 1 kg for nanoparticles and 1 barrel for chemicals. The cost is bound to decrease notably for field scale purchase orders.

**Table 7.22:** Summary of cost and viscosity performance of all test fluids prepared with heavy oil Sample A

Type of Test Fluid			Cost (USD / bbl of oil)	Average Change in Viscosity (%)			
Nano Particle Type	Nanoparticle concentration (wt%)	S/W Emulsion to Oil Volume Ratio (vol%)		100°F	120°F	140°F	160°F
<b>Copper Oxide (CuO)</b>	0.50	-	< 191	-13	-56	-56	-59
	0.10	-	< 38	-28	-46	-51	-56
	0.05	-	< 19	-17	-41	-50	-56
	0.002	5	< 7	-22	-22	-36	-27
	0.002	10	< 13	-44	-52	-48	-42
<b>Iron Oxide (Fe<sub>2</sub>O<sub>3</sub>)</b>	0.50	-	< 160	-22	-62	-65	-52
	0.10	-	< 32	-2	-48	-50	-48
	0.05	-	< 16	4	-22	-30	-35
	0.002	5	< 7	-16	-10	-6	-26
	0.002	10	< 13	-15	-29	-28	-36
<b>Nickel Oxide (NiO)</b>	0.50	-	< 375	17	17	-7	-11
	0.10	-	< 75	-7	-51	-70	-65
	0.05	-	< 37	1	-12	-35	-46
	0.002	5	< 7	-11	-8	-7	-11
	0.002	10	< 13	-44	-38	-41	-41
-	-	5	< 6	-11	-17	-17	-32
	-	10	< 12	-23	-31	-29	-35
	-	15	< 18	-24	-48	-41	-42
	-	20	< 24	-88	-89	-79	-67
<p>* Cost of nanoparticles and chemicals is based on purchase quote of 1 kg and 1 bbl respectively</p> <p>** Costs would further decrease for field scale bulk orders</p> <p>*** Highlighted test fluids provided at least 30% viscosity reduction at a cost less than \$25</p>							

**Table 7.23:** Summary of cost and viscosity performance of all test fluids prepared with heavy oil Sample B

Type of Test Fluid			Cost	Average Change in Viscosity (%)			
Nano Particle Type	Nanoparticle concentration (wt%)	S/W Emulsion to Oil Volume Ratio (vol%)	(USD / bbl of oil)	100°F	120°F	140°F	160°F
<b>Copper Oxide (CuO)</b>	0.50	-	< 195	-8	-18	-23	-36
	0.10	-	< 39	-19	-24	-20	-30
	0.05	-	< 19	-9	-9	-14	-25
	0.002	5	< 7	-56	-49	-37	-54
	0.002	10	< 13	-44	-47	-49	-63
<b>Iron Oxide (Fe<sub>2</sub>O<sub>3</sub>)</b>	0.50	-	< 164	-16	-8	-3	-17
	0.10	-	< 33	-18	-28	-28	-65
	0.05	-	< 16	-9	-20	-19	-48
	0.002	5	< 7	-46	-40	-36	-55
	0.002	10	< 13	-43	-41	-53	-69
<b>Nickel Oxide (NiO)</b>	0.50	-	< 384	-17	-24	-13	-17
	0.10	-	< 77	-36	-50	-53	-64
	0.05	-	< 38	-29	-30	-32	-53
	0.002	5	< 8	-39	-33	-28	-57
	0.002	10	< 14	-29	-57	-75	-73
-	-	5	< 6	-43	-45	-37	-51
	-	10	< 12	-43	-41	-43	-68
	-	15	< 18	-85	-83	-77	-74
	-	20	< 24	-93	-91	-91	-92
<p>* Cost of nanoparticles and chemicals is based on purchase quote of 1 kg and 1 bbl respectively</p> <p>** Costs would further decrease for field scale bulk orders</p> <p>*** Highlighted test fluids provided at least 30% viscosity reduction at a cost less than \$25</p>							

The cost of heat generation is a major constraint on all existing thermal recovery methods. Currently, steam is generated with natural gas, and when the cost of natural gas rises, operating costs rise considerably. At a fuel price of \$6/MMBTU, the cost of steam generation typically ranges from \$17 to \$27/ton (Chaar et al., 2015). This is one of the major reasons why thermal EOR is employed only in reservoirs with thick payzone and high oil in place. One of the approaches to improve economics is to minimize the ratio of barrel of steam injected to barrel of oil produced (SOR). For example, SAGD is about twice as thermally efficient as cyclic steam stimulation for similar cases, with steam-oil ratios that are now approaching two instead of four for cyclic steam method (Speight, 2009).

Use of nanoparticles can improve not only the mobility of heavy oil but also heat transfer efficiency. This would minimize effective steam-oil ratio and as a result may offset additional cost of nanoparticles. Additionally, results of the present study confirm that nanoparticles and solvent based emulsion have the ability to reduce viscosity even at low temperatures. This indicates that application of solvent based emulsion in chemical flooding, with or without nanoparticles, has the potential to provide a cheaper alternative to cost intensive thermal methods.

## 8. Conclusions and Recommendations

This experimental work was focused on investigating three different approaches for reducing viscosity of heavy oil: (i) nano-sized metal oxide particles, (ii) solvent-in-water emulsion, and (iii) solvent based emulsion containing nanoparticles. Major conclusions from this study are as follows.

### 8.1 Conclusions

- Viscosity of heavy oil Sample A varied from 67,702 cP at 80°F to 432 cP at 160°F. Sample B was approximately five times more viscous than Sample A with viscosity of 333,439 cP at 80°F and 2624 cP at 160°F. When characterized by Ostwald-de Waele power law model, both samples displayed fluid behavior index 'n' of greater than 0.9, indicating highly Newtonian behavior.
- Addition of nanoparticles provided notable viscosity reduction. At the optimum nanoparticle concentration, depending on the metal type, viscosity reduction of 59 to 70% and 36 to 65% was achieved for Sample A and Sample B respectively.
- The degree of viscosity reduction was observed to be a function of type of nanoparticles, their concentration, oil composition, and temperature of fluid. In most of the cases, optimum concentration point was observed to occur near 0.1 wt% and shifted towards 0.5 wt% (or more) with increase in temperature.
- Low volume fractions of S/W emulsion i.e. 5 and 10 vol%, did not cause noteworthy change in rheological characteristics of heavy oil samples. Addition of 15 vol% S/W emulsion resulted in development of shear thinning property only in Sample B.

However, in case of 20 vol% S/W emulsion, both samples exhibited significant shear thinning behavior.

- Addition of 5, 10, 15 and 20 vol% S/W emulsion to heavy oil Sample A, reduced its viscosity by approximately 20, 30, 40 and 80% respectively. For Sample B, corresponding viscosity reduction was approximately 45, 50, 80 and 90% respectively. Interestingly, the viscosity reduction remained fairly constant irrespective of fluid temperatures tested.
- Viscosity alteration observed in nano-emulsions strongly depended on type of nanoparticles. Addition of copper oxide nanoparticles to S/W emulsion provided additional viscosity reduction of approximately 10% to 30%. On the other hand, mixing iron oxide nanoparticles with S/W emulsion either had no effect or resulted in increased viscosity. Interestingly, nickel oxide nanoparticles had negative effect on the performance of 5 vol% S/W emulsion, and resulted in viscosity increment. However, the same amount of NiO particles, when added to 10 vol% emulsion, provided additional viscosity reduction of 10% to 30%.
- All the test fluid samples except for those having nanoparticles concentration of 0.1 wt% or more, cost less than \$25 per barrel of oil. Some of the samples provided 40 to 50% viscosity reduction at a cost less than \$16 per barrel of oil. The cost presented were calculated based on purchase quote for small quantity and would reduce significantly for a field scale application.

Remarkable results obtained in this study confirms the efficacy of nanoparticles in improving mobility of highly viscous heavy oil. It reinforces the industry's interest in

developing an economically feasible technique that can efficiently harness the potential of nanoparticles, and replicate these laboratory-scale results in field. Moreover, notable viscosity reduction achieved with S/W emulsion and S/W emulsion containing nanoparticles, rekindles the interest in improving efficiency of non-thermal heavy oil recovery technique such as chemical flooding. This study also lays the foundation for further research in the area of nanoparticles stabilized solvent based emulsion flooding.

## **8.2 Future Work and Recommendations**

The experimental work presented in this document was performed on extremely viscous heavy oil with limited information to begin with. This study helped delineate some of the problems associated with heavy oil viscosity measurement. The viscosity data generated may not be 100% accurate but it certainly helped confirm efficacy of nanoparticles and S/W emulsion. Moreover, the results also helped establish the trends of viscosity variation with change in nanoparticles concentration and temperature.

Following are the recommendations for future work:

- Acquisition, transportation and storage of heavy oil sample should be carefully planned so that the sample remains uncontaminated and representative of reservoir as much as practically possible.
- Considering the presence of viscous heating and high temperature sensitivity of heavy oil viscosity; employ a viscometer capable of providing excellent temperature control; possibly through simultaneous use of a heating and a cooling system.

- Good temperature control would improve reproducibility of viscosity data. This may enable detection of minor viscosity alteration caused by 0.002 wt% nanoparticles. This would provide additional insights into synergistic effects of S/W emulsion and nanoparticles discussed in the present work.
- Concentration of surfactant and solvent in S/W emulsion can also be varied to determine an optimum balance between viscosity reduction and cost.
- Cheaper alternatives of xylene solvent and Triton<sup>TM</sup> X – 100 surfactant can also be explored to improve economics.
- Once enough rheological data has been acquired, core flooding studies should be conducted to understand efficiency of in-situ emulsification and estimate enhancement in oil recovery. Investigating interfacial tension between heavy oil and S/W emulsion would also support analysis of core-flooding performance.
- Possibility of introducing nanoparticles into the reservoir by viscosified water flooding can also be investigated by conducting core flooding experiments.



## Nomenclature

$k_{eff}$	Thermal conductivity of fluid in presence of nanoparticles, W/mK
$k_f$	Thermal conductivity of fluid, W/mK
$k_p$	Thermal conductivity of nanoparticles, W/mK
$k_{rd}$	Relative permeability of displacing fluid, mD
$k_{ro}$	Relative permeability of oil, mD
$n$	Fluid behavior index, dimensionless
$s$	Empirical shape factor, dimensionless
$v$	Darcy velocity of displacing fluid, m/s
$K_v$	Viscometer consistency index, lbf.s <sup>n</sup> /ft <sup>2</sup>
$M$	Mobility Ratio, dimensionless
$N_c$	Capillary number, dimensionless

### Greek Symbols:

$\alpha$	Volume fraction of nanoparticles in fluid, dimensionless
$\gamma$	Shear Rate, s <sup>-1</sup>
$\eta$	Viscosity of nano-suspension, cP
$\eta_0$	Viscosity of carrier fluid, cP
$\mu$	Newtonian Viscosity, cP
$\mu_a$	Apparent viscosity, cP
$\mu_d$	Viscosity of displacing fluid, Pa.s
$\mu_o$	Viscosity of oil, Pa.s
$\sigma$	Interfacial tension, N/m
$\tau$	Shear Stress, lbf/ft <sup>2</sup>
$\phi$	Volume fraction of solid in suspension, dimensionless
$\Psi$	Sphericity of particles, dimensionless

## References

- Akeredolu, B. 2014. *Rheological Characterization of Alaska Heavy Oils*. Master's Thesis. Colorado School of Mines. Golden, CO.
- Akstinat, M. H. 1981. *Surfactants for EOR Process in High-Salinity System: Product Selection and Evaluation*, F. J. Fayers (ed). New York, Elsevier.
- Alkandari, H., Alomair, O., and Elsharkawy, A. 2012. *Heavy Oil Viscosity Measurements; Accuracy, Reliability, and Repeatability*. Society of Petroleum Engineers. <http://dx.doi.org/10.2118/160879-MS>.
- Alomair, O. A., Matar, K. M., and Alsaeed, Y. H. 2014. *Nanofluids Application for Heavy Oil Recovery*. Society of Petroleum Engineers. <http://dx.doi.org/10.2118/171539-MS>.
- Amanullah, Md., Al-Arfaj, M. K., and Al-Abdullatif, Z. 2011. *Preliminary Test Results of Nano-Based Drilling Fluids for Oil and Gas Field Applications*. Paper SPE/IADC 139534 presented at the SPE/IADC Drilling Conference and Exhibition, Amsterdam, The Netherlands, 1-3 March.
- Argillier, J. F., Coustet, C., and Henaut, I. 2002. *Heavy Oil Rheology as a Function of Asphaltene and Resin Content and Temperature*. Society of Petroleum Engineers. <http://dx.doi.org/10.2118/79496-MS>.
- Binder, G. G. Jr. and Russel, C. D. 1965. *Method of Secondary Recovery*. U.S. Patent #3208517, 28 September.
- Berlin, J. M., Yu, J., Lu, W. et al. 2011. *Engineer Nanoparticles for Hydrocarbon Detection in Oil-Field Rocks*. Paper SPE 141528 presented at the SPE International Symposium on Oilfield Chemistry, The Woodlands, Texas, USA, 11-13 April.
- Bryan, J. and Kantzas, A. 2007. *Enhanced Heavy-Oil Recovery by Alkali-Surfactant Flooding*. Paper SPE 110738-MS presented at the SPE Annual Technical Conference and Exhibition, Anaheim, California, USA, 11-14 November.
- Bryan, J., Mai, A., and Kantzas, A. 2008. *Investigation into the Processes Responsible for Heavy Oil Recovery by Alkali-Surfactant Flooding*. Paper SPE 113993-MS presented at the SPE/DOE Symposium on Improved Oil Recovery, Tulsa, Oklahoma, USA, 20-23 April.
- Bousaid, I. S. 1978. *Oil Recovery Process Using an Emulsion Slug with Tapered Surfactant Concentration*. U.S. Patent #4074759. February 21.

- Chaar, M., Venetos, M., Dargin, J. et al. 2015. *Economics of Steam Generation For Thermal Enhanced Oil Recovery*. Society of Petroleum Engineers. doi:10.2118/172004-PA.
- Chen, X. 2006. *Heavy Oils, Part 1*. SIAM News, Society of Industrial and Applied Mathematics. 393.
- Clark, P. D. and Hyne, J.B. 1984. *Steam-oil chemical reactions: mechanisms for the aquathermolysis of heavy oils*. AOSTRA J. Res. 1 1, 15–20.
- Clark, P. D., Clarke, R.A., Hyne, J.B. et al. 1990. *Studies on the effect of Metal Species on Oil Sands Undergoing Steam Treatments*. AOSTRA J Res 6 1: pp. 53-64.
- Crews, J. B. and Huang, T. 2008. *Performance Enhancements of Viscoelastic Surfactant Stimulation Fluids with Nanoparticles*. Society of Petroleum Engineers. <http://dx.doi.org/10.2118/113533-MS>.
- Crews, J. B. and Gomaa, A. M. 2012. *Nanoparticle Associated Surfactant Micellar Fluids: An Alternative to Crosslinked Polymer Systems*. Society of Petroleum Engineers. <http://dx.doi.org/10.2118/157055-MS>.
- Dion, M. 2011. *Modelling the Rheology of Complex Fluids: Cases of Bitumen and Heavy Oils at Low Temperatures*. Masters Thesis. University of Alberta. Edmonton, Alberta, Canada.
- El-Diasty, A. I. and Aly, A. M. 2015. *Understanding the Mechanism of Nanoparticles Applications in Enhanced Oil Recovery*. Society of Petroleum Engineers. <http://dx.doi.org/10.2118/175806-MS>.
- El-Kemary, M. Nagy, N, and El-Mehasseb, I. 2013. *Nickel oxide nanoparticles: Synthesis and spectral studies of interactions with glucose*, *Materials Science in Semiconductor Processing*, Volume 16, Issue 6, Pages 1747-1752, ISSN 1369-8001, <http://dx.doi.org/10.1016/j.mssp.2013.05.018>.
- Fakoya, M. F. and Shah, S. N. 2013. *Rheological Properties of Surfactant Based and Polymeric Nano-Fluids*. Paper SPE 163921, presented at the SPE Coiled Tubing and Well Intervention Conference and Exhibition, Woodlands, Texas, USA, 26-27 March.
- Fakoya, M. F. and Shah, S. N. 2016. *Relative Viscosity of Hydraulic Fracturing Fluids Containing Nanoparticles*. Paper SPE 180458 MS, presented at the SPE Western Regional Meeting, Anchorage, Alaska, USA, 23-26 May.
- Fan, H., Liu, Y., Zhang, L. et al. 2002. *The Study on Composition Changes of Heavy Oils during Steam Stimulation Processes*. Fuel 81 13: pp. 1733-1738.

Fan, H., Zhang, Y., and Lin, Y. 2004. *The Catalytic Effects of Minerals on Aquathermolysis of Heavy Oil*. Fuel 83 14-15: pp. 2035-2039.

Farooqui, J., Babadagli, T., and Li, H. A. 2015. *Improvement of the Recovery Factor Using Nano-Metal Particles at the Late Stages of Cyclic Steam Stimulation*. Society of Petroleum Engineers. <http://dx.doi.org/10.2118/174478-MS>.

Green, D. and Willhite, G. 1998 *Enhanced Oil Recovery*. Society of Petroleum Engineers Textbook Series Vol. 6. ISBN: 978-1-55563-077-5. Richardson, Texas.

Greff, J. and Babadagli, T. 2011. *Catalytic Effects of Nano-Size Metal Ions in Breaking Asphaltene Molecules during Thermal Recovery of Heavy-Oil*. Society of Petroleum Engineers. <http://dx.doi.org/10.2118/146604-MS>.

Hascakir, B. 2008. *Investigation of Productivity of Heavy Oil Carbonate Reservoirs and Oil Shales Using Electrical Heating Methods*. Master's Thesis. Middle East Technical University. Ankara, Turkey.

Hascakir, B., Babadagli, T., and Akin, S. 2010. *Experimental and Numerical Modeling of Heavy-Oil Recovery by Electrical Heating*. Paper SPE 117669 presented at the International Thermal Operations and Heavy Oil Symposium, Calgary Canada.

Helgeson, M. E., Hodgdon, T. K., Kaler, E. W. et al. 2010. *Formation and Rheology of Viscoelastic Double Networks in Wormlike Micelle – Nanoparticle Mixtures*. Langmuir, Vol. 26 11: pp. 8049-8060.

Henaut, I., Barre, L., Argillier, J. F. et al. 2001. *Rheological and Structural Properties of Heavy Crude Oils in Relation with their Asphaltenes Content*. Society of Petroleum Engineers. <http://dx.doi.org/10.2118/65020-MS>.

Huang, T., Crews, J.B., and Willingham, J. R. 2008. *Nanoparticles for Formation Fines Fixation and Improving Performance of Surfactant Structure Fluids*. Paper IPTC 12414 presented at the International Petroleum Technology Conference, Kuala Lumpur, Malaysia, 3-5 December.

Jiang, L., Li, S., Yu, W. et al. 2016. *Interfacial study on the interaction between hydrophobic nanoparticles and ionic surfactants*. Colloids and Surfaces A: Physicochemical and Engineering Aspects. Volume 488, Pages 20-27, ISSN 0927-7757, <http://dx.doi.org/10.1016/j.colsurfa.2015.10.007>.

Johannesen, E. B. and Graue, A. 2007. *Mobilization of Remaining Oil - Emphasis on Capillary Number and Wettability*. Society of Petroleum Engineers. <http://dx.doi.org/10.2118/108724-MS>.

Karpinski, P. H. and Wey, J. S. 2002. *Handbook of Industrial Crystallization*. Butterworth-Heinemann, Boston, <http://dx.doi.org/10.1002/aic.690400622>.

- Kershaw J. R., Barrass G., and Gray D. 1980. *Chemical nature of coal hydrogenation oils part I: The effect of catalysts*. Fuel Processing Technology 3-2: pp. 115-129.
- Kovscek, T. 2005. *Overview: Heavy Oil*. Society of Petroleum Engineers. <http://dx.doi.org/10.2118/0605-0062-JPT>.
- Lake, L. W. 1989. *Enhanced Oil Recovery*. First edition, Prentice-Hall Inc., Englewood Cliffs, NJ.
- Larson, R. G. 1999. *The structure and rheology of complex fluids*. New York: Oxford University Press.
- Li, W., Zhu, J., and Qi, J. 2007. *Application of Nano-nickel Catalyst in the Viscosity Reduction of Liaohe-heavy Oil by Aquathermolysis*. J Fuel Chem. Technology 35 2: pp. 176-180.
- Lohne, A. and Fjelde, I. 2012. *Surfactant Flooding in Heterogeneous Formations*. Society of Petroleum Engineers. <http://dx.doi.org/10.2118/154178-MS>.
- Maserati, G., Daturi, E., Belloni, A. et al. 2010. *Nano-emulsions as Cement Spacer Improve the Cleaning of Casing Bore during Cementing Operations*. Paper SPE 133033 presented at the SPE Annual Technical Conference and Exhibition, Florence, Italy, 19-22 September.
- Meyer, R. F., Attanasi, E. D., and Freeman, P. A. 2007. *Heavy Oil and Natural Bitumen Resources in Geological Basins of the World*. US geological survey Open File-Report 2007-1084. <http://pubs.usgs.gov/of/2007/1084/OF2007-1084v1.pdf> Accessed on 2 February 2016.
- Mcauliffe, C. D. 1973. *O/W Emulsions and Their Flow Properties in Porous Media*. Journal of Petroleum Technology, pp. 727-733.
- McElfresh, P., Olguin, C., and Ector, D. 2012. *The Application of Nanoparticle Dispersions to Remove Paraffin and Polymer Filter Cake Damage*. Paper SPE 151848 presented at the SPE International Symposium and Exhibition on Formation Damage Control, Lafayette, Louisiana, USA, 15-17 February.
- Miller, K. A. and Erno, B. P. 1995. *Use and Misuse of Heavy Oil and Bitumen Viscosity Data*. Petroleum Society of Canada. <http://dx.doi.org/10.2118/95-93>.
- Miller, K. A., Nelson, L. A., and Almond, R. M. 2003. *Should You Trust Your Heavy Oil Viscosity Measurement?* Petroleum Society of Canada. <http://dx.doi.org/10.2118/06-04-02>.
- Model 900 OFITE viscometer Instruction Manual. [http://www.ofite.com/joomlatools-files/docman-files/130-76-C\\_instructions.pdf](http://www.ofite.com/joomlatools-files/docman-files/130-76-C_instructions.pdf) Accessed on: February 11, 2016.

- Nassar, N., Husein, M., and Pereira-Almao, P. 2011. *In-Situ prepared nanoparticles in support of oilsands industry meeting future environmental challenges*. Exploration and Production: Oil and Gas Review 01/2011; 91:46-48.
- Ogolo, N. A., Olafuyi, O. A., and Onyekonwu, M. O. 2012. *Enhanced Oil Recovery Using Nanoparticles*. Society of Petroleum Engineers. <http://dx.doi.org/10.2118/160847-MS>.
- Muraza, O. and Galadima, A. 2015. *Aquathermolysis of heavy oil: A review and perspective on catalyst development*. Fuel. Volume 157. Pages 219-231, ISSN 0016-2361, <http://dx.doi.org/10.1016/j.fuel.2015.04.065>.
- Pei, H. H., Zhang, G. C., Ge, J. J. et al. 2015. *Investigation of Nanoparticle and Surfactant Stabilized Emulsion to Enhance Oil Recovery in Waterflooded Heavy Oil Reservoirs*. Society of Petroleum Engineers. <http://dx.doi.org/10.2118/174488-MS>.
- Pierre, C., Barre, L., Pina, A., and Moan, M. 2004. *Composition and Heavy Oil Rheology*. Oil & Gas Science and Technology – Rev. IFP, Vol. 59, No. 5, pp. 489-501.
- Qiu, F. 2010. *The Potential Applications in Heavy Oil EOR With the Nanoparticle and Surfactant Stabilized Solvent-Based Emulsion*. Paper SPE 134613 prepared for presentation at the Canadian Unconventional Resources & International Petroleum Conference held in Calgary, Alberta, Canada, 19–21 October.
- Rudiyak, V. 2013 *Viscosity of Nanofluids. Why it is not Described by the Classical Theories*. Advances in Nanoparticles, 2, 266-279. <http://dx.doi.org/10.4236/anp.2013.23037>.
- Rodriguez, E., Roberts, M. R., Yu, H. et al. 2009. *Enhanced Migration of Surface-Treated Nanoparticles in Sedimentary Rocks*. Paper SPE 124418 presented at the SPE Annual Technical Conference and Exhibition, New Orleans, Louisiana, USA, 4-7 October.
- Sarma, H. K., Maini, B. B., and Jha, K. 1998. *Evaluation of Emulsified Solvent Flooding For Heavy Oil Recovery*. Petroleum Society of Canada. <http://dx.doi.org/10.2118/98-07-06>.
- Schlumberger Oilfield glossary. <http://www.glossary.oilfield.slb.com>.
- Schlumberger 2006. *Highlighting Heavy Oil*. Oilfield Review. Volume 18, Issue 2.
- Sensoy, T., Chenevert, M. E., and Sharma, M. M. 2009. *Minimizing Water Invasion in Shale Using Nanoparticles*. Paper SPE 124429 presented at the SPE Annual Technical Conference and Exhibition, New Orleans, Louisiana, USA, 4-7 October.
- Sezai, U. 2015. Personal communication. October 21.

Sharma, M. and Shah, D. 1985. *Introduction to Macro- and Microemulsions*. ACS Symposium Series. American Chemical Society. Washington, DC.

Shokrlu, Y. H. and Babadagli, T. 2010. *Effects of Nano Sized Metals on Viscosity Reduction of Heavy Oil/Bitumen during Thermal Applications*. Paper CSUG/SPE 137540 presented at the Canadian Unconventional Resources & International Petroleum Conference, Calgary, Alberta, Canada, 19-21 October.

Shokrlu, Y. H. and Babadagli, T. 2011. *Transportation and Interaction of Nano and Micro Size Metal Particles Injected to Improve Thermal Recovery of Heavy-Oil*. Society of Petroleum Engineers. <http://dx.doi.org/10.2118/146661-MS>.

Shokrlu, Y. H. and Babadagli, T. 2014. *Viscosity reduction of heavy oil/bitumen using micro- and nano-metal particles during aqueous and non-aqueous thermal applications*. Journal of Petroleum Science and Engineering, Volume 119, Pages 210-220, ISSN 0920-4105, <http://dx.doi.org/10.1016/j.petrol.2014.05.012>.

Singh, P. and Bhat, S. 2006. *Nanologging: Use of Nanorobots for Logging*. Society of Petroleum Engineers. <http://dx.doi.org/10.2118/104280-MS>.

Singh, S. and Ahmed, R. 2010. *Vital Role of Nanopolymers in Drilling and Stimulations Fluid Applications*. Paper SPE 130413 presented at the SPE Annual Technical Conference and Exhibition, Florence, Italy, 19-22 September.

Speight, J. G 2009. *Enhanced Recovery Methods for Heavy Oil and Tar Sands*. Gulf Publishing Company, Pages 185-260, ISBN 9781933762258, <http://dx.doi.org/10.1016/B978-1-933762-25-8.50011-0>.

Srinivasan, A. 2014. *Surfactant-Based Fluids Containing Copper-Oxide Nanoparticles for Heavy Oil Viscosity Reduction*. Master's Thesis. The University of Oklahoma. Norman, OK.

Srinivasan, A. and Shah, S. N. 2014. *Surfactant-Based Fluids Containing Copper-Oxide Nanoparticles for Heavy Oil Viscosity Reduction*. Society of Petroleum Engineers. <http://dx.doi.org/10.2118/170800-MS>.

Tarek, M. 2015. *Investigating Nano-Fluid Mixture Effects to Enhance Oil Recovery*. Society of Petroleum Engineers. <http://dx.doi.org/10.2118/178739-STU>.

Torsaeter, O., and Abtahi, M. 2003. *Experimental reservoir engineering laboratory workbook*. Norwegian University of Science and Technology.

Qiu, F. and Mamora, D. D. 2010. *Experimental Study of Solvent-Based Emulsion Injection to Enhance Heavy Oil Recovery in Alaska North Slope Area*. Society of Petroleum Engineers. <http://dx.doi.org/10.2118/136758-MS>.

Van Der Knaap, W., Van Daalen, F., and Florian, L. 1970. *Method of Recovering Crude Oil from a Subsurface Formation*. U.S. Patent #3500916A. March 17.

Wasan, D., Nikolov, A., and Kondiparty, K. 2010. *The wetting and spreading of nanofluids on solids: Role of the structural disjoining pressure*. *Current Opinion in Colloid & Interface Science*, Volume 16, Issue 4, Pages 344-349, ISSN 1359-0294, <http://dx.doi.org/10.1016/j.cocis.2011.02.001>.

Wu, C. H. 1977. *A Critical Review of Steamflood Mechanisms*. Society of Petroleum Engineers. <http://dx.doi.org/10.2118/6550-MS>.

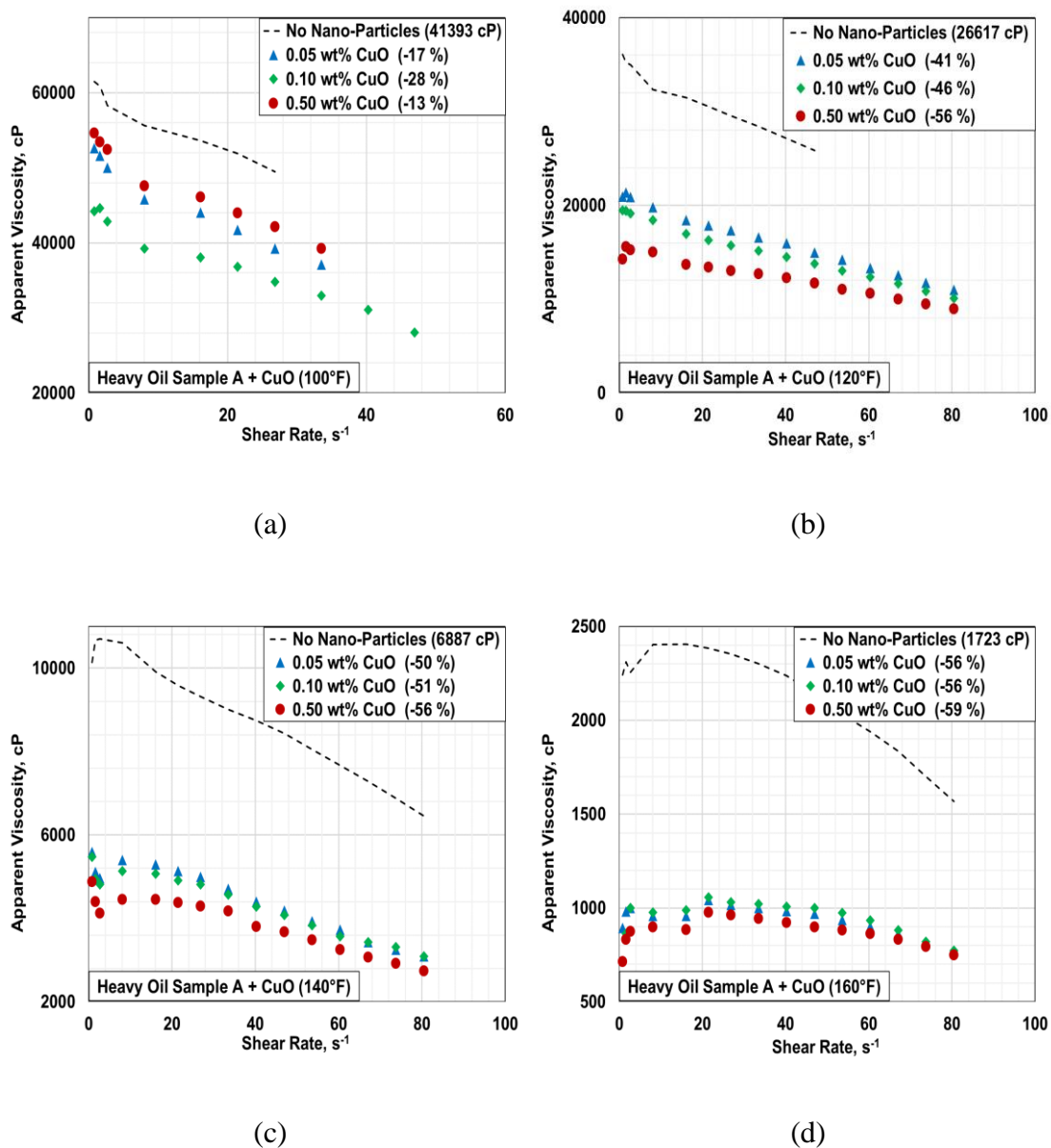
Yokoyama, T., Masuda, H., Suzuki, M. et al. 2008. *Basic properties and measuring methods of nanoparticles*. *Nanoparticle technology handbook*. ed, Chap.1, 5-48, Elsevier B.V.

Zhang, T., Roberts, M. R., Bryant, S. L. et al. 2009. *Foams and Emulsions Stabilized with Nanoparticles for Potential Conformance Control Applications*. Paper SPE 121744 presented at the SPE International Symposium on Oilfield Chemistry, The Woodlands, Texas, USA, 20-22 April.

Zhang, T., Davidson, A., Bryant, S.L. et al. 2010. *Nanoparticle-Stabilized Emulsions for Applications in Enhanced Oil Recovery*. Paper SPE 129885 presented at the SPE Improved Oil Recovery Symposium, Tulsa, Oklahoma, USA, 24-28 April.

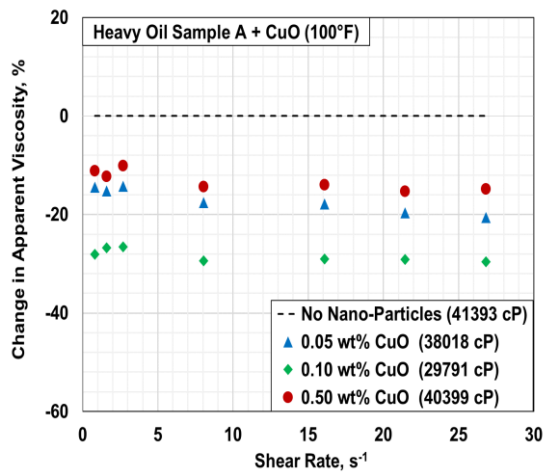


## Appendix A: Rheology of Heavy Oil Containing Nanoparticles

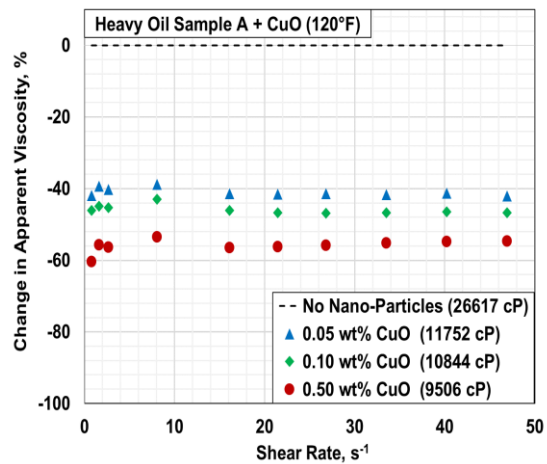


**Figure A.1:** Apparent viscosity of heavy oil Sample A containing copper oxide nanoparticles at (a) 100°F (b) 120°F (c) 140°F and (d) 160°F

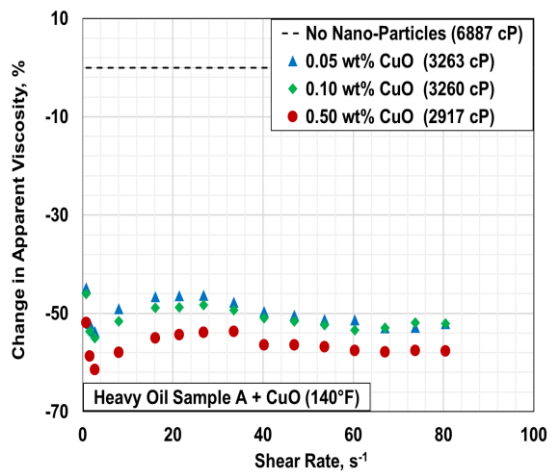
\* Average percentage change in apparent viscosity is mentioned in parenthesis



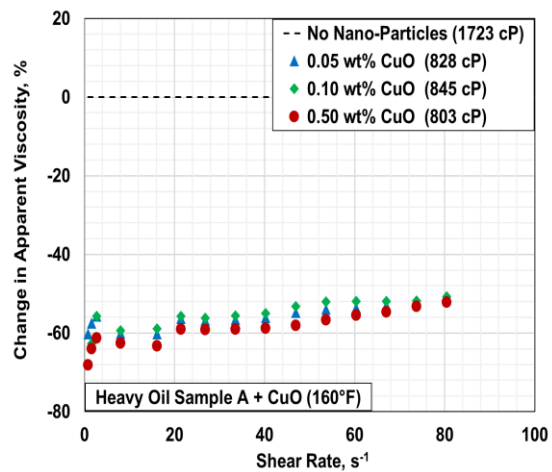
(a)



(b)



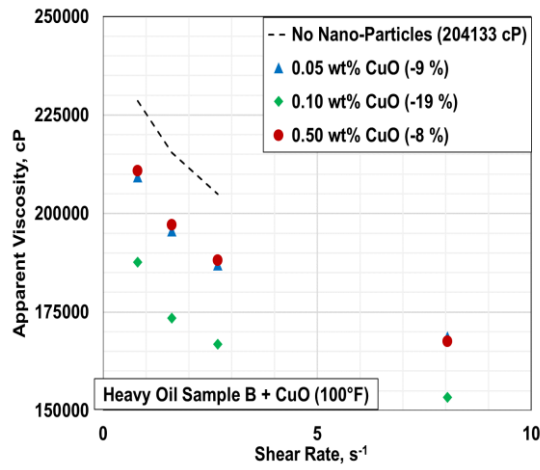
(c)



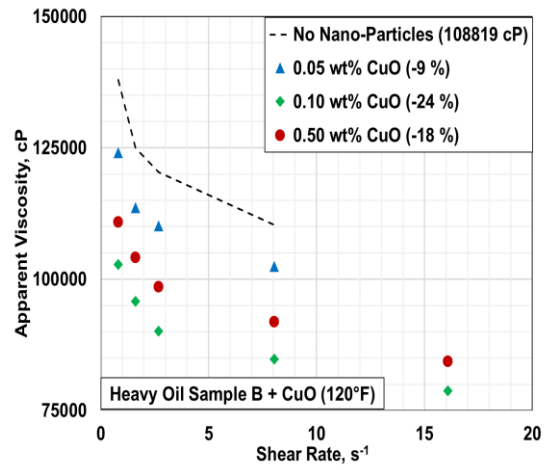
(d)

**Figure A.2:** Percentage change in apparent viscosity of heavy oil Sample A by copper oxide nanoparticles at (a) 100°F (b) 120°F (c) 140°F and (d) 160°F

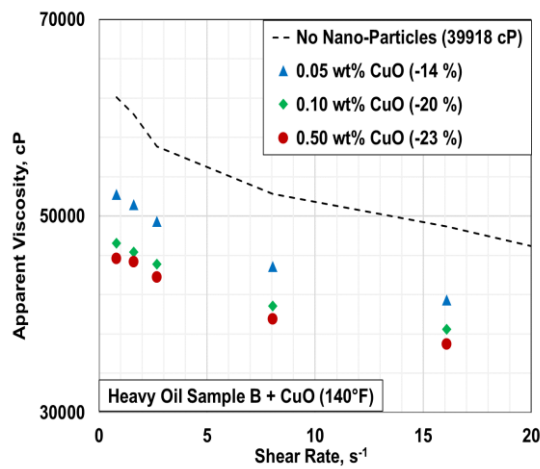
\* Viscosity mentioned in parenthesis corresponds to Newtonian viscosity



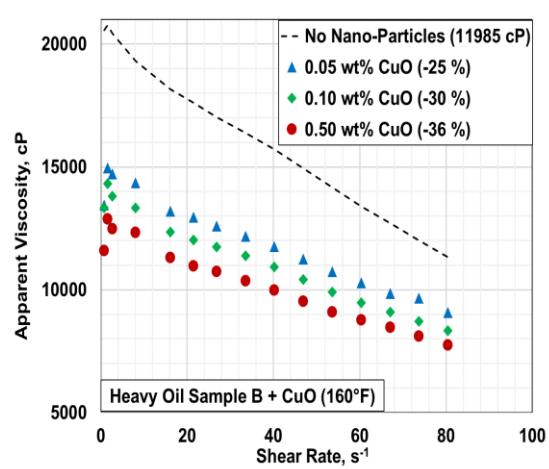
(a)



(b)



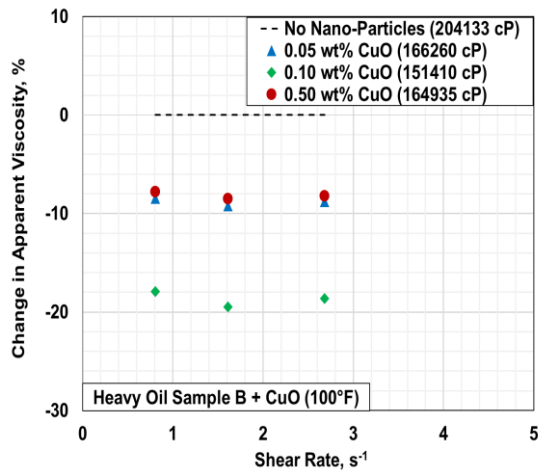
(c)



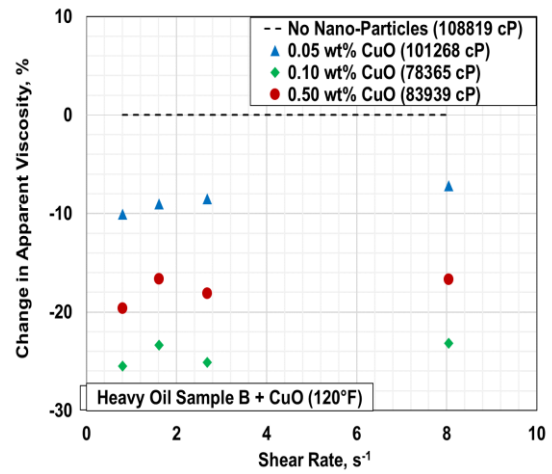
(d)

**Figure A.3:** Apparent viscosity of heavy oil Sample B containing copper oxide nanoparticles at (a) 100°F (b) 120°F (c) 140°F and (d) 160°F

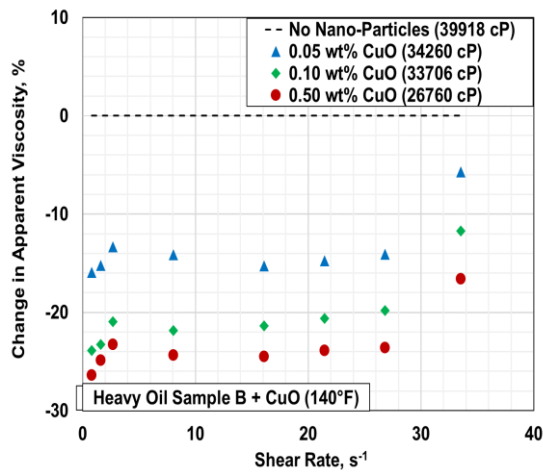
\* Average percentage change in apparent viscosity is mentioned in parenthesis



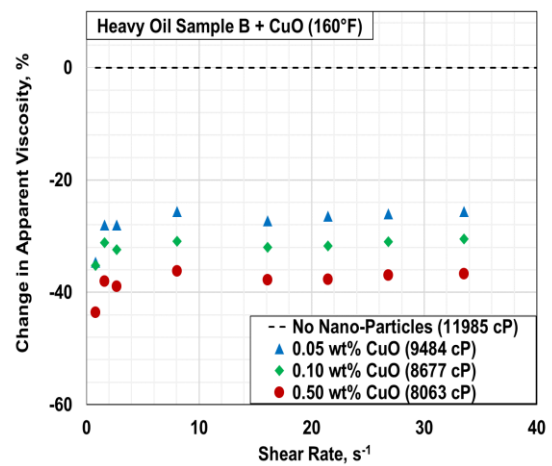
(a)



(b)



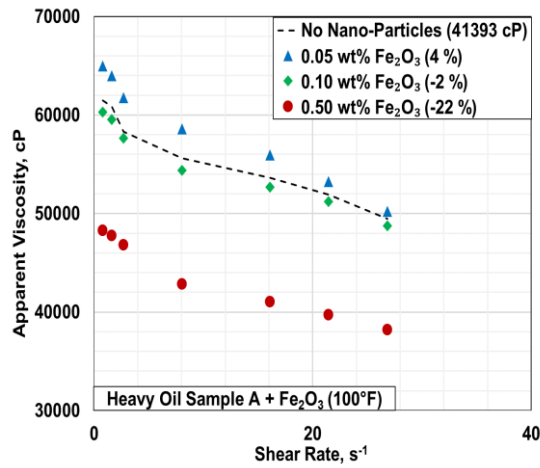
(c)



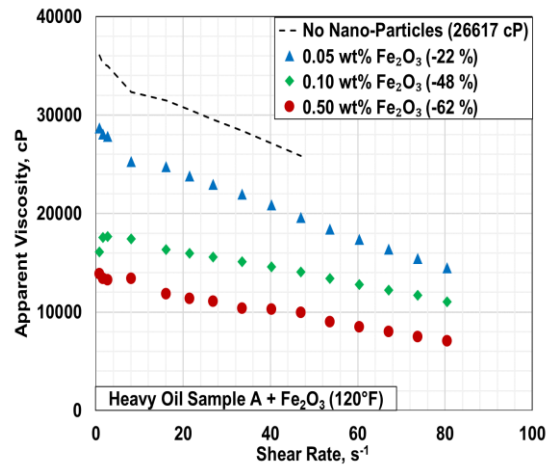
(d)

**Figure A.4:** Percentage change in apparent viscosity of heavy oil Sample B by copper oxide nanoparticles at (a) 100°F (b) 120°F (c) 140°F and (d) 160°F

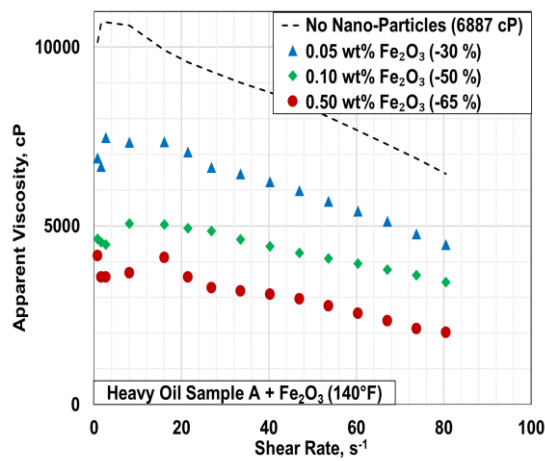
\* Viscosity mentioned in parenthesis corresponds to Newtonian viscosity



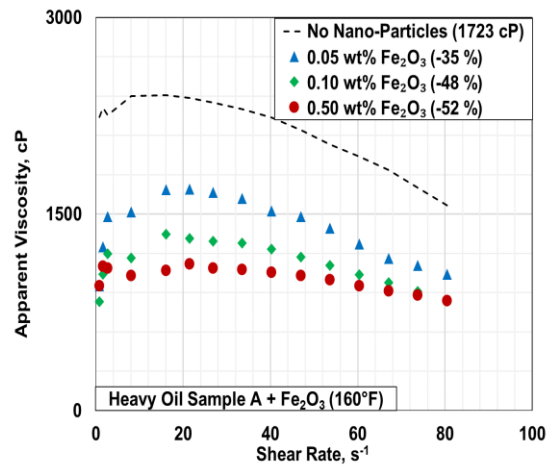
(a)



(b)



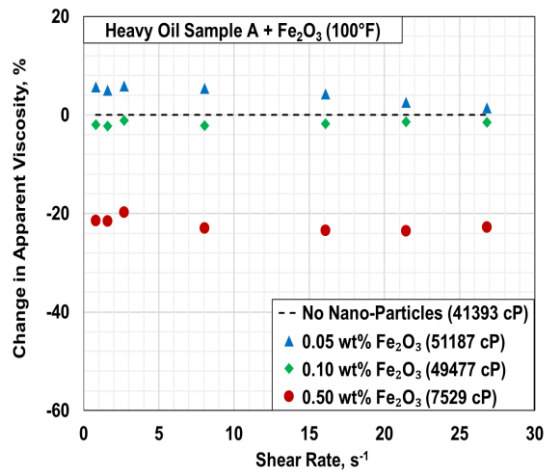
(c)



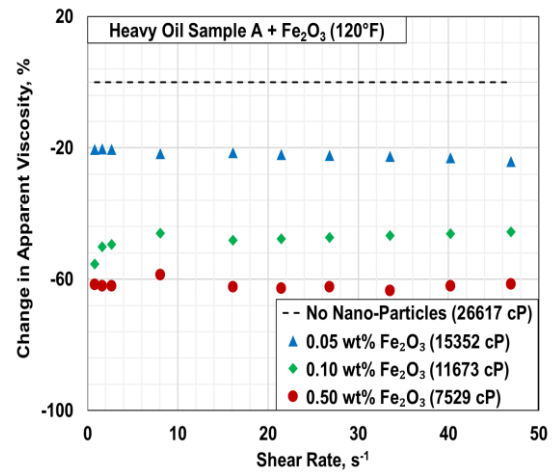
(d)

**Figure A.5:** Apparent viscosity of heavy oil Sample A containing iron oxide nanoparticles at (a) 100°F (b) 120°F (c) 140°F and (d) 160°F

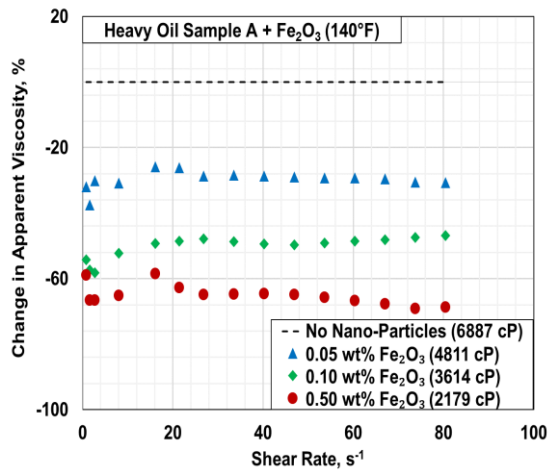
\* Average percentage change in apparent viscosity is mentioned in parenthesis



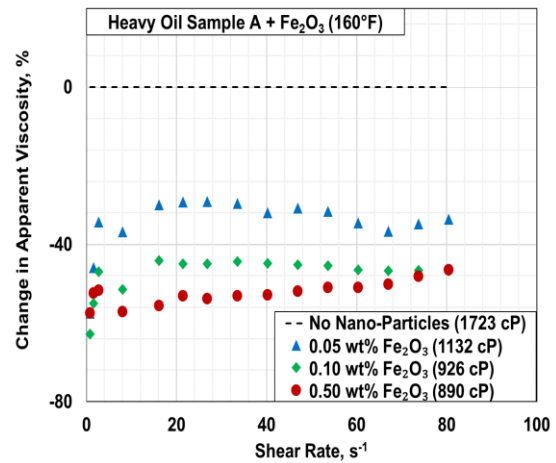
(a)



(b)



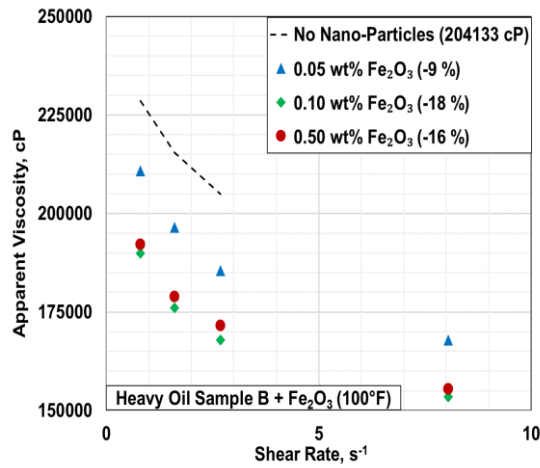
(c)



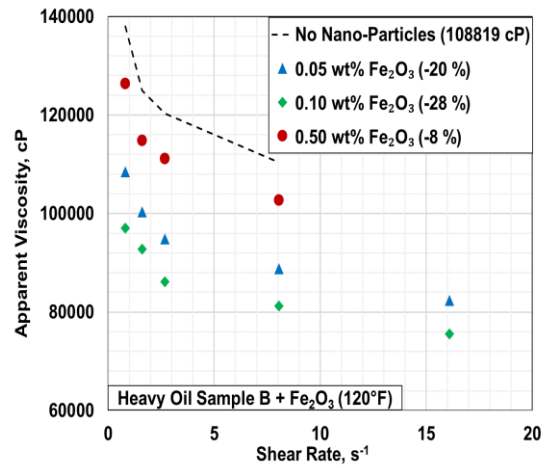
(d)

**Figure A.6:** Percentage change in apparent viscosity of heavy oil Sample A by iron oxide nanoparticles at (a) 100°F (b) 120°F (c) 140°F and (d) 160°F

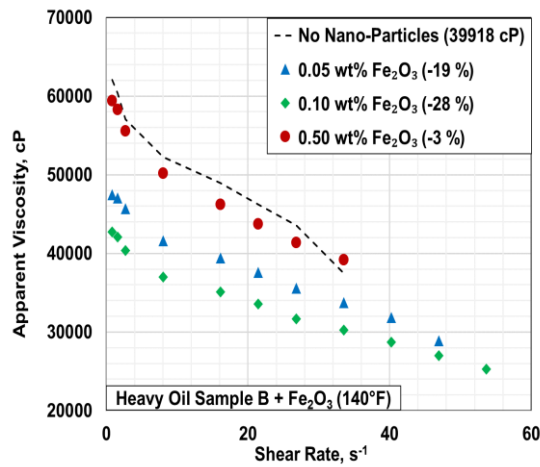
\* Viscosity mentioned in parenthesis corresponds to Newtonian viscosity



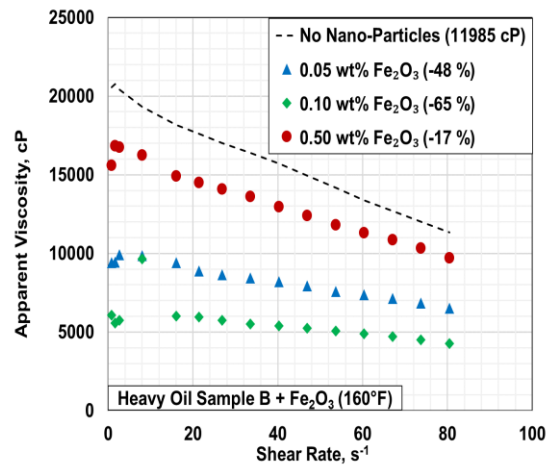
(a)



(b)



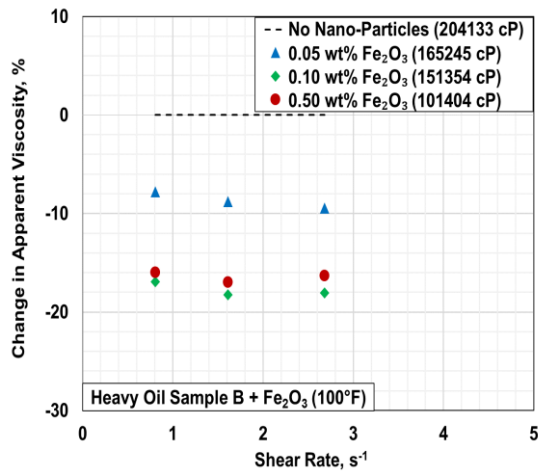
(c)



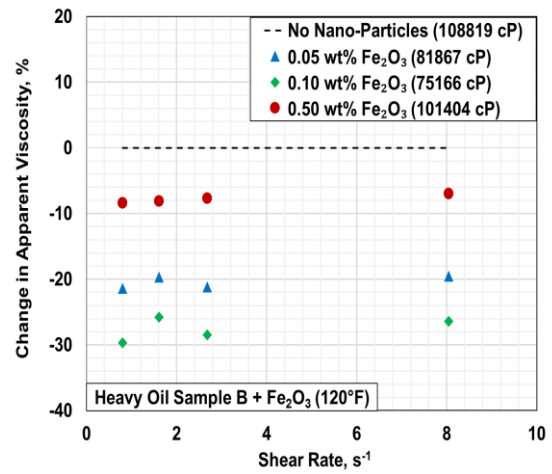
(d)

**Figure A.7:** Apparent viscosity of heavy oil Sample B containing iron oxide nanoparticles at (a) 100°F (b) 120°F (c) 140°F and (d) 160°F

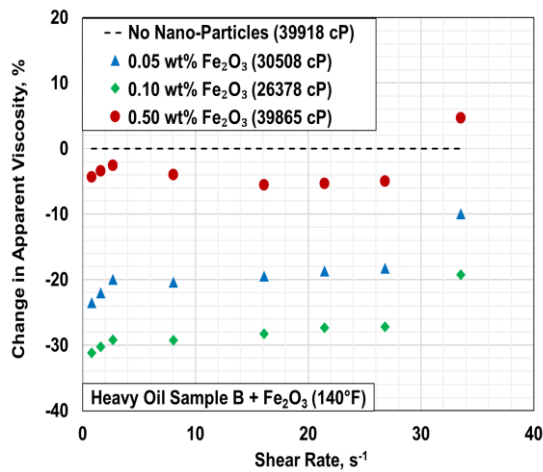
\* Average percentage change in apparent viscosity is mentioned in parenthesis



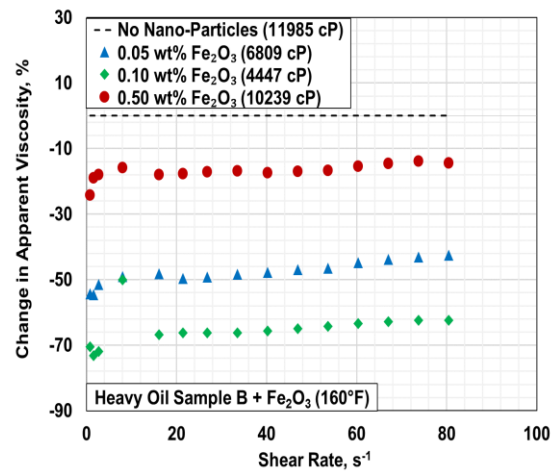
(a)



(b)



(c)

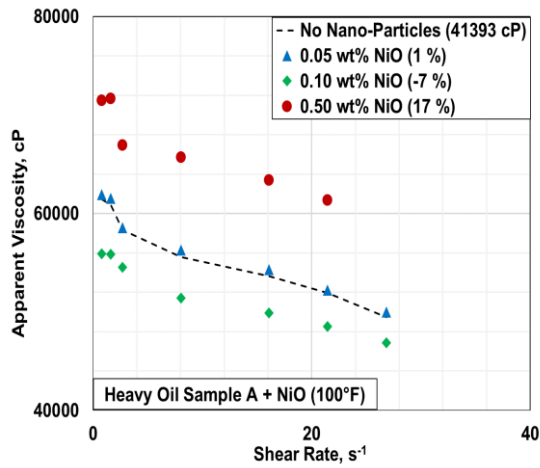


(d)

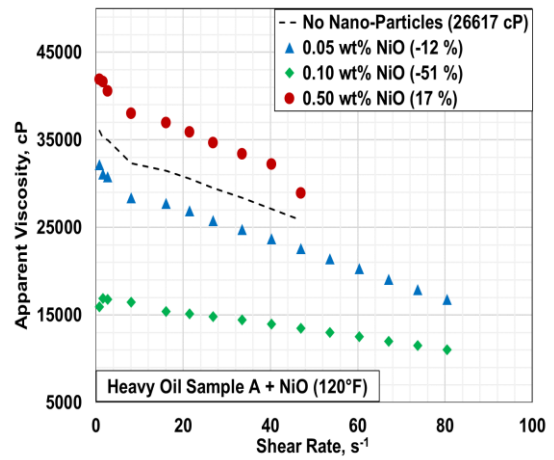
**Figure A.8:** Percentage change in apparent viscosity of heavy oil Sample B by iron oxide nanoparticles at (a) 100°F (b) 120°F (c) 140°F and (d) 160°F

\* Viscosity mentioned in parenthesis corresponds to Newtonian viscosity

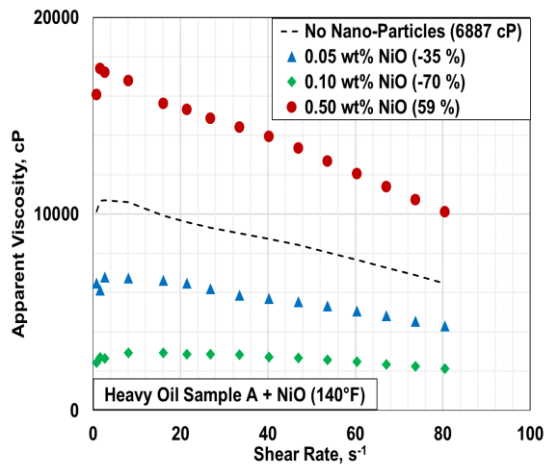




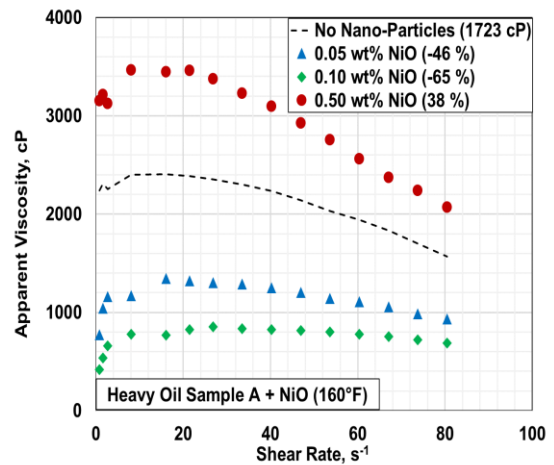
(a)



(b)



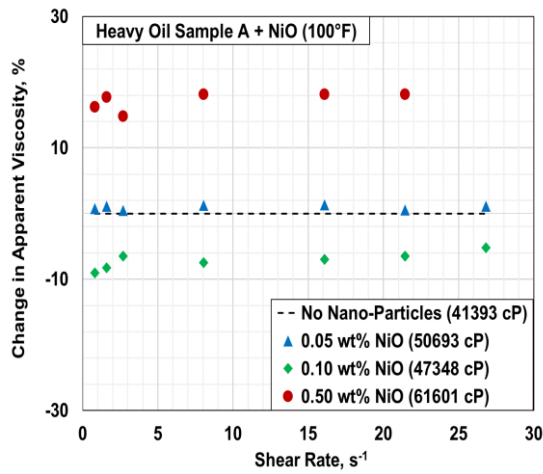
(c)



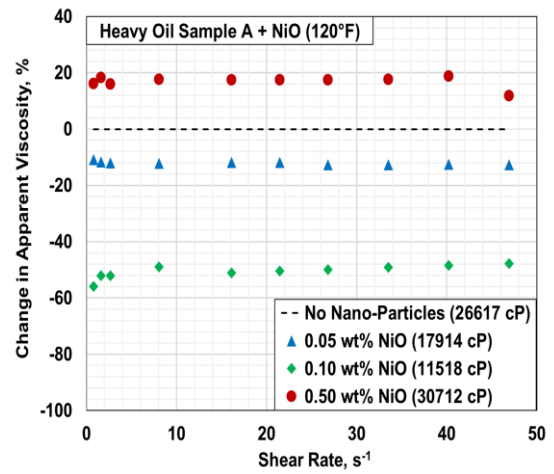
(d)

**Figure A.9:** Apparent viscosity of heavy oil Sample A containing nickel oxide nanoparticles at (a) 100°F (b) 120°F (c) 140°F and (d) 160°F

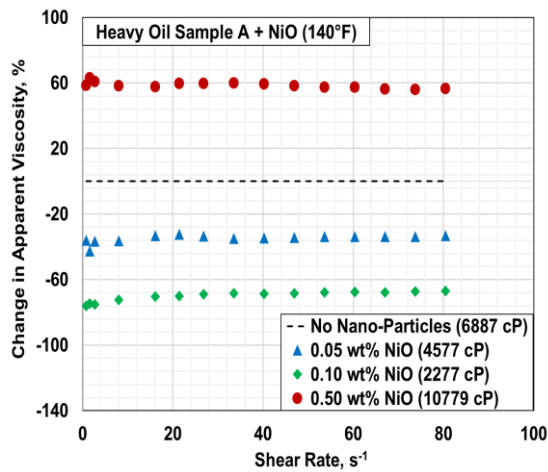
\* Average percentage change in apparent viscosity is mentioned in parenthesis



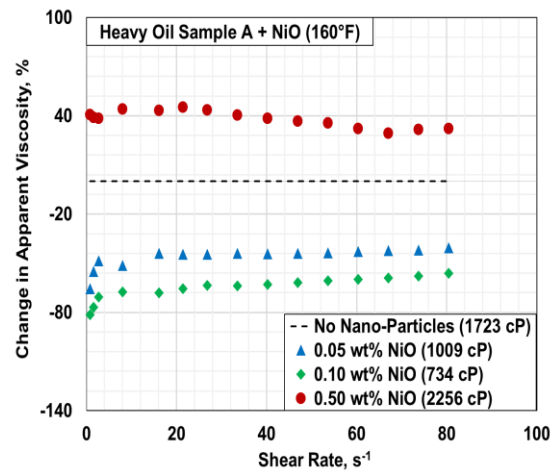
(a)



(b)



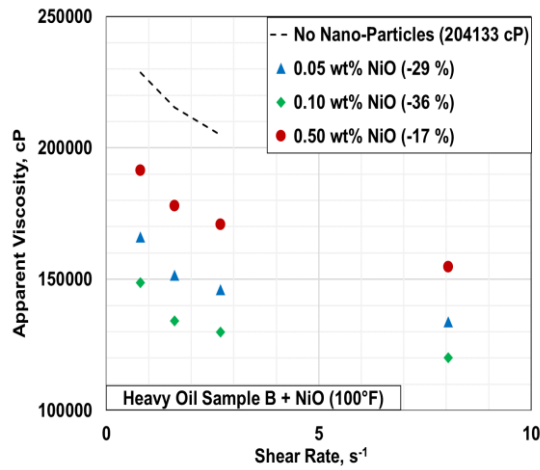
(c)



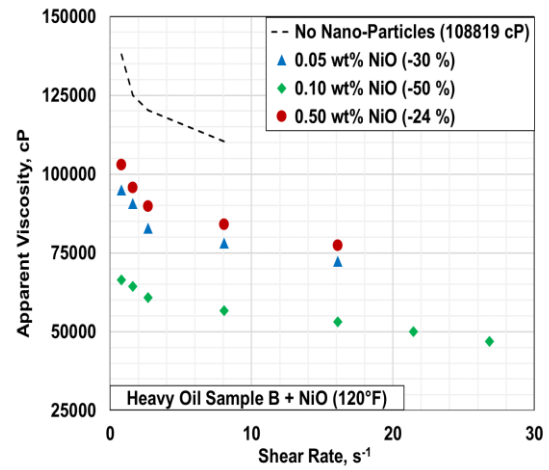
(d)

**Figure A.10:** Percentage change in apparent viscosity of heavy oil Sample A by nickel oxide nanoparticles at (a) 100°F (b) 120°F (c) 140°F and (d) 160°F

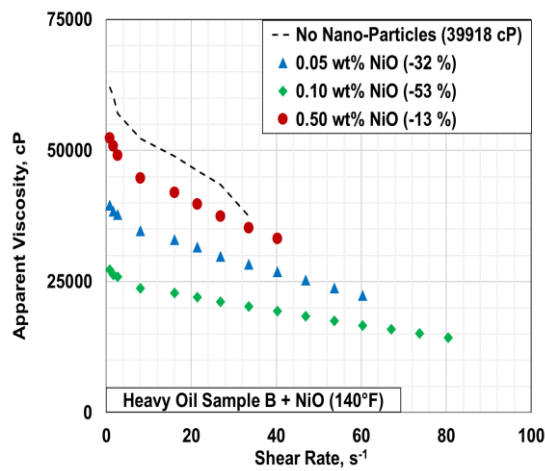
\* Viscosity mentioned in parenthesis corresponds to Newtonian viscosity



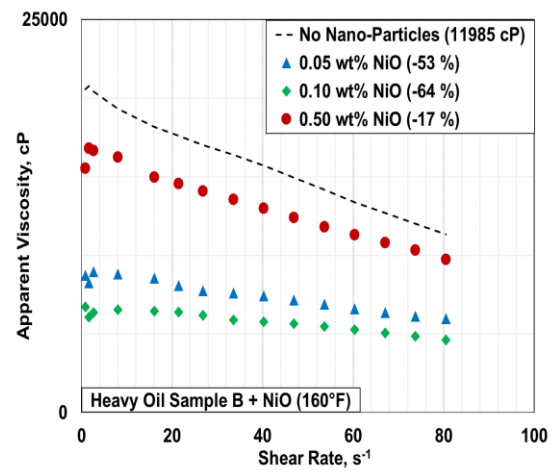
(a)



(b)



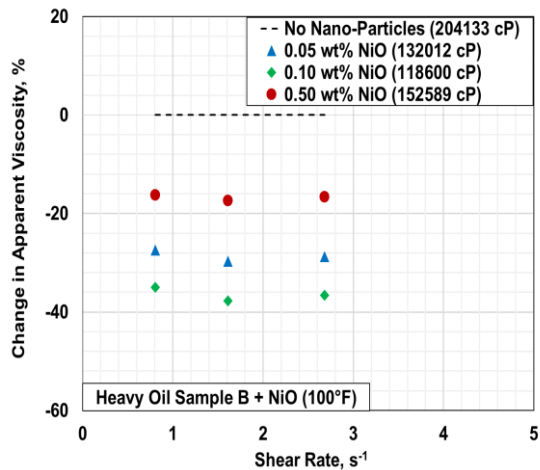
(c)



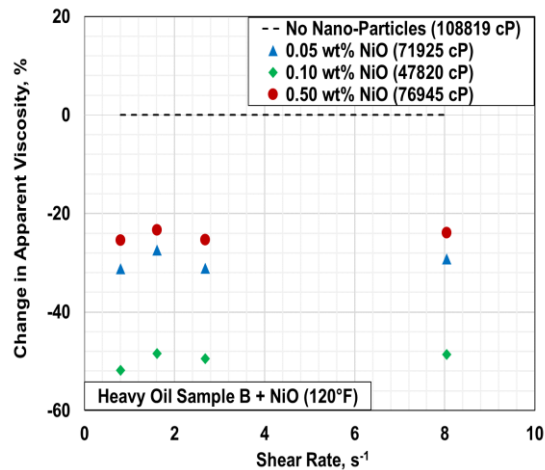
(d)

**Figure A.11:** Apparent viscosity of heavy oil Sample B containing nickel oxide nanoparticles at (a) 100°F (b) 120°F (c) 140°F and (d) 160°F

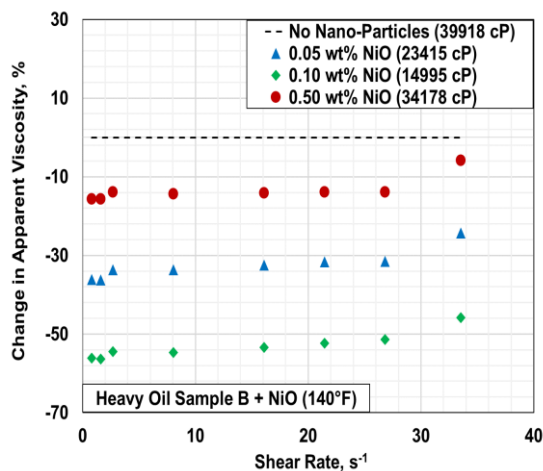
\* Average percentage change in apparent viscosity is mentioned in parenthesis



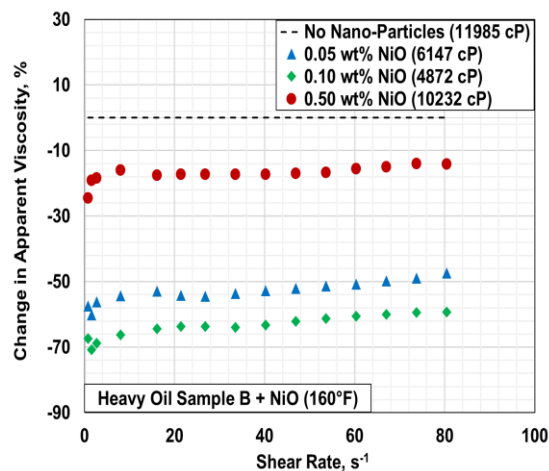
(a)



(b)



(c)



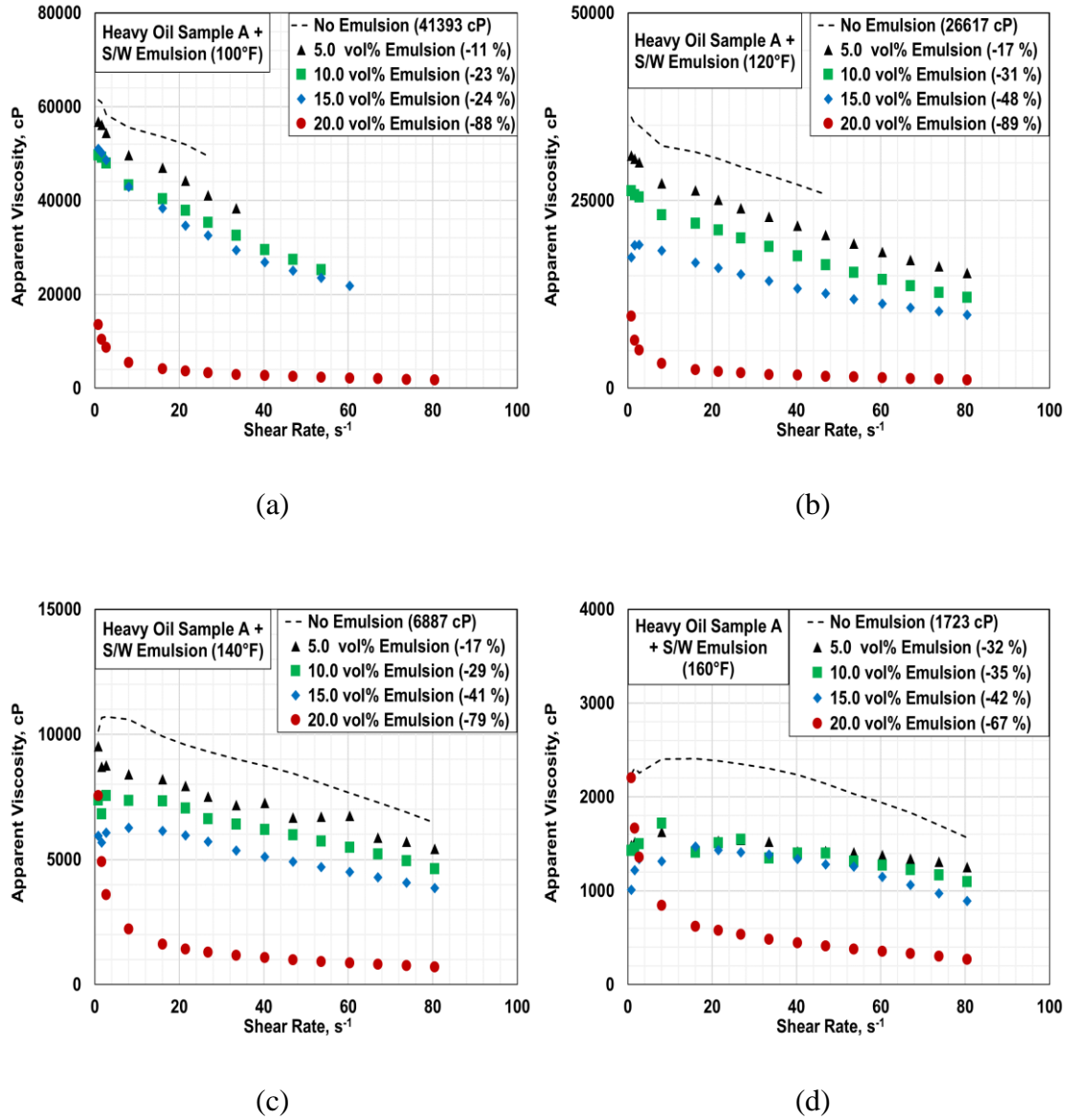
(d)

**Figure A.12:** Percentage change in apparent viscosity of heavy oil Sample B by nickel oxide nanoparticles at (a) 100°F (b) 120°F (c) 140°F and (d) 160°F

\* Viscosity mentioned in parenthesis corresponds to Newtonian viscosity

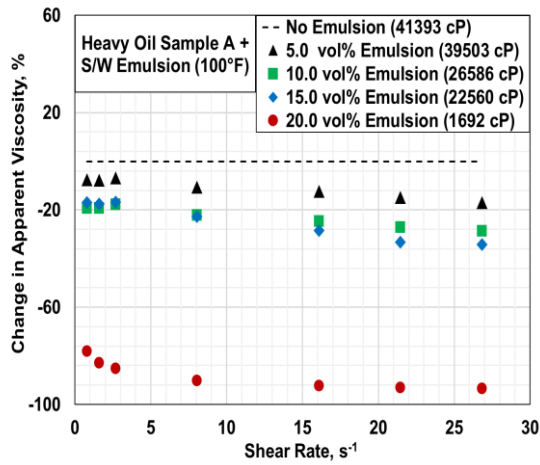
## Appendix B: Rheology of Heavy Oil Emulsion Containing S/W Emulsion

### Emulsion

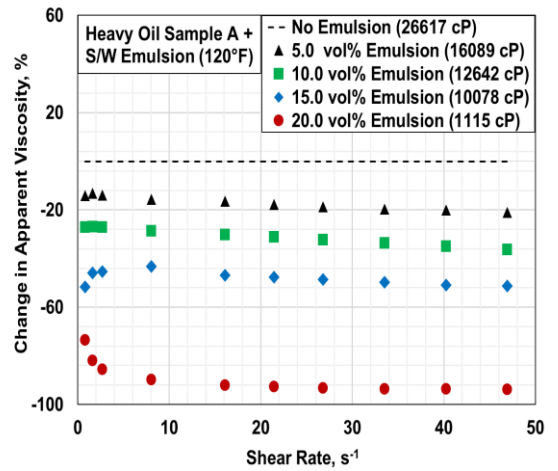


**Figure B.1:** Apparent viscosity of heavy oil emulsion (Sample A) at (a) 100°F (b) 120°F (c) 140°F and (d) 160°F

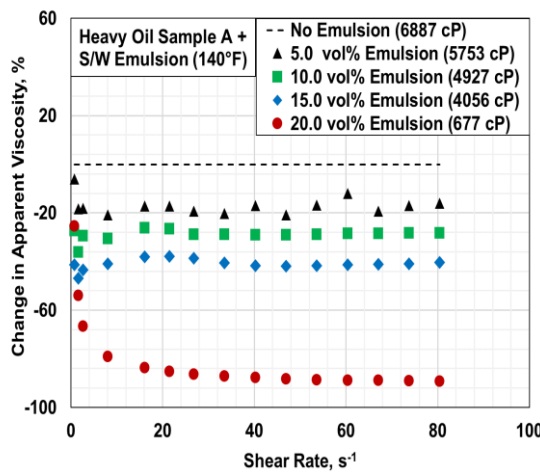
\* Average percentage change in apparent viscosity is mentioned in parenthesis



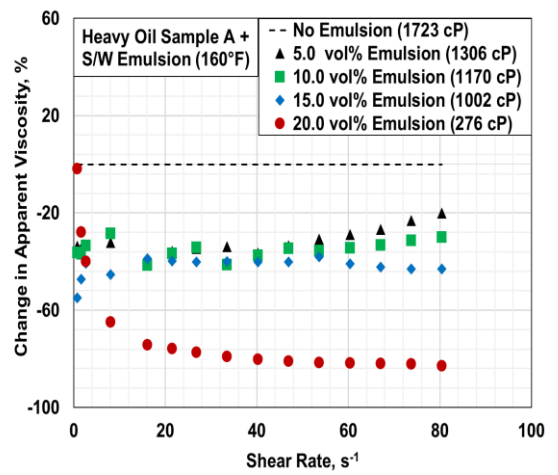
(a)



(b)



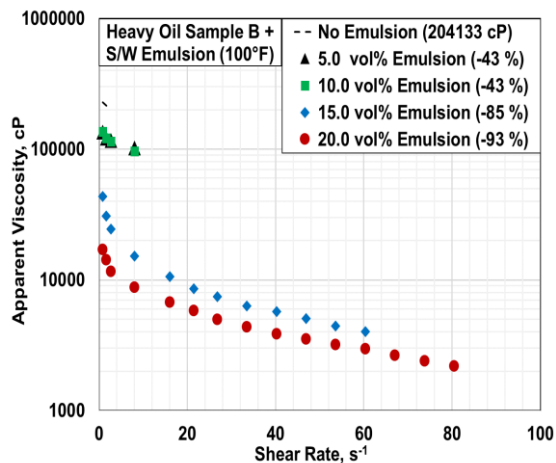
(c)



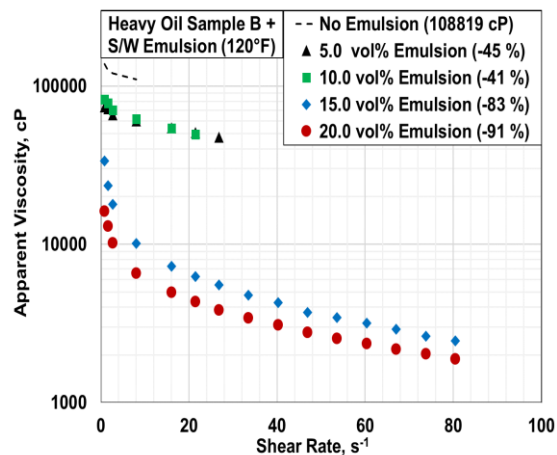
(d)

**Figure B.2:** Percentage change in apparent viscosity of heavy oil Sample A by S/W emulsion at (a) 100°F (b) 120°F (c) 140°F and (d) 160°F

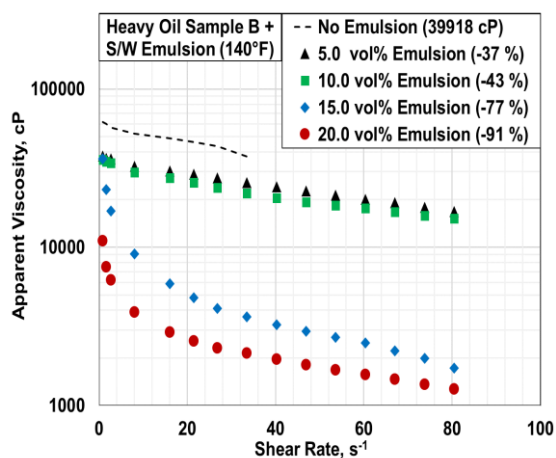
\* Viscosity mentioned in parenthesis corresponds to Newtonian viscosity



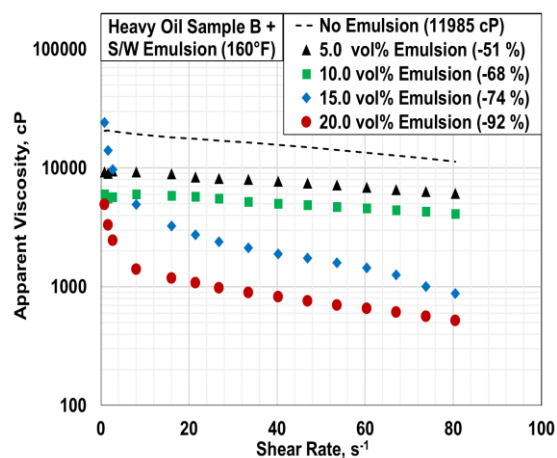
(a)



(b)



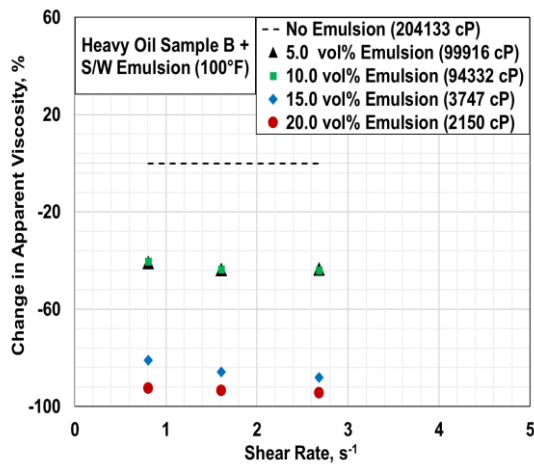
(c)



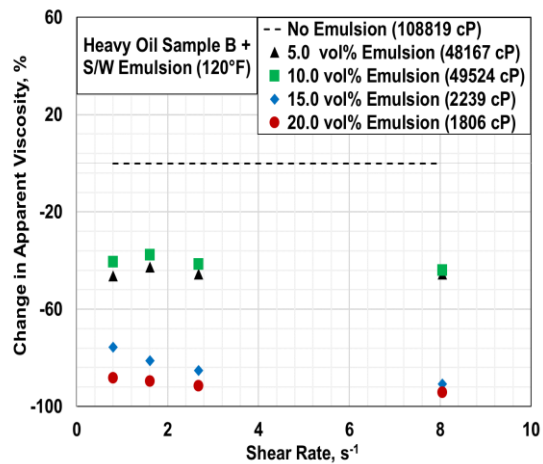
(d)

**Figure B.3:** Apparent viscosity of heavy oil emulsion (Sample B) at (a) 100°F (b) 120°F (c) 140°F and (d) 160°F

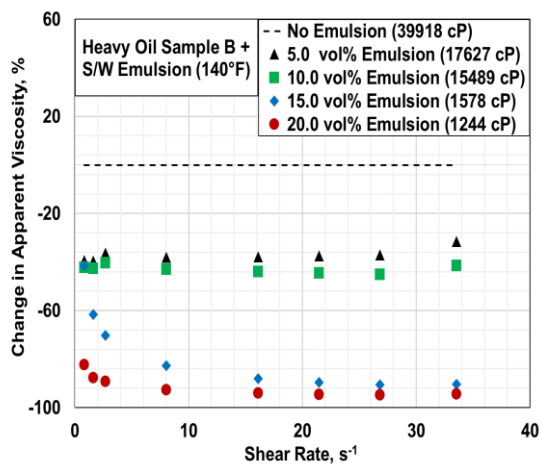
\* Average percentage change in apparent viscosity is mentioned in parenthesis



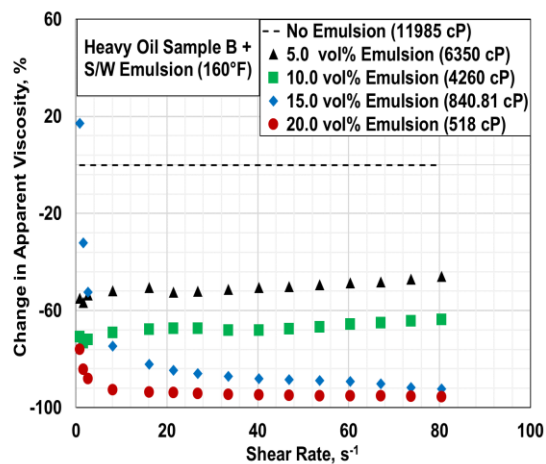
(a)



(b)



(c)



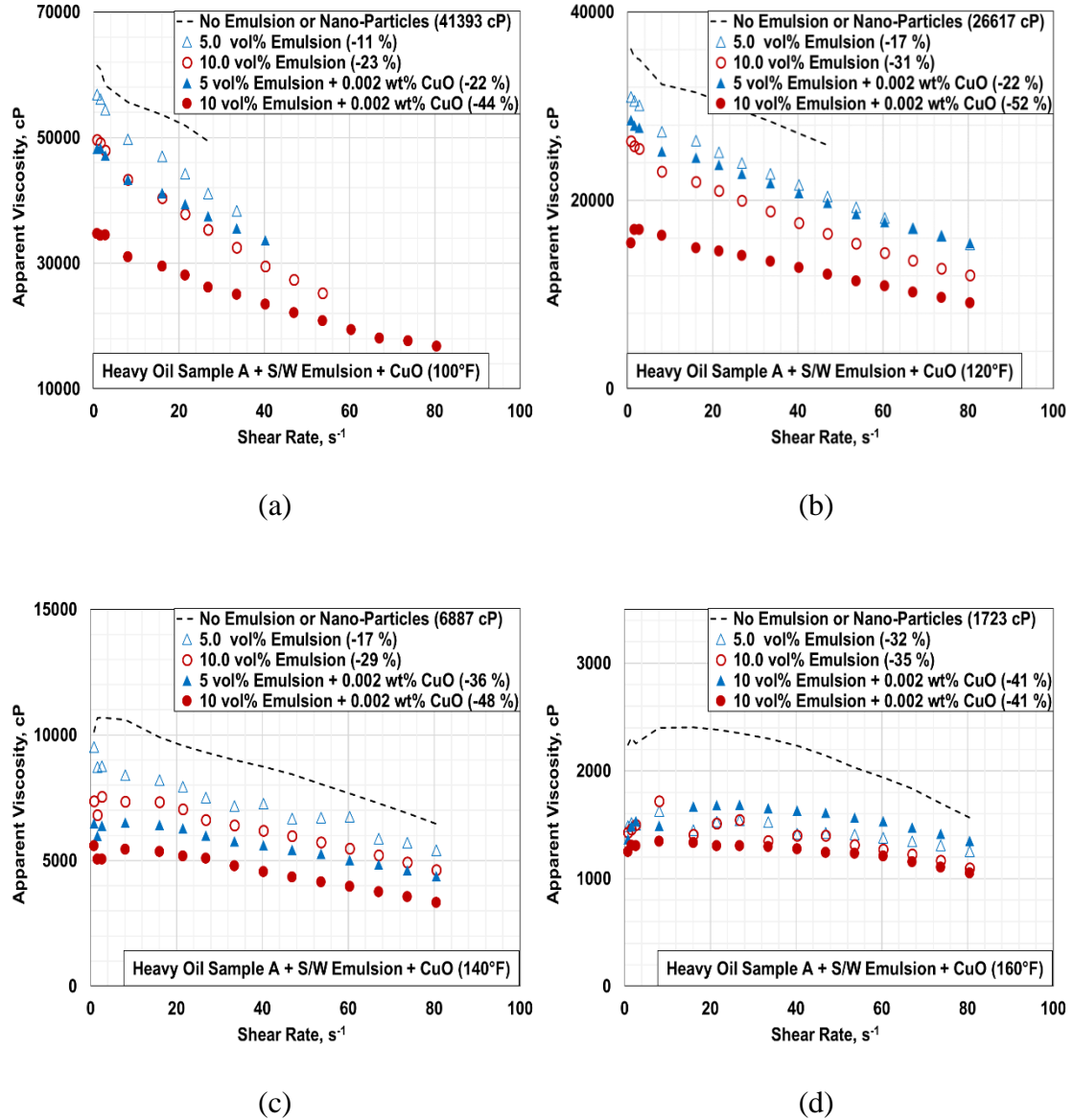
(d)

**Figure B.4:** Percentage change in apparent viscosity of heavy oil Sample B by S/W emulsion at (a) 100°F (b) 120°F (c) 140°F and (d) 160°F

\* Viscosity mentioned in parenthesis corresponds to Newtonian viscosity

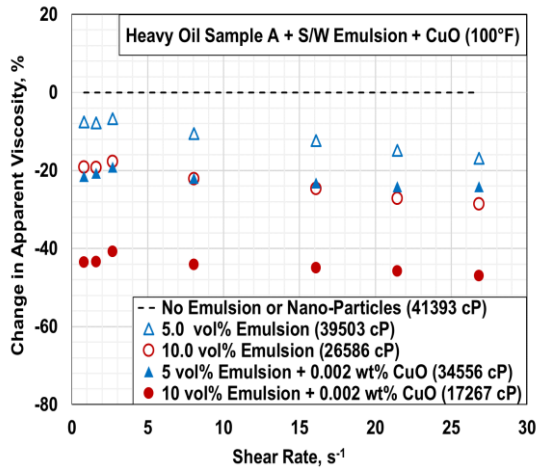


## Appendix C: Rheology of Heavy Oil Nano-Emulsion Containing S/W Emulsion and Nanoparticles

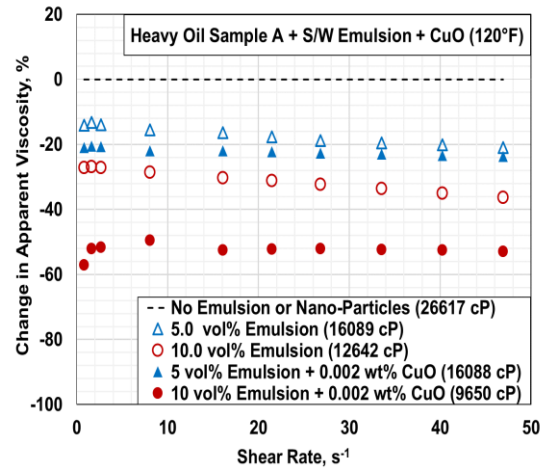


**Figure C.1:** Apparent viscosity of heavy oil nano-emulsion (Sample A) containing copper oxide nanoparticles at (a) 100°F (b) 120°F (c) 140°F and (d) 160°F

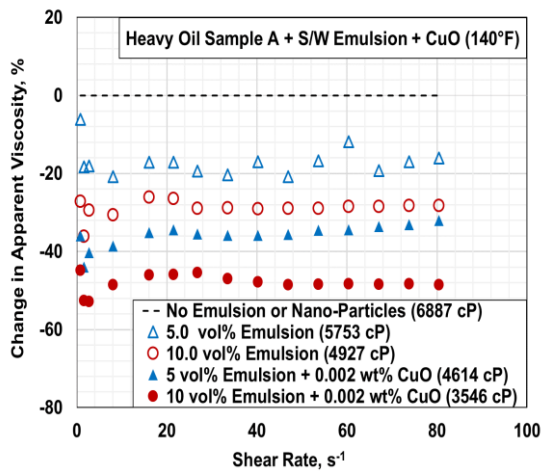
\* Average percentage change in apparent viscosity is mentioned in parenthesis



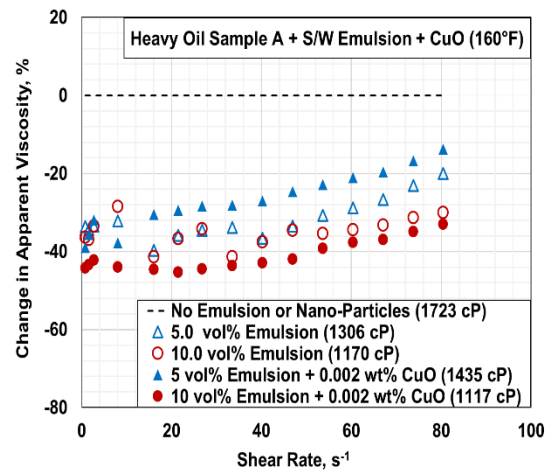
(a)



(b)



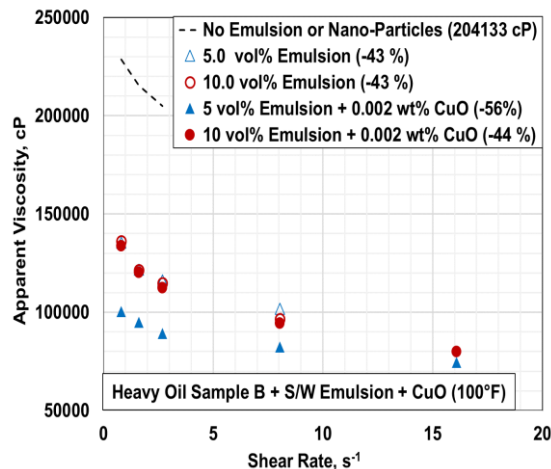
(c)



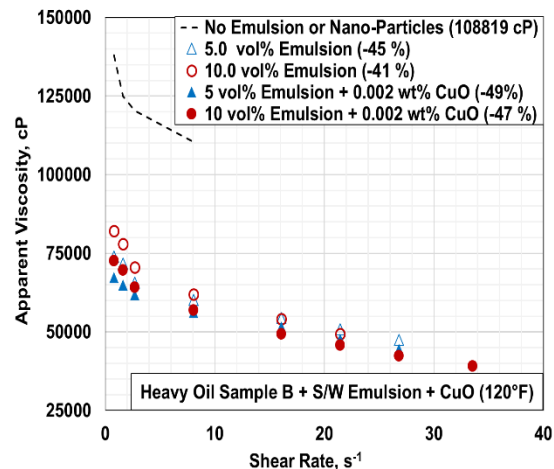
(d)

**Figure C.2:** Percentage change in apparent viscosity of heavy oil Sample A by S/W emulsion containing copper oxide nanoparticles at (a) 100°F (b) 120°F (c) 140°F and (d) 160°F

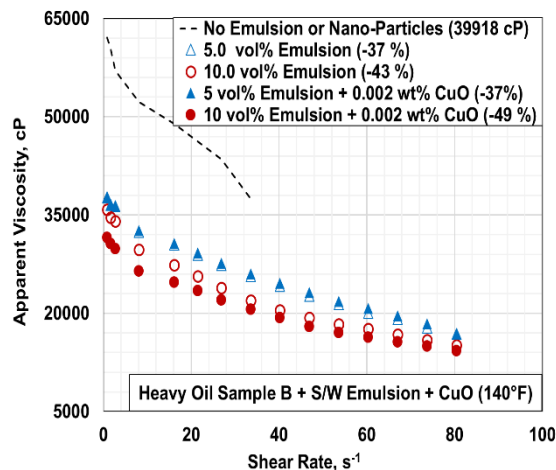
\* Viscosity mentioned in parenthesis corresponds to Newtonian viscosity



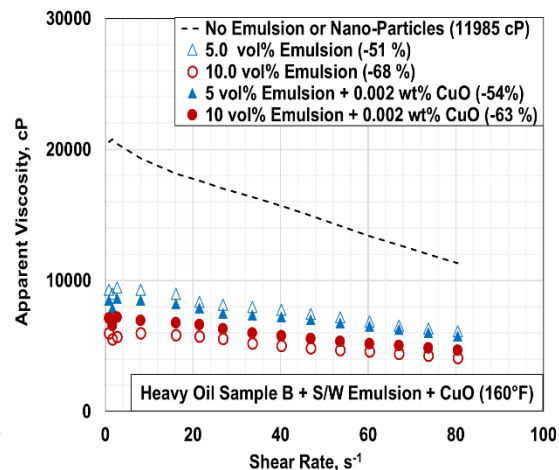
(a)



(b)



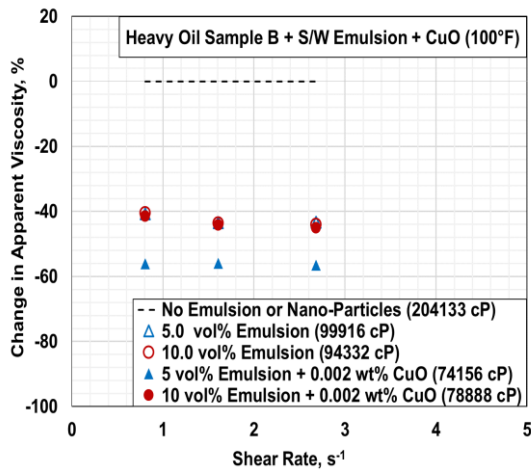
(c)



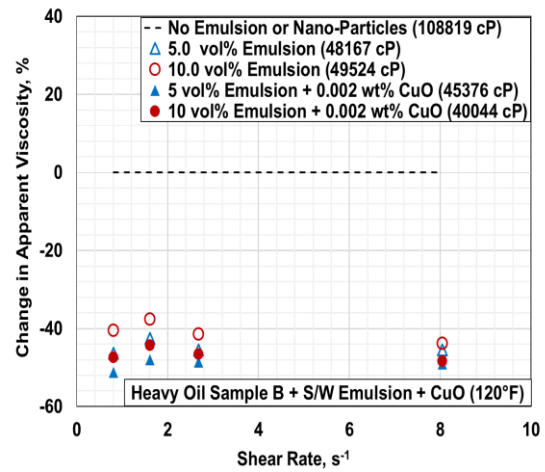
(d)

**Figure C.3:** Apparent viscosity of heavy oil nano-emulsion (Sample B) containing copper oxide nanoparticles at (a) 100°F (b) 120°F (c) 140°F and (d) 160°F

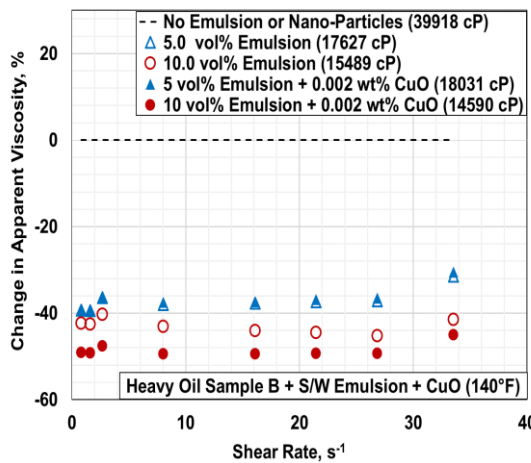
\* Average percentage change in apparent viscosity is mentioned in parenthesis



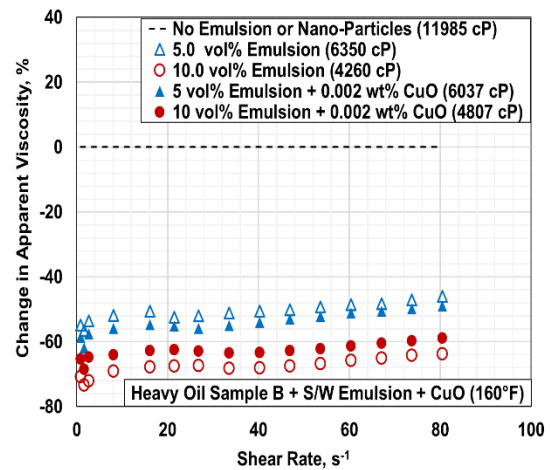
(a)



(b)



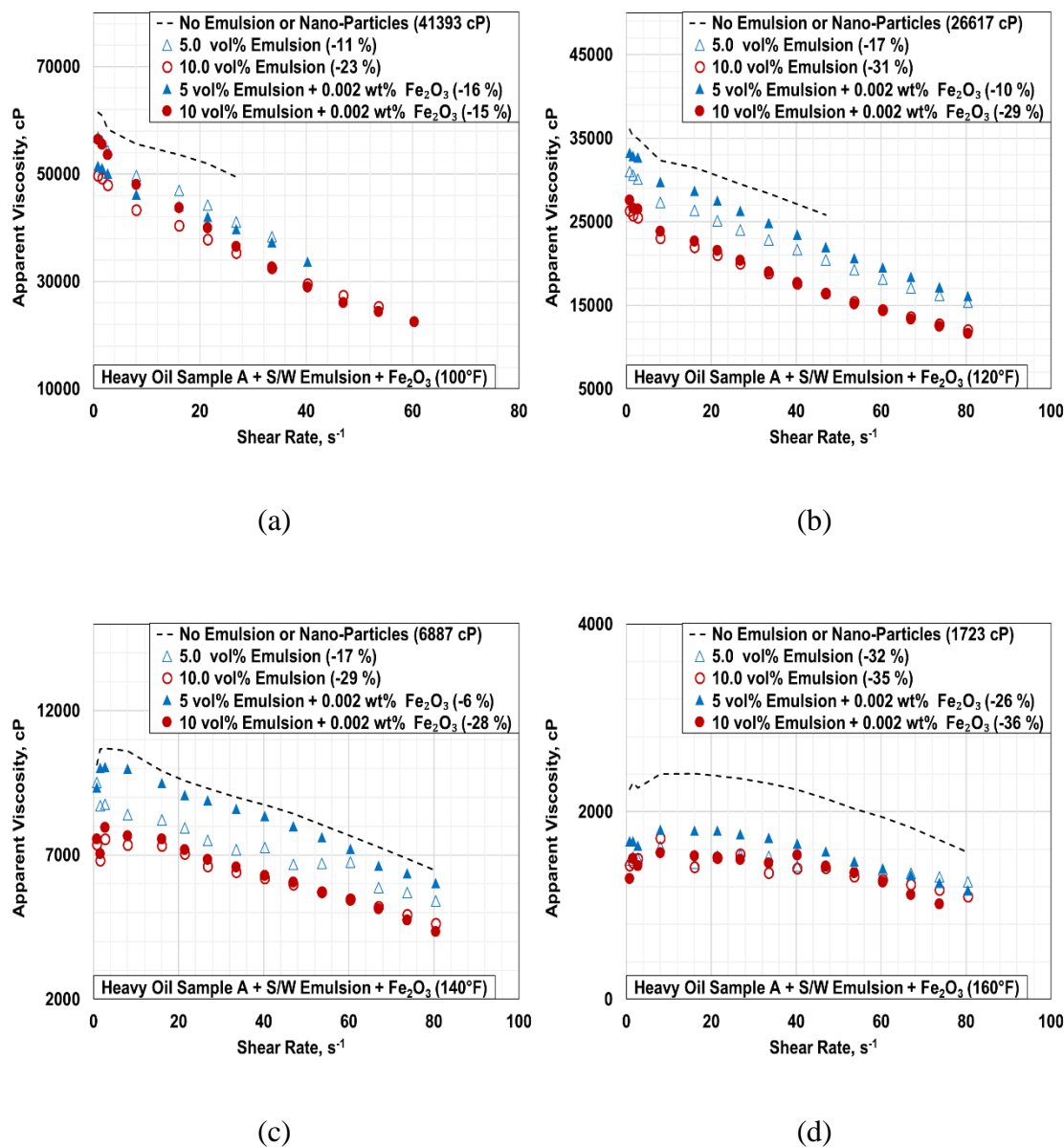
(c)



(d)

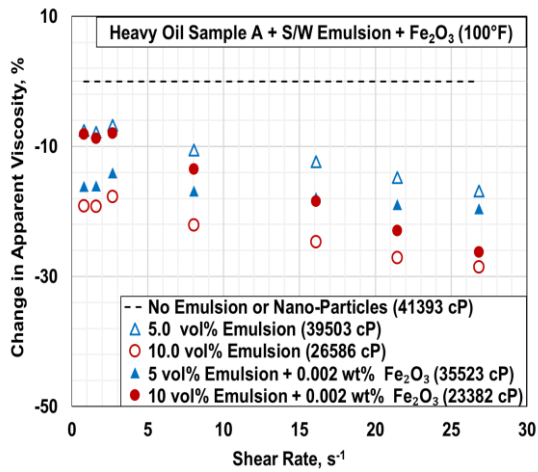
**Figure C.4:** Percentage change in apparent viscosity of heavy oil Sample B by S/W emulsion containing copper oxide nanoparticles at (a) 100°F (b) 120°F (c) 140°F and (d) 160°F

\* Viscosity mentioned in parenthesis corresponds to Newtonian viscosity

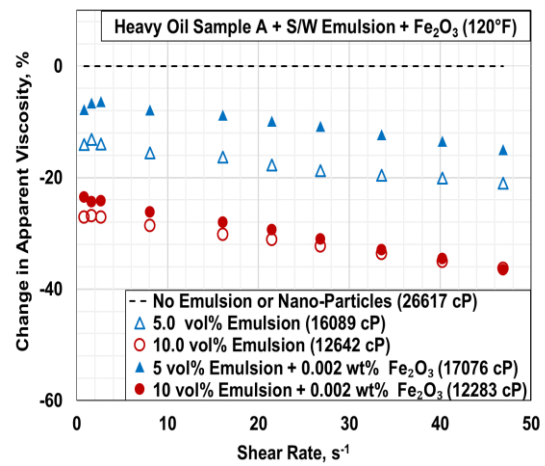


**Figure C.5:** Apparent viscosity of heavy oil nano-emulsion (Sample A) containing iron oxide nanoparticles at (a) 100°F (b) 120°F (c) 140°F and (d) 160°F

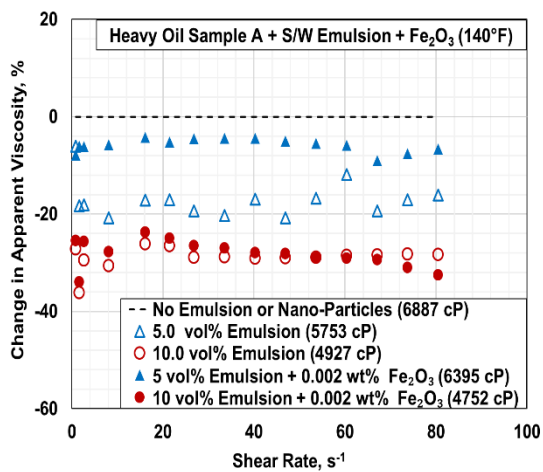
\* Average percentage change in apparent viscosity is mentioned in parenthesis



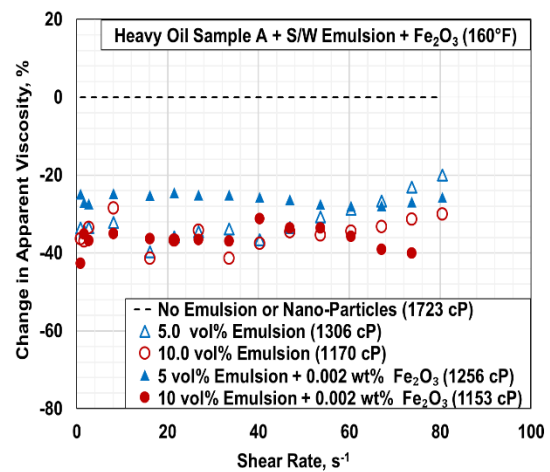
(a)



(b)



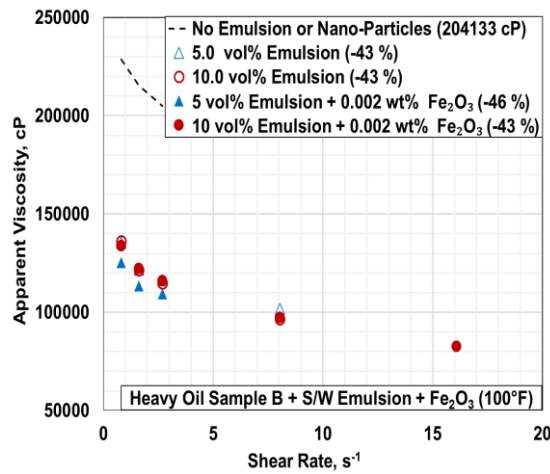
(c)



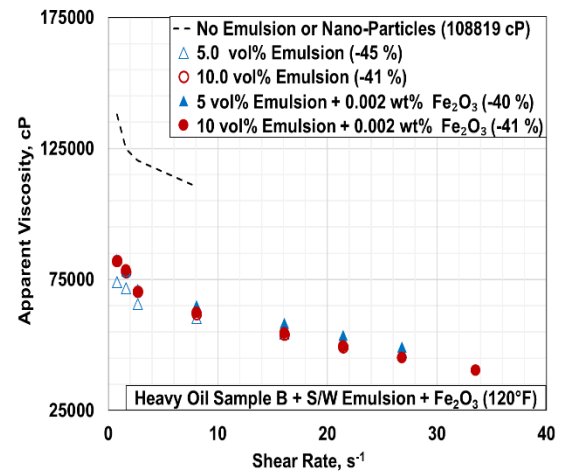
(d)

**Figure C.6:** Percentage change in apparent viscosity of heavy oil Sample A by S/W emulsion containing iron oxide nanoparticles at (a) 100°F (b) 120°F (c) 140°F and (d) 160°F

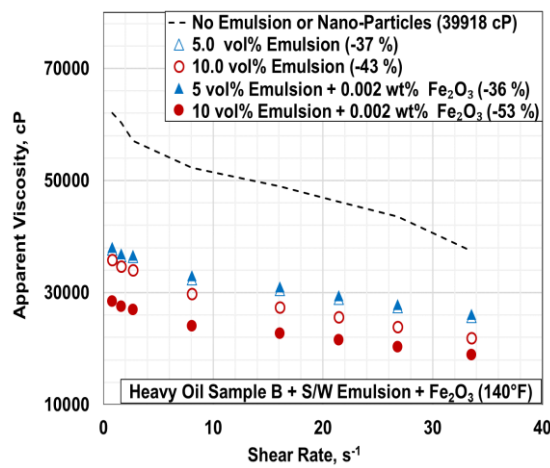
\* Viscosity mentioned in parenthesis corresponds to Newtonian viscosity



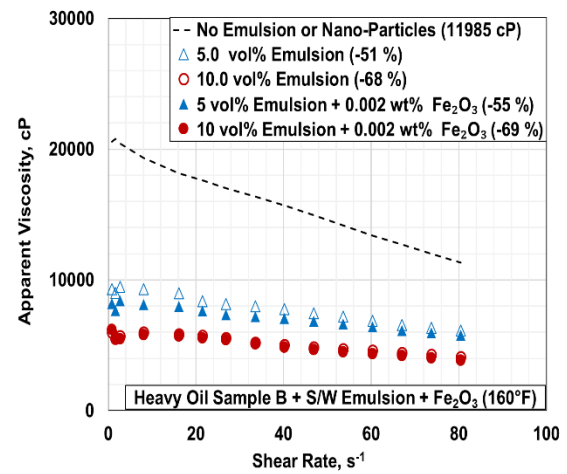
(a)



(b)



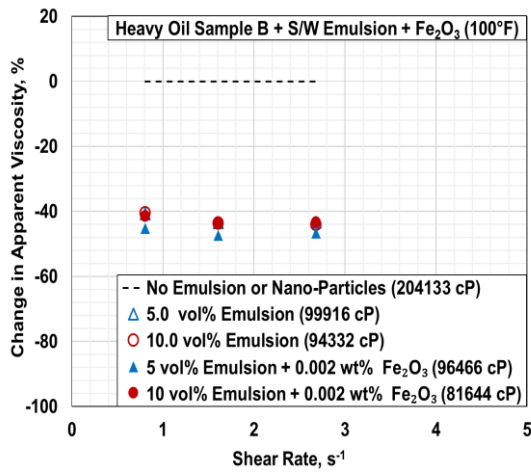
(c)



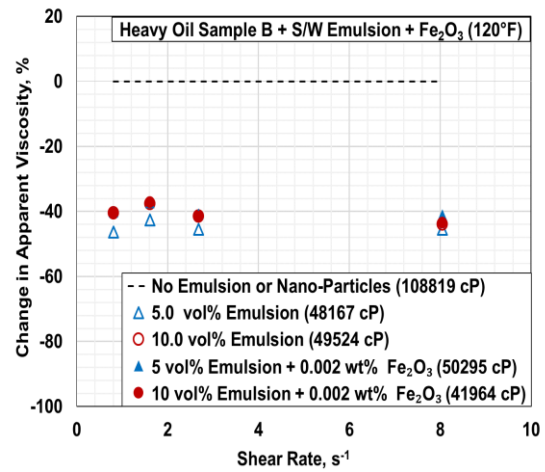
(d)

**Figure C.7:** Apparent viscosity of heavy oil nano-emulsion (Sample B) containing iron oxide nanoparticles at (a) 100°F (b) 120°F (c) 140°F and (d) 160°F

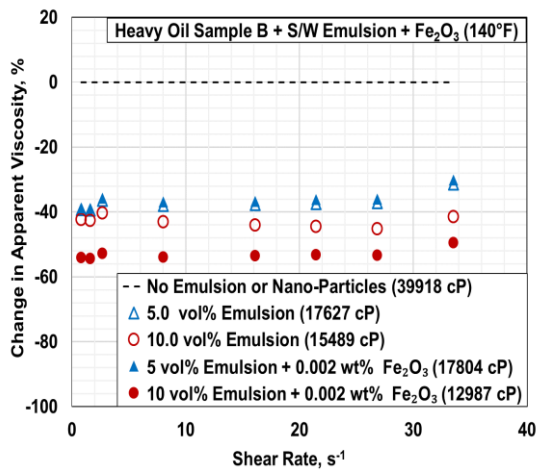
\* Average percentage change in apparent viscosity is mentioned in parenthesis



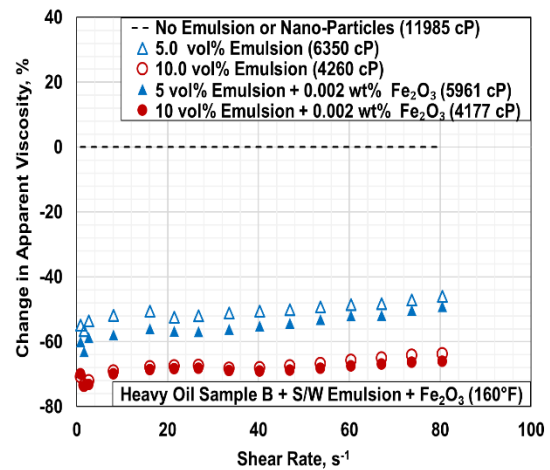
(a)



(b)



(c)

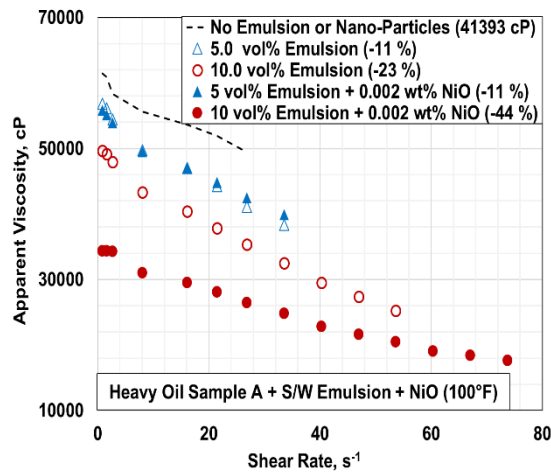


(d)

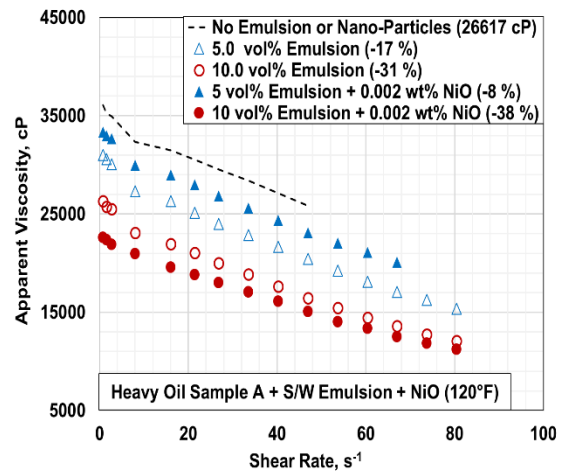
**Figure C.8:** Percentage change in apparent viscosity of heavy oil Sample B by S/W emulsion containing iron oxide nanoparticles at (a) 100°F (b) 120°F (c) 140°F and (d) 160°F

\* Viscosity mentioned in parenthesis corresponds to Newtonian viscosity

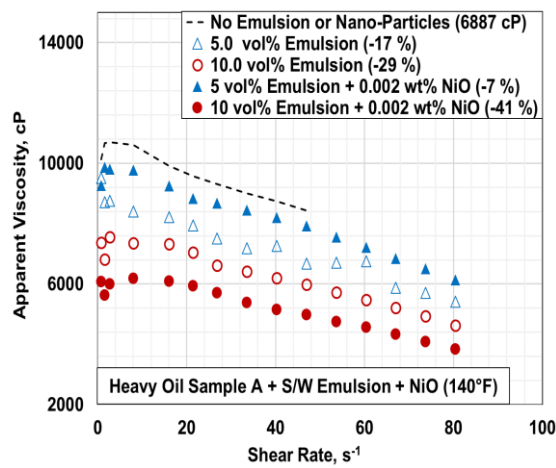




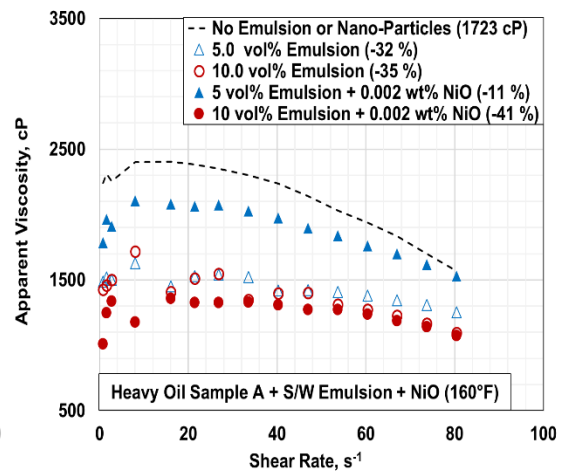
(a)



(b)



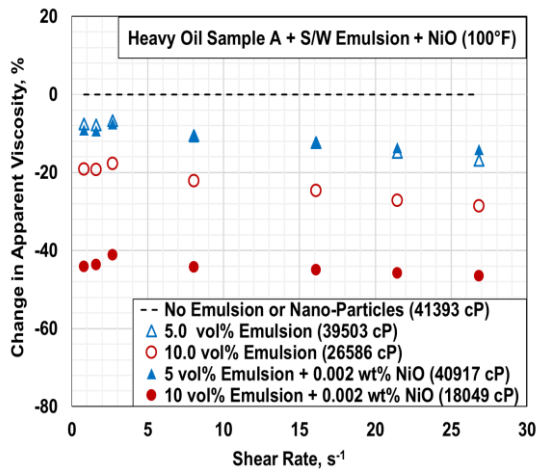
(c)



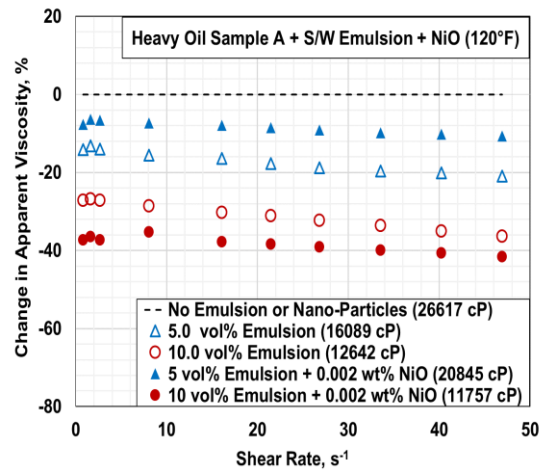
(d)

**Figure C.9:** Apparent viscosity of heavy oil nano-emulsion (Sample A) containing nickel oxide nanoparticles at (a) 100°F (b) 120°F (c) 140°F and (d) 160°F

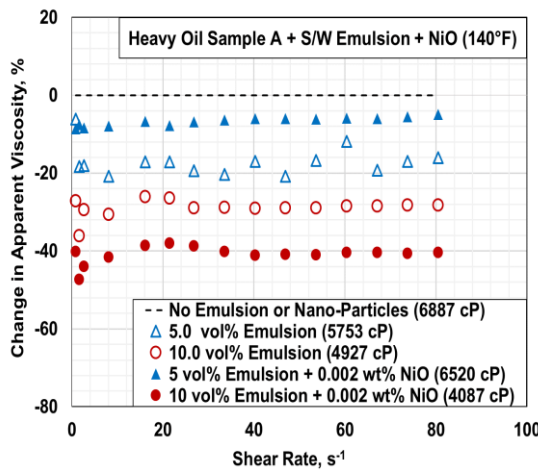
\* Average percentage change in apparent viscosity is mentioned in parenthesis



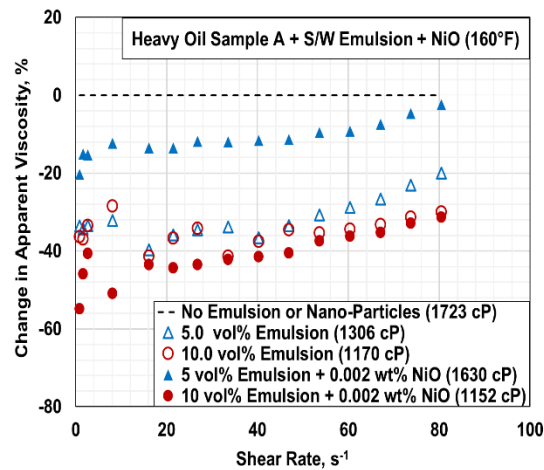
(a)



(b)



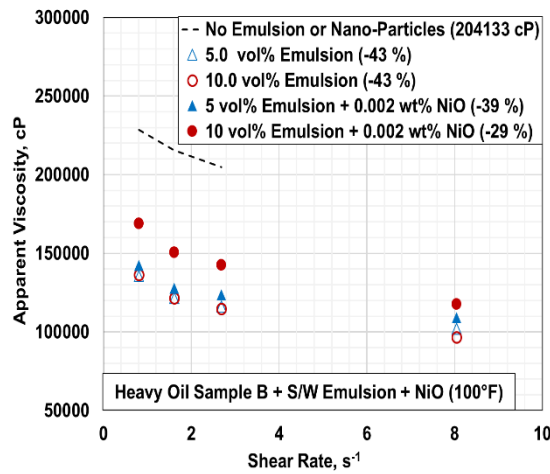
(c)



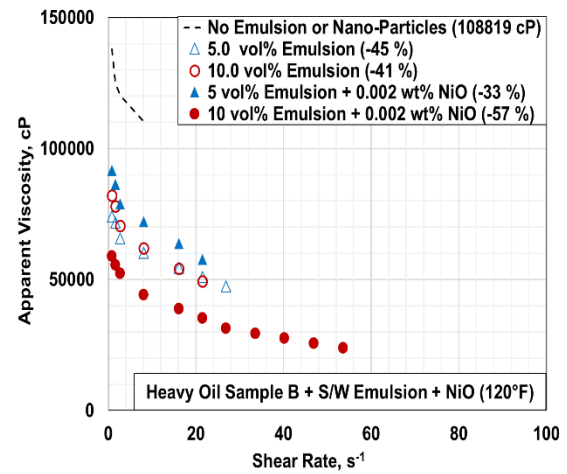
(d)

**Figure C.10:** Percentage change in apparent viscosity of heavy oil Sample A by S/W emulsion containing nickel oxide nanoparticles at (a) 100°F (b) 120°F (c) 140°F and (d) 160°F

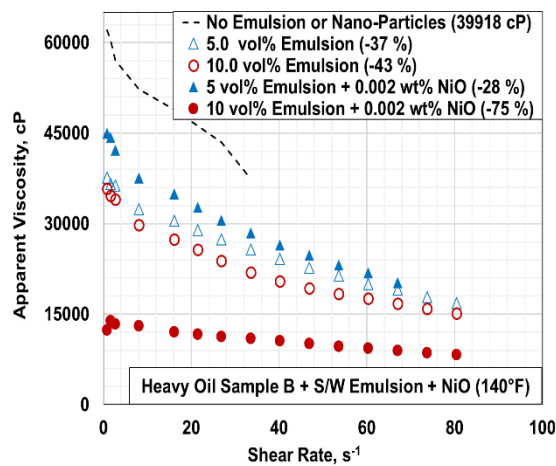
\* Viscosity mentioned in parenthesis corresponds to Newtonian viscosity



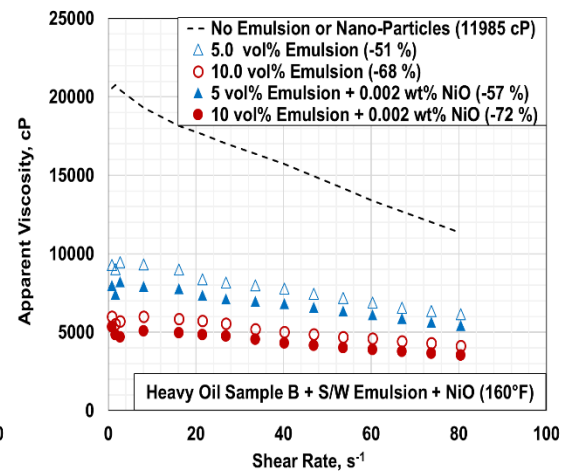
(a)



(b)



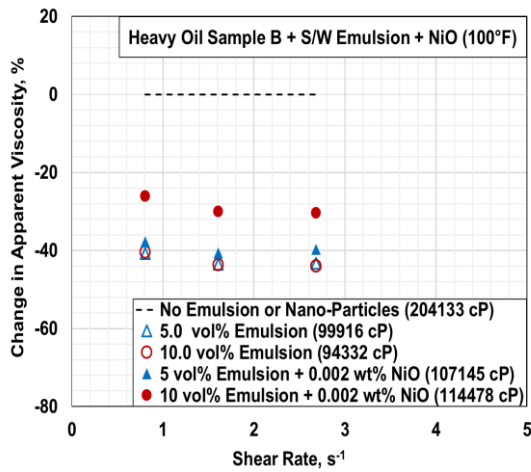
(c)



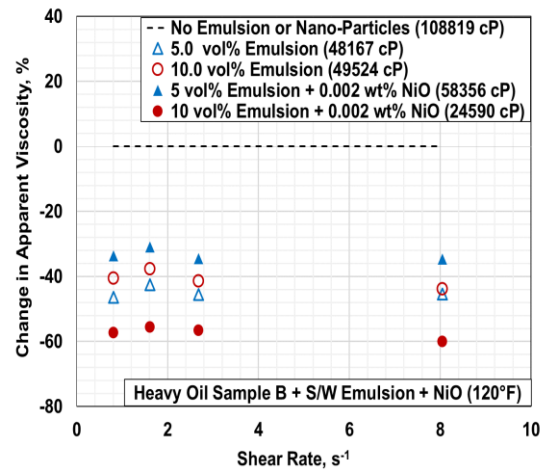
(d)

**Figure C.11:** Apparent viscosity of heavy oil nano-emulsion (Sample B) containing nickel oxide nanoparticles at (a) 100°F (b) 120°F (c) 140°F and (d) 160°F

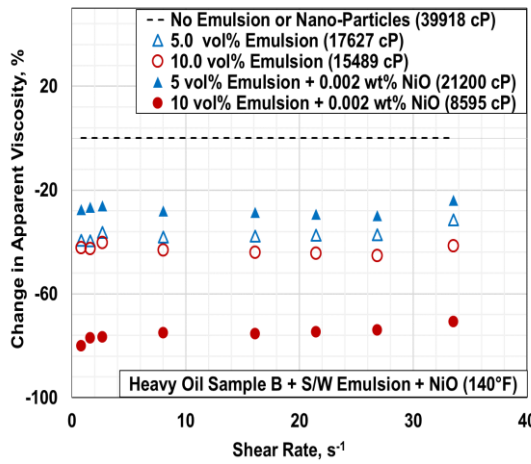
\* Average percentage change in apparent viscosity is mentioned in parenthesis



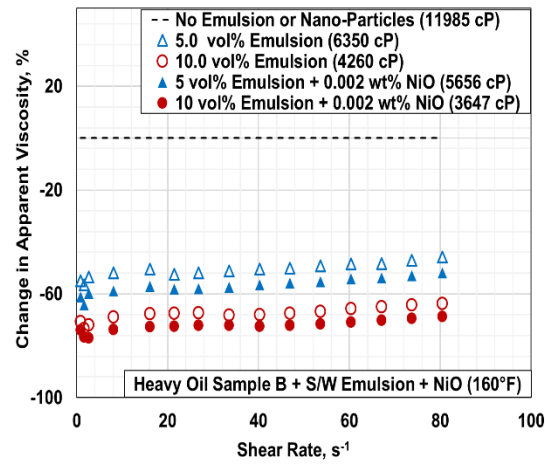
(a)



(b)



(c)



(d)

**Figure C.12:** Percentage change in apparent viscosity of heavy oil Sample B by S/W emulsion containing nickel oxide nanoparticles at (a) 100°F (b) 120°F (c) 140°F and (d) 160°F

\* Viscosity mentioned in parenthesis corresponds to Newtonian viscosity